MINISTRY OF EDUCATION AND TRAINING

QUY NHON UNIVERSITY

PHAN DANG CAM TU

STUDY ON STABILITY AND NATURE OF INTERACTIONS OF FUNCTIONAL ORGANIC MOLECULES WITH CO_2 AND H_2O BY USING QUANTUM CHEMICAL METHOD

DOCTORAL DISSERTATION

BINH DINH - 2022

MINISTRY OF EDUCATION AND TRAINING

QUY NHON UNIVERSITY

PHAN DANG CAM TU

STUDY ON STABILITY AND NATURE OF INTERACTIONS OF FUNCTIONAL ORGANIC MOLECULES WITH CO_2 AND H_2O BY USING QUANTUM CHEMICAL METHOD

Major: Theoretical and Physical Chemistry

Code No.: 9440119

Reviewer 1: Assoc. Prof. Dr. Tran Van Man

Reviewer 2: Assoc. Prof. Dr. Ngo Tuan Cuong

Reviewer 3: Dr. Nguyen Minh Tam

Supervisor: Assoc. Prof. Dr. NGUYEN TIEN TRUNG

BINH DINH - 2022

DECLARATION

This dissertation was done at the Laboratory of Computational Chemistry and Modelling (LCCM), Quy Nhon University, Binh Dinh province, under the supervision of Assoc. Prof. Dr. Nguyen Tien Trung. I hereby declare that the results presented are new and original. Most of them were published in peer-reviewed journals. For using results from joint papers, I have gotten permissions from my co-authors.

Binh Dinh, 2022

Author

Phan Dang Cam Tu

ACKNOWLEDGEMENT

To all the family members, teachers, and friends, I would not complete this dissertation without their help and support.

First, I am kindly thankful to my supervisor, Assoc. Prof. Dr. Nguyen Tien Trung for his advice and encouragement during my PhD life. I also express thanks to Assoc. Prof. Dr. Vu Thi Ngan and Prof. Minh Tho Nguyen for their valuable advice and discussing some research problems.

I am thankful to all the past and present members of the LCCM lab for outgoing activities and valuable discussions during my research time. It is a pleasure for me to say thank to my seniors, Ho Quoc Dai and Nguyen Ngoc Tri for morning coffee chatting and for solving all the technical problems. I gratefully acknowledge the lectures of Department of Chemistry, Faculty of Natural Sciences and the staffs in Office of Postgraduate Management, Quy Nhon University.

I sincerely thanks to the Vietnam National Foundation for Science and Technology Development (NAFOSTED) under grant number 104.06-2017.11; Domestic PhD Scholarship Programme of Vingroup Innovation Foundation (VinIF), Vietnam; and the VLIR-TEAM project awarded to Quy Nhon University with Grant number ZEIN2016PR431 (2016-2020) for the financial support.

I heartily thank to my longtime friends, Nhung and Nga, who always be here, by my side and share with me all the difficulties in life; to Tran Quang Tue for helping me to understand some mathematical aspects in the study of quantum chemistry; and to Nguyen Duy Phi, who encouraged me in the first two years of my PhD.

Last but most important, words are never enough to express my gratitude to my parents. To dad, the first person I asked for the decision of doing PhD and the most influential person in my life, I wish you are here, at this moment and proudly smile to your little daughter. To mom, with your love and endless patience, you make me feel stronger and ready to overcome all challenges.

TABLE OF CONTENTS

List of symbols and notations

AIM	Atoms in Molecules
aco	Acetone
acs	Thioacetone
BCP	Bond critical point
BSHB	Blue-shifting hydrogen bond
BSSE	Basis set superposition error
ChB	Chalcogen bond
CCSD(T)	Coupled-cluster singles and doubles methods
DME	Dimethyl ether
DMSO	Dimethyl sulfoxide
DMS	Dimethyl sulfide
DPE	Deprotonation energy
EDT	Electron density transfer
E_{int}	Interaction energy
E_{coop}	Cooperative energy
HF	Hartree Fock method
HB	Hydrogen bond
MEP	Molecular electrostatic potential
MP2	Second-order Moller-Plesset perturbation method
NBO	Natural bond orbital
NCIplot	Noncovalent Interaction plot
PA	Proton affinity
RSHB	Red-shifting hydrogen bond
SAPT	Symmetry-adapted perturbation theory
TtB	Tetrel bond
ZPE	Zero-point vibrational energy
$\rho(r)$	Electron density
$\nabla^2\rho(r)$	Laplacian of electron density
$H(r)$	Total energy density
$E^{(2)}$	Second-order energy of intermolecular interaction
Lp	Lone pair

List of figures

List of tables

GENERAL INTRODUCTION

1. Research introduction

Economic development and industrialization cause a significant increase in concentration of gases emitted into the environment. Therefore, air pollution is one of the hottest topics which attracts a lot of attention. Increasing amount of carbon dioxide (CO_2) in the air is the main factor that significantly affects the greenhouse effect. The enhancing applications of supercritical CO_2 (hereafter denoted by $scCO_2$) in manufacturing industries help to partially solve emission problems, while also save other resources. $ScCO_2$ has attracted much attention due to its environmentally friendly applications, as compared to toxic organic solvents.[1] Compressed CO_2 has indeed been widely used as a solvent for extraction purposes or in organic solvent elimination/purification processes, also as an antisolvent in polymerization of some organic molecules and precipitation of polymers. With the aim of finding the new materials and solvents which preferred CO_2, it is essential to clarify interactions between CO_2 and functional organic compounds and their electronic characteristics at molecular level. These understandings require a systematic study combining the experiments and modelling, and importantly, a quantum computational approach.

Up to now, various experimental researches on the interactions between solutes and $scCO_2$ solvent have been undertaken to better investigate the solubility in $scCO_2$. In general, some functional organic compounds including hydroxyl, carbonyl, thiocarbonyl, carboxyl, sulfonyl, amine, … are considered as CO_2 - philic ones. Furthermore, the use of polarized compounds as H_2O, small alcohols (CH_3OH, C_2H_5OH) as cosolvents was reported to affect the thermodynamic and even kinetic properties of reactions involving CO_2. Addition of H_2O into $scCO_2$ solvent helps to increase the solubility and extraction yield of organic compounds. Therefore, the systematic research on interactions between CO_2, H_2O and organic functional compounds will open the doors to the nature and role of formed interactions, the effect of cooperativity in the solvent – cosolvent – solute system.

The achieved results are hopefully to provide a more comprehensive look at $scCO_2$ application and also contribute to the understanding of the intrinsic characteristics of weak noncovalent interactions.

2. Object and scope of the research

- Research object: Geometrical structure, stability of complexes involving CO_2; nature and role of noncovalent interactions including tetrel bond, hydrogen bond.
- Scopes: complexes of functional organic compounds including dimethyl sulfoxide, acetone, thioacetone, methanol, ethanol, ethanethiol, dimethyl ether and its halogen/methyl substitution with some molecules of CO_2 and/or H_2O.

3. Novelty and scientific significance

This work represents the geometries, stability, properties of noncovalent interactions in complexes of dimethyl sulfoxide, acetone, thioacetone, dimethyl ether and its di-halogen/methyl derivative, dimethyl sulfide, methanol, ethanol, ethanethiol with CO_2 and/or H_2O. Remarkably, general trend of complexes with mentioned organic compounds and CO_2 and/or H_2O is determined using high level *ab initio* calculations. The bonding features of complexes with CO_2 and/or H_2O are also analysed in detail. In addition, the effect of H_2O presence leads to a significant increase in stability and positive cooperativity as compared to complexes containing only CO_2. The O–H···O HBs contribute largely into the cooperativity among other weak interactions including C···O/S TtBs, C−H···O HBs and O···O ChBs. Especially, it is found the growth pattern in complexes of ethanol with 1-5 CO_2 molecules which is expected to be useful for understanding the ethanol solvation in $scCO_2$. It is important that the comparison of stability of complexes and strength of noncovalent interactions are thoroughly investigated.

The systematically theoretical investigation on complexes between functional organic molecules and a number of CO_2 and/or H_2O ones could provide useful information for the development of promising functionalized materials for CO_2 capture/sequestration and increase knowledge in noncovalent interactions. These obtained results can play as the valuable references for future works on

$scCO_2$ and benchmark of noncovalent interactions.

This dissertation is also hoped to be an effective reference for lectures, researchers, students, etc in studying about computational chemistry at molecular level, especially noncovalent interactions and complexes involving CO_2.

Chapter 1. DISSERTATION OVERVIEW

1.1. Overview of the research

Human emissions of CO_2 and other greenhouse gases are the primary driver of climate change which is one of the present world's most pressing challenges. The relation between the cumulative CO_2 emissions and global temperature has been clearly discovered.[2] It is said that CO_2 is the key atmospheric gas that exerts control over the strength of the greenhouse effect. Innovating the use of CO_2 is an urgent mission with the aim of decreasing its concentration in ambient air. CO_2 is abundant, reusable and non-toxic, and it reaches a supercritical point at an easily controlled temperature and pressure. $ScCO_2$ is a well-known effective solvent for the development of green chemical reactions instead of conventional toxic organic solvents. $ScCO_2$ is used in extensive applications in nanomaterials, food science, pharmaceuticals, especially in separation and synthetic processes.[3,4] The effective use of $scCO_2$ in extraction and fractional processes of separation has been reported in many previous works.[3,5,6] Nevertheless, the solvent has drawbacks in solute polar organic compounds and high molecular-mass ones. Thus, many efforts have been made to find out the interacting species and effective thermodynamic reaction conditions aiming to enhance the solubility in $scCO_2$. Fluorocarbons, fluoropolymers, and carbonyl-based compounds are previously considered as CO_2-philic functional groups.[7,8,9] While high cost and toxicity are the limitations of the first two compounds, carbonyl-based compounds have been paid much attention thanks to their simple synthesis process and lower cost. Efforts for enhanced applicability of $scCO_2$ with the use of CO_2-philes have been pursued *via* series of experimental and theoretical works.[10,11,12,13,14,15]

Dimethyl sulfoxide (DMSO) is a common solvent in biological and physicochemical studies, which is widely used in supercritical antisolvent processes,[16,17] with many valuable applications such as micronization of pharmaceutical compounds, polymers, catalysts, superconductors and colouring materials.[18] The use of the mixture of DMSO and CO_2 in PCA (Precipitation with a

Compressed Antisolvent) process to precipitate proteins and polar polymers confronts some difficulties in both operation regions that are below and upper the critical pressure of the DMSO-CO_2 mixture. Some experimental studies suggested the use of water as a cosolvent of DMSO to modify the phase behaviour of DMSO-CO_2 and solve limitations of the PCA process.[19] In this approach, water molecules help to shape particle morphology by changing the mechanism of particle formation. Experimental phase equilibrium data on binary mixtures of DMSO-CO_2 and ternary mixtures of DMSO-CO_2-H_2O were measured.[20,21] Wallen *et al.*[9] reported that DMSO interacts strongly with CO_2, and the complex strength is contributed by both the S=O···C Lewis acid-base interaction and the C–H···O HB, in which the more crucial role of the former was suggested by Trung *et al.* [22] Intermolecular interaction of DMSO and H_2O was classified into the class of O−H···O red-shifting and C−H···O blue-shifting hydrogen bonds by Kirchner and Reiher.[23] Lei *et al.* revealed that the weak C−H···O and strong O−H···O contacts represent a consistent concentration dependence in interaction between DMSO and H_2O, implying a cooperative effect between two hydrogen bonded types.[24] Overall, the phase behaviour of these binary and ternary mixtures can be controlled when the interactions and stability of DMSO with both H_2O and CO_2 at the molecular level are elucidated.

Many experimental investigations showed that the addition of a small amount of cosolvents into the scCO_2 solvent resulted in an increase in the solubility of solutes.[25,26,27] In particular, some alkanes were added to scCO_2 to dissolve the nonpolar compounds, whereas functional organic compounds or H_2O were used for the polar ones.[28,29,30] Alcohols including methanol, ethanol, and propanol were extensively used as cosolvents to improve both solubility and selectivity processes.[27,30,31] According to Hosseini *et al.*, the presence of alcohols as a cosolvent affects the shape of complexes formed, in which each alcohol has different impacts on the aggregation of CO_2 around the drugs.[30] The solubility of Disperse Red 82 and modified Disperse Yellow 119 increases substantially up to

25-fold by adding 5% of ethanol cosolvent to the $scCO_2$.[31] Vapor-liquid equilibria and critical properties of the CO_2···ethanol binary mixture were experimentally investigated using a variety of experimental techniques and equipment.[32,33,34,35] Becker *et al*. reported that the addition of CO_2 to pure ethanol leads to a reduction of interfacial tension in the liquid phase.[32] The addition of H_2O into $scCO_2$ solvent was reported that induces an increase in the solubility and extraction yield of organic compounds.[36,37]

From the theoretical viewpoint, it is important to elucidate the interactions, stability and structures of complexes between organic compounds and CO_2 with/without H_2O at molecular level. The mechanism of the CO_2 capture could also be understood *via* the investigation into CO_2 complexes. In which, the intrinsic strength of the noncovalent interactions between CO_2 and adsorbents is determined as a key to demanded captured abilities. Furthermore, a systematically theoretical investigation into complexes between organic compounds and CO_2 with/without H_2O at molecular level could give information for solvent-solute and solvent-cosolvent interactions in systems involving CO_2.

As previously mentioned, the molecules containing carbonyl group have been paid much attention. Indeed, they have been pursued by series of experimental and theoretical works.[15,38,39,40,41,42,43,44,45,46,47] The structures of complexes and strengths of intermolecular interactions have been reported through numerous studies on systems bound by CO_2 and various organic compounds: simple alcohols,[48,49] formamide,[50] isopropyl amine,[51] 2-methoxy pyridine,[52] … According to *ab initio* calculations, three types of geometries were reported as presented in Fig. 1.1. The conventional structure is supported by theoretical and experimental data, whereas two remaining ones are less favoured. The parallel geometry (also called non-conventional structure) is similar to the $(CO_2)_2$ dimer and carbonyl-carbonyl arrangements in crystallographic structures. However, this structure is rarely reported, with the exception of methyl acetate-CO_2 complexes. For carbonyl

complexes, C···O tetrel bond (previously called Lewis acid-base interaction) was addressed as the bonding feature.

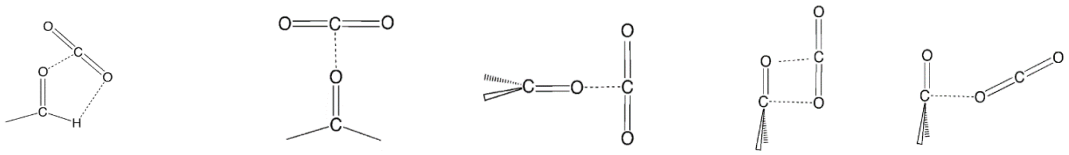

Conventional structures | T-shaped structures | Non-conventional structures

Figure 1.1. Three types of CO_2 complexes

In 2002, Raveendran and Wallen reported the cooperative effect of C-H···O hydrogen bond in systems of CO_2 with different organic molecules including formaldehyde, acetaldehyde, acetic acid, and methyl acetate, as model carbonyl compounds, and dimethyl sulfoxide as a model system for the sulfonyl group.[9] In which the hydrogen atom attaches to the carbonyl carbon or the α-carbon directly interacted with oxygen one of CO_2. However, the investigations that were combined by *ab initio* calculations and experimental infrared spectra showed that the complex of dimethyl ether and CO_2 is stabilized by C···O tetrel bond with the C_s symmetry and without the additional contribution of C–H···O hydrogen bond.[47,53]

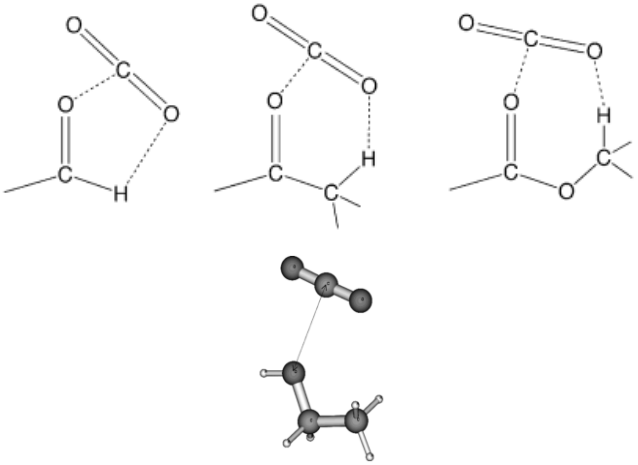

a) Stable structures of complexes formed by carbonyl compounds and CO_2 (Ref. 44)

b) Stable structures of complexes formed by ethanol and CO_2 (Ref. 48)

Figure 1.2. Stable geometries of complexes involving CO_2

Similarly, the principal role of C···O tetrel bond was detected in complexes of CO_2 with CO[54], HCN[55], H_2O[56], C_2H_5OH, CH_3OH, … In systems of formamide and CO_2, the C···O over the C···N tetrel bond is the primary factor in stabilizing the complexes.[50] Many rotational data were reported for the nature of interactions

between CO_2 and partner molecules, from solvent or lattice effects. The rotational spectra using the high-resolution Fourier transform microwave (FTMW) reveals information on intermolecular interactions and geometrical structures, which is used to compare with obtained results taken from theoretical calculations.[46,49,50,52] For complexes of simple alcohols with CO_2, many works proposed the primary role of C···O tetrel bond with additional contribution of C–H···O hydrogen bond.[48,49] For the aggregation of CO_2 around ethanol, molecular dynamic simulations of ethanol···64CO_2 system under supercritical conditions showed the higher probability of CO_2 around the lone pairs of oxygen atom in ethanol.[57] Another investigation into structures of ethanol and 1-4 and 6 molecules of CO_2 in 2017 also gives the same result that the CO_2 molecules preferably locate around the oxygen atom of ethanol.[58]

It is useful to compare features of compounds containing oxygen and sulur element. A previously comparative study on interactions between CO_2 and compounds functionalized by >S=O and >S=S groups reported the larger stability of $(CH_3)_2(S=O)\cdots CO_2$ complexes as compared to $(CH_3)_2(S=S)\cdots CO_2$ ones, which is due to a larger contribution of the attractive electrostatic interaction of the >S=O relative to the >S=S.[22] The complexes of CO_2 with thioformaldehyde and its halogen/methyl-derivatives were exclusively reported to be slightly less stable than those with substituted formaldehydes.[42] Different with the great attention of carbonyl compounds, thiocarbonyl ones have been rarely studied in searching for an effective cosolvent in scCO_2. Thiocarbonyl compounds have been used in syntheses and have provided several unique organocatalysts thanks to their higher reactivity and less polarity in comparison with carbonyl ones.[59] Moreover, the compounds involving >C=S group are predicted to be key functions in molecular materials and biologically relevant substrates.[60] Accordingly, understanding of interactions of thioacetone (acs) with popular solvents and cosolvents used in synthesis, extraction, separation processes such as scCO_2 and/or H_2O is essential.

Up to now, most of studies concentrated on the geometries, stability and interactions of binary complexes involving CO_2. Nevertheless, the aggregation and growth mechanism of complexes with more CO_2 molecules, which are important to understand the absorption processes and their properties, have not been reported yet. Besides, the solvation structures and stability of complexes formed by interactions of organic compounds with a small number of CO_2 and H_2O molecules have not yet been discovered.

From perspective of noncovalent interactions, the behaviour and origin of weak interactions such as hydrogen, tetrel, chalcogen, and halogen bond have been widely investigated because of their considerable influence on crystal packing, material structures, and biological systems.[61,62,63,64,65,66,67] Hydrogen bond (HB), especially blue-shifting HB has extensively been reported thanks to its ubiquity and significance in crystal engineering and biochemical processing.[42,68,69,70] A general scheme that can unravel the origin of blue-shifting HB remains an objective of both theoretical and experimental investigations. The C–H···O, which is known as a typical blue-shifting HB,[71,72] is revealed to play a cooperative role in stabilization of complexes between CO_2 and some organic molecules *via* IR spectra and *ab initio* calculations.[9,45] Different with hydrogen bond, other types of noncovalent interaction including tetrel, chalcogen, pnictogen bonds have been named in very recent years. Therefore, it is lack of a comprehensive theory of these interactions and especially, the molecular level characterization and interpretation of tetrel bond are still far from being satisfactory. On the other hand, mutual influence of two or more noncovalent interactions is also an important issue in order to clarify their characteristics. The cooperativity effects involving hydrogen bonds in living organisms are well-known phenomena as previously reported.[73,74,75] A largely positive effect was found between hydrogen bonds in water clusters.[75,76] For complexes of DMSO with two molecules of H_2O, the interaction energies of the O−H···O and C−H···O hydrogen bonds were reported to be increased by 53% and 58% respectively, demonstrating the presence of large cooperativity.[77] In addition to

hydrogen-bonded complexes, the cooperative effect was also found in other noncovalent ones including cation-π, π-π, halogen, tetrel bonds, etc.[45,78] In 2015, Scheiner *et al.* determined a small cooperativity in complexes of carbonyl compounds with CO_2 molecules.[45] Because of the importance of cooperativity in life sciences and biochemistry, the quantitative study of cooperative effect is thus important to explore how noncovalent interactions influence each other and can shed new light on the cooperativity effect in biological as well as supramolecular chemistry.

The investigation of various noncovalent interactions helps to provide the quantum mechanical basis for understanding energetically favourable motifs. The presence of both H_2O and CO_2 in a system could lead to the existence of C···O tetrel bond, O–H···O and C–H···O hydrogen bonds. The investigation into such systems helps to discover the characteristics of the noncovalent interactions and their mutual influence. It is clear that the phase behaviour of these binary and ternary mixtures should be controlled when the interaction and stability of organic compounds with both H_2O and CO_2 molecules at the molecular level is elucidated. However, as mentioned above, a systematically theoretical investigation into these systems has not been reported in the literature.

In short, a systematic study on the complexes of organic compounds with CO_2 and H_2O using reliable high-level computational methods is essential to thoroughly understand the solvent capacity and adsorption of CO_2, the characteristics of noncovalent interactions and evaluate the cooperative effect derived from multiple interactions within the ternary systems. Another important objective of the study is to investigate the influence of H_2O to structures and stability of complexes and characteristics of noncovalent interactions. Further, changes in C(O)–H bond length and its stretching frequency are determined for the various complexes considered, with respect to relevant monomers, in order to obtain a deeper understanding on characteristic of C–H···O blue-shifting hydrogen bond. The obtained results lead to the understanding of geometrical trend and all

interesting characteristics of noncovalent interactions and complexes as mentioned above. In addition, these obtained results will be useful for scientists in searching of novel materials to adsorb CO_2 gas effectively.

1.2. Objectives of the research

This work has four main objectives detailed as follows:

1) To determine stable structures and to compare the strength of the complexes formed by interaction of basic organic compounds functionalized by various groups with CO_2 and H_2O molecules, and also to find out functional groups that interact strongly with CO_2 as valuable candidates in searching of novel materials to adsorb CO_2 gas phase.
2) To specify the existence and the role of noncovalent interactions in stabilizing the complexes, to unravel their cooperativity, especially the cooperativity of hydrogen bonds and tetrel bonds; and also to gain further insights into the origin of noncovalent interaction. Furthermore, this research was investigated to clarify role of H_2O in stabilization of noncovalent interactions and complexes, which leads to a clearer understanding of importance of H_2O as cosolvent in supercritical CO_2.
3) To investigate the effect of different substitution groups including halogen and methyl on the geometry and stability of complexes formed by interaction of functional organic compounds with CO_2 and/or H_2O.
4) To discover the trend of geometrical structures and characteristic of noncovalent interactions when increasing number of CO_2/H_2O molecules. This gives information of the aggregation of CO_2 around organic compounds, with/without H_2O.

1.3. Research content

In order to obtain the aims of research project, the complexes of functional organic molecules including $(CH_3)_2SO$, $(CH_3)_2CO$, $(CH_3)_2CS$, $(CH_3)_2O$, $(CH_3)_2S$, CH_3OH, C_2H_5OH, C_2H_5SH with nCO_2 and/or nH_2O (n=1-2) were investigated. Additionally, the effect of methyl and halogen substitution is also examined.

With those systems, the following contents were performed:

- Choosing the computational methods along with basis sets which are suitable for both monomers and complexes based on available experimental data, or reliable results reported in the literature.

- Simulating the structures of monomers and complexes, and then optimizing these structures to obtain stable geometries with minima of energy on potential energy surfaces.

- Calculating infrared spectra of monomers and complexes, and estimating the change of C(O)−H bond lengths, its stretching vibrational frequencies and infrared intensities in the complexes compared to the relevant monomers with purpose of classifying which type of hydrogen bond formed.

- Calculating interaction energy of complexes and comparing their strength. Many electronic analysed tools including MEP, AIM, NBO and NCIplot were used to specify existence and stability of the noncovalent interactions in the complexes, and then along with PA, deprotonation energy DPE to unravel their cooperativity to stability of complexes. Besides, the contribution of separate components of energy to the complex stabilisation on the basis of SAPT2+ approach was also estimated to gain a clearer view in the cooperativity of interactions in the complexes.

- Estimating cooperative energy of ternary complexes to evaluate the cooperation between noncovalent interactions in complexes. The effect of addition another CO_2 or H_2O molecule into complexes will be explored.

- Investigating the effect of DPE and PA to the formation of blue-shifting HB involving C−H covalent bond, in order to give more elucidation of origin of blue-shifting HB on the basis of PA of proton acceptor and DPE of C−H bond in the isolated monomers.

1.4. Research methodology

Investigation into complexes of functional organic molecules and CO_2 with/without H_2O at molecular level was carried out using high level computational chemical methods. Optimization calculations were done at MP2/6-6-

311++G(2d,2p), which is highly reliable. Vibrational frequency analyses were performed at the same level to specify minimum and estimate the zero-point energy. Single point energies with the geometries optimized at MP2/6-311++G(2d,2p) were computed at CCSD(T)/6-311++G(2d,2p) or MP2/aug-cc-pVTZ which depends on the size of investigated complexes. Interaction energies and cooperative energies are corrected for ZPE and the BSSE. The depth of intermolecular interactions was discovered with wave function calculations at MP2/6-311++G(2d,2p) or MP2/aug-cc-pVTZ. NBO analyses with ωB97X-D or MP2 method was used to quantitatively determine the charge-transfer effects and the characteristics of noncovalent interactions. To further identify the noncovalent behaviours, interactions between carbon dioxide and ethanol were assessed with NCIplot at MP2/6-311++G(2d,2p). MEP of isolated monomers was plotted at MP2/aug-cc-pVTZ. All quantum calculations mentioned above were carried out *via* the Gaussian09 package.

The SAPT2+ analysis executed by PSI4 program was applied to decompose the interaction energy into physically meaningful components including electrostatic, induction, dispersion and exchange terms. SAPT2+ calculations are performed with density-fitted integrals with the standard aug-cc-pVDZ basis set.

Besides, software such as Molden, Gaussview, Origin and Excel will be employed to help in analysing calculated results. Research methodology and techniques appropriate for each issue are described more detail in the next chapter.

Chapter 2. THEORETICAL BACKGROUNDS AND COMPUTATIONAL METHODS

2.1. Theoretical background of computational chemistry

2.1.1. The Hartree–Fock method

The origin of Hartree-Fock (HF) method existed soon after the discovery of Schrödinger's equation (1926). In 1928, Hartree introduced for the first time a procedure called the *self-consistent field* (SCF) method to calculate approximate wave functions and energies for atoms and ions.[79] Hartree assumed that the appropriate potential for a core electron is total potential of the nucleus and the whole electronic distribution of charge. Another assumption in Hartree's original paper is that the distribution of charge for a closed shell electron configuration is centrally symmetrical and the nucleus together with the electrons formed a spherically symmetric field. The following diagram briefly expresses the process of SCF method.

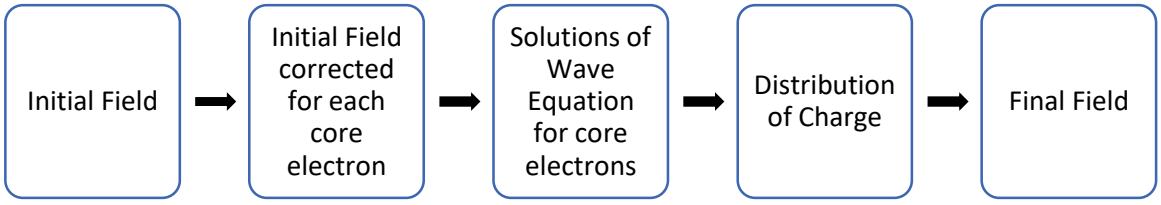

According to Hartree's approach,[79] SCF method gives solutions to Schrödinger's equation for systems with individual electrons 1, 2, 3, … in the states χ_1, χ_2, χ_3, … The electronic wave function of system is separated into product of wave functions of the individual electrons $\chi(r)$, is known as *Hartree product.* With the full set of coordinates, the *Hartree product* becomes

$$\Phi_{el} = \chi_1(x_1)\chi_2(x_2)...\chi_N(x_N)$$

This method attracted much attention and was independently modified by Slater and Fock in 1930. The Hartree product which assumes that electrons are independent did not satisfy the *anti*-symmetric requirement. The *anti*-symmetry of the wave function can be achieved by building it from Slater determinants.

$$\Phi_{el} = \left| \chi_i(\mathrm{x}_1)\chi_j(\mathrm{x}_2)...\chi_k(\mathrm{x}_N) \right\rangle$$

In order to derive the HF equation, the expression of energy of a single Slater determinant is needed to be described. Based on the Born-Oppenheimer approximation, it is allowed that the wave functions of atomic nuclei and electrons in a molecule can be treated separately:

$$\Psi_{total} = \Phi_{el}\Phi_{nu}$$

Then the Hamiltonian describes the system of N electrons around nuclei is recalled as:

$$\hat{\mathrm{H}}_{el} = -\sum_{i=1}^{N}\frac{1}{2}\nabla_i^2 - \sum_{i=1}^{N}\sum_{A=1}^{M}\frac{Z_A}{r_{iA}} + \sum_{\mathrm{i=1}}^{\mathrm{N}}\sum_{\mathrm{j>i}}^{\mathrm{N}}\frac{1}{\mathrm{r_{ij}}} + \sum_{\mathrm{A=1}}^{\mathrm{M}}\sum_{\mathrm{B>A}}^{\mathrm{M}}\frac{\mathrm{Z_A Z_B}}{\mathrm{R_{AB}}}$$

$$= \quad T_e \quad + \quad V_{ne} \quad + \quad V_{ee} \quad + \quad V_{nn}$$

Here, the first term is the kinetic energies of electrons. The second one is the attraction of electrons to nuclei. Two first terms depend on only one electron coordinate. The third term is repulsion between electrons and depends on two electrons. The repulsion between nuclei is added onto the energy at the end of the equation. The last term does not depend on electron coordinates and is a constant for a given nuclear geometry. These operators may be collected according to the number of electron indices (used atomic units to shorten the equation):

$$\hat{h}_i = -\frac{1}{2}\nabla_i^2 - \sum_{A=1}^{M}\frac{Z_A}{r_{iA}} \text{ and } \hat{v}(\mathrm{i,j}) = \frac{1}{r_{ij}}$$

$$\hat{H}_e = \sum_{i}^{Nel}\hat{h}_i + \sum_{j>i}^{Nel}\hat{v}(\mathrm{i,j}) + \mathrm{V}_{nn}$$

The energy is now written in terms of the permutation operator as:

$$\begin{aligned}
E_{el} &= \left\langle \Phi_{el} \middle| \hat{H}_e \middle| \Phi_{el} \right\rangle \\
&= \left\langle \Phi_{el} \middle| \sum_i \hat{h}_i \middle| \Phi_{el} \right\rangle + \left\langle \Phi_{el} \middle| \sum_i \sum_{j>i} \hat{v}(i,j) \middle| \Phi_{el} \right\rangle + V_{nn} \\
&= \sum_i \left\langle \Phi_{el} \middle| \hat{h}_i \middle| \Phi_{el} \right\rangle + \sum_i \sum_{j>i} \left\langle \Phi_{el} \middle| \hat{v}(i,j) \middle| \Phi_{el} \right\rangle + V_{nn} \\
&= \sum_i \left\langle \chi_i \middle| \hat{h}_i \middle| \chi_i \right\rangle + \frac{1}{2}\left[\sum_{ij} \left\langle \chi_i\chi_j \middle| \frac{1}{r_{ij}} \middle| \chi_i\chi_j \right\rangle - \sum_{ij} \left\langle \chi_i\chi_j \middle| \frac{1}{r_{ij}} \middle| \chi_j\chi_i \right\rangle \right] + V_{nn}
\end{aligned}$$

According to variational theorem, the idea of HF method is to find out the minimum of E_{el} when $\chi_i \to \chi_i + \delta\chi_j$ (is handled by means of Lagrange multipliers).

One of the advantages of the method is that it breaks the many-electron Schrodinger equation into many simpler one-electron equations. Each one-electron equation is solved to yield a single-electron wave function which called an orbital; and energy, called an orbital energy. The orbital describes the behaviour of an electron in the net field of all the other electrons.

$$\hat{f}\,\chi_i(x_1) = \varepsilon\chi_i(x_1)$$

Where f is Fock operator, $\chi_i(x_i)$ is a set of one-electron wave functions, called the HF molecular orbitals.

In computational chemistry, the simplified algorithmic flowchart of HF method is described in Fig. 2.1. The Hartree-Fock algorithm produces the optimal single-determinant electronic configuration for any set of nuclear coordinates. From this, the Fock matrix is constructed and diagonalized. After that, it solves the eigen value problem based on the obtained Fock matrix. A new density matrix is constructed, and this process will be repeated until the convergence test is satisfied.

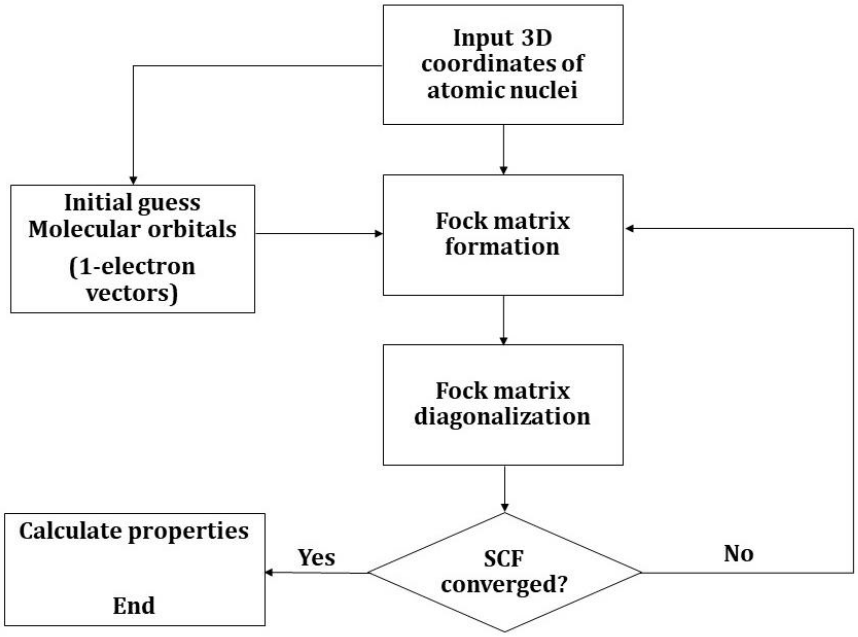

Figure 2.1. The flowchart illustrating Hartree–Fock method

The main defect of the HF method is that it does not treat electron correlation properly: each electron is considered to move in an electrostatic field composing by the average positions of the other electrons, whereas the fact is that electrons avoid each other better than the model predicts, since any electron A really sees any other one B as a moving particle and the two mutually adjust (correlate) their motions to minimize their interaction energy. The electron correlation is treated better in post-HF methods, which are represented in the following section.

2.1.2. The post–Hartree-Fock method

There is a number of different methods that go beyond HF calculations, called post-Hartree-Fock methods. They add electron correlation which is a more accurate way of including the repulsions between electrons than in the HF method where repulsions are on averaged. One of the widely used approaches is perturbation theory.

❖ In perturbation theory, the HF solution is treated as the first term in a Taylor series. One of the most common forms of perturbation was developed by Møller and Plesset.[80] Because it is a perturbational treatment, Møller-Plesset (MP) theory can be applied considering the perturbation series to include different numbers of terms (i.e., to different orders). Second order MP theory (MP2) is often used for geometry optimizations and fourth order (MP4) for refining calculated energies. The second order perturbation was utilized in the present work.

The MP perturbation theory considers an unperturbed Hamiltonian operator $\hat{H}_0$, to which a small perturbation *V* is added.

$$\hat{H} = \hat{H}_0 + \lambda\hat{V}$$

Here, λ is an arbitrary real parameter. Expanding the exact wave function and energy in term of HF wave function and energy yields:

$$E = E^{(0)} + \lambda E^{(1)} + \lambda^2 E^{(2)} + \lambda^3 E^{(3)} + \ldots$$

And

$$\psi = \psi_0 + \lambda\psi^{(1)} + \lambda^2\psi^{(2)} + \lambda^3\psi^{(3)} + \ldots$$

Substituting these expansions into the Schrödinger equation and collecting terms according to powers of λ yields

$$H_0\psi_0 = E^{(0)}\psi_0$$

$$H_0\psi^{(1)} + V\psi_0 = E^{(0)}\psi^{(1)} + E^{(1)}\psi_0$$

$$H_0\psi^{(2)} + V\psi^{(1)} = E^{(0)}\psi^{(2)} + E^{(1)}\psi^{(1)} + E^{(2)}\psi_0$$

…

After a number of transformations, the nth-order MP energy is expressed as:

$$E^{(0)} = \langle \psi_0 | H_0 | \psi_0 \rangle$$

$$E^{(1)} = \langle \psi_0 | V | \psi_0 \rangle$$

$$E^{(2)} = \langle \psi_0 | V | \psi^{(1)} \rangle$$

Thus, the HF energy is the sum of zero- and first- order energy

$$E_0 = E^{(0)} + E^{(1)}$$

The correlation energy can then be written as

$$E_{corr} = E_0^{(2)} + E_0^{(3)} + ...$$

There are a number of other techniques to include electron correlation that can potentially provide very accurate results, such calculations can however become very time consuming and at present they tend to be used for small molecules. Such time-consuming methods are used to calculate single-point energy in some small complexes in the present work.

❖ Couple cluster (CC) method takes the basic HF molecular orbital method and constructs multi-electron wave function using the exponential cluster operator to account for electron correlation. The wave function of the coupled-cluster theory is written as an exponential ansatz:

$$|\Psi_{CC}\rangle = e^{\hat{T}} |\Phi_0\rangle \qquad (2.1)$$

Where Φ_0 is the reference wave function which is typically a Slater determinant constructed from HF molecular orbitals, and $\hat{T}$ is cluster operator. The cluster operator is written in the Taylor expansion form:

$$\hat{T} = \hat{T}_1 + \hat{T}_2 + \hat{T}_3 + ... + \hat{T}_N = \sum_p^N \hat{T}_p$$

Where $\hat{T}_1$ is the operator of all single excitations, $\hat{T}_2$ is the operator of all double excitations, and so forth. For the determination of the amplitudes, the wave function (2.1) is inserted in the Schrödinger equation:

$$\hat{H}\ e^{\hat{T}} \left|\Phi_0\right\rangle = E\ e^{\hat{T}} \left|\Phi_0\right\rangle$$

The exponential operator can be written as a Taylor expansion. The correlation energy is obtained by subtraction of the HF energy on both sides of the equation:

$$\underbrace{\left(\hat{H} - \left\langle \Phi_0 \left| \hat{H} \right| \Phi_0 \right\rangle\right)}_{\hat{H}_N}\ e^{\hat{T}} \left|\Phi_0\right\rangle = \underbrace{\left(E - E_{HF}\right)}_{E_{corr}}\ e^{\hat{T}} \left|\Phi_0\right\rangle \qquad (2.2)$$

The $\hat{H}_N$ is introduced the first time and called the normal order Hamiltonian, which consists of the one-electron ($\hat{f}_N$) and two-electron ($\hat{W}_N$) contributions; the E_{coor} is denoted for electron correlation energy. Due to its complexity and the resulting computational effort the coupled-cluster problem is normally not solved in a variational manner. By multiplication from the left of equation (2.2), it is projected onto the reference determinant as well as onto all excited determinants. The couple cluster energy is thus considered as the expectation value of a similarity transformed Hamiltonian.

$$E_{CC} = \left\langle \Phi_0 \left| e^{-\hat{T}} \hat{H}_N e^{\hat{T}} \right| \Phi_0 \right\rangle$$

The classification of traditional coupled-cluster methods rests on the highest number of excitations allowed in the definition of $\hat{T}$. The abbreviations for coupled-cluster methods usually begin with the letters "CC" and follow by:

S – for single excitations (shortened to singles in coupled-cluster terminology),

D – for double excitations (doubles),

T – for triple excitations (triples),

Q – for quadruple excitations (quadruples).

Thus, the $\hat{T}$ operator in CCSDT has the form: $\hat{T} = \hat{T}_1 + \hat{T}_2 + \hat{T}_3$

Terms in round brackets indicate that these terms are calculated based on perturbation theory. For example, the CCSD(T) method means:

- Coupled cluster with a full treatment singles and doubles.
- An estimate to the connected triples contribution is calculated non-iteratively using many-body perturbation theory arguments.

The CCSD(T) method is often called the "gold standard" of computational chemistry, because it is one of the most accurate methods applicable to reasonably large molecules.

❖ Configuration interaction (CI) solves the problem of electron correlation by considering more than a single occupation scheme for the MOs and by mixing the microstates obtained by permuting the electron occupancies over the available MOs. In its simplest form, a CI calculation consists of a preliminary SCF calculation, which gives the MOs that are used unchanged throughout the rest of the calculation. Microstates are then constructed by moving electrons from occupied orbitals to vacant ones according to preset schemes. However, the problem is that if you want to consider every possible arrangement of all the electrons in all the MOs (a full CI), the calculations will become far too large even for moderate-sized molecules with a large basis set. Thus, two types of restriction are usually used: only a limited number of MOs are included in the CI, and only certain types of rearrangement (excitation) of the electrons are used. The most economical form is that in which only one electron is promoted from the ground state to a virtual orbital (single excitations). This is abbreviated as CIS and has traditionally been used for calculating spectra. Adding all double excitations (in which two electrons are promoted) gives CISD, and so on.

To sum up: *ab initio* calculations, in general, give very good qualitative results and can yield increasingly accurate quantitative results as the molecules in question become smaller. The advantage of *ab initio* methods is that they eventually converge to the exact solution once all the approximations are made sufficiently

small in magnitude. In general, the relative accuracy of results is:

HF << MP2 < CISD ≅ MP4 ≅ CCSD < CCSD(T) < CCSDT < FullCI

In *ab initio* calculations, there are four sources of error including the Born-Oppenheimer approximation, the use of an incomplete basis set, incomplete correlation, the omission of relativistic effects.

The disadvantage of *ab initio* methods is that they are computational expensive. These methods often take enormous amounts of computer CPU time, memory, and disk space. The HF method scales as N^4, where N is the number of basis functions. This means that a calculation twice as big takes 16 times as long (2^4) to complete. Correlated calculations often scale much worse than this. In practice, extremely accurate solutions are only obtainable when the molecule contains a dozen electrons or less. However, results with an accuracy rivalling that of many experimental techniques can be obtained for moderate sized organic molecules. The minimally correlated methods, such as MP2, are often used when correlation is important to the description of molecules.

2.1.3. Density functional theory

The initial work on density functional theory (DFT) was reported in two publications: the first is of Hohenberg and Kohn, 1964[81] and the next is of Kohn and Sham, 1965.[82] DFT is an alternative approach to the theory of electronic structure, in which the electron density distribution $p(r)$, rather than the many-electron wave function, plays a central role.

According to DFT theory, the kinetic energy of the non-interacting electron density is calculated and corrected to the real energy in interacting system approximately. The correction to the non-interacting kinetic energy is known as the *exchange correlation (XC) energy* and is calculated as a function of the electron density. As the electron density itself is a function, the XC energy is a function of a function, which is known as a *functional*; hence the name “density functional theory”. Its basic principles are described more fully by Koch and Holthausen (2001).[83]

The advantage of using electron density is that the integrals for Coulomb repulsion need be done only over the electron density, which is a three-dimensional function, thus scaling as N^3. Furthermore, at least some electron correlation can be included in the calculation. This results in faster calculations than HF calculations (which scale as N^4) and computations those are a bit more accurate as well.

The problem is that one does not know the functional(s) that translate the electron density into the XC energy. There are now many alternative functionals available, but there is no way to say that functional A is better than functional B. Thus, the major advantage of ab-initio theory, the ability to improve it systematically, is lost in DFT.

This is of importance in the present work to analyse the intermolecular interaction using NBO and in particular, the 2nd perturbation method to estimate their delocalization energies using ωB97X-D method.

The ωB97X-D results from the re-optimizing of a recently proposed long-range corrected hybrid density functional, with empirical dispersion corrections. Chai *et. al* introduced an empirical dispersion correction to the ωB97X, to provide the missing pieces of the long-range vdW interactions and following Grimme's work, he denoted the new functional as ωB97X-D.[84] The following equation represents the total energy:

$$E_{DFT-D} = E_{KS-DFT} + E_{disp}$$

where ωB97X approximation is used for E_{KS-DFT}.

The performance of ω-D type of functionals was tested by comparing with the results obtained with three well-established DFT-D functionals (B97D, B3LYP-D, and BLYP-D) and with long-range corrected hybrid functionals (ωB97X and ωB97) for atomization energies, equilibrium geometries, reaction energies, non-covalent interaction energies, and a charge transfer excited states.[85] The optimized functional such as ωB97X-D is shown to be significantly superior for non-bonded interactions and very similar in performance for bonded interactions.

2.1.4. Basis set

A basis set is a set of mathematical functions from which a wave function can be constructed. From HF theory, each MO is expressed as a linear combination of basis functions, and the coefficients are determined from the iterative solution of the HF-SCF procedure. The full HF wave function is expressed as a Slater determinant formed from the individual occupied MOs.

Most semi-empirical methods use a predefined basis set. When *ab initio* or DFT calculations are done, a basis set must be specified. Although it is possible to create a basis set from scratch, most calculations are done using existing basis sets. The type of calculation and basis set mainly determine the accuracy of results.

The physically best motivated basis set are Slater type orbitals (STOs), which are solutions to the Schrödinger's equation of hydrogen-like atoms (1 electron). However, hydrogen-like atoms lack many-electron interactions, thus the orbitals do not accurately describe electron state correlations. Calculating integrals with STOs is computationally difficult and it was later realized that STOs could be approximated as linear combinations of Gaussian type orbitals (GTOs). Therefore, the orbitals used in *ab initio* calculations usually have the forms of GTOs: $\varphi = Y_{ml} \sum_i C_i \sum_{ij} C_{ij} e^{-\varsigma_{ij} r^2}$. Fig. 2.2 shows the difference of GTO and STO in describing the atomic orbitals.

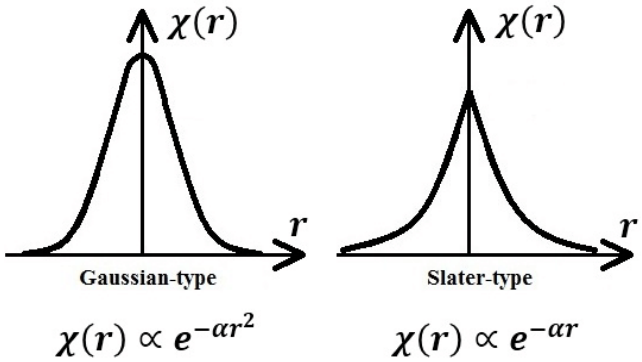

Figure 2.2. Plots of GTO and STO basis functions

The smallest basis sets are called *minimal basis sets*. A minimal basis set is one in which, on each atom in the molecule, a single basis function is used for each

orbital in a HF calculation on the free atom. In the next level, additional functions are added to describe polarization of the electron density of the atom in molecules. These are called *polarization functions*. For example, while the minimal basis set for hydrogen is one function approximating the 1s atomic orbital, a simple polarized basis set typically has two *s*- and one *p*-function (which consists of three basis functions: *px*, *py* and *pz*). This adds flexibility to the basis set, effectively allowing molecular orbitals involving the hydrogen atom to be more asymmetric about the hydrogen nucleus. This is very important for modelling chemical bonding, because the bonds are often polarized. Similarly, *d*-type functions can be added to a basis set with valence p orbitals, and *f*-functions to a basis set with d-type orbitals, and so on.

Another common addition to basis sets is the addition of *diffuse functions*. These are extended Gaussian basis functions with a small exponent, which give flexibility to the "tail" portion of the atomic orbitals, far away from the nucleus. Diffuse basis functions are important for describing anions or dipole moments, but they can also be important for accurate modelling of intra- and intermolecular bonding.

Pople basis set

The Pople basis set notation is X-YZG*, where X is the number of Gaussian primitives used for each inner-shell orbitals. The hyphen indicates a split-basis set where the valence orbitals are double zeta. The Y indicates the number of primitives that form the large zeta function (for the inner valence region), and Z indicates the number that form the small zeta function (for the outer valence region). G identifies the set a being Gaussian. A single asterisk means that a set of *d*-primitives has been added to atoms other than hydrogen. A double asterisk means that a single set of Gaussian 2p functions is included for each hydrogen atom.

List of commonly used split-valence basis sets of this type including 3-21G, 3-21G*, 3-21G**, 3-21+G, 3-21++G, 6-31+G*, 6-311G, 6-311G*, 6-311+G*, 6-311++G**…

Correlation-consistent (Dunning) basis set

A series of basis sets for correlated calculations has also been developed by Dunning *et al*.[86] These basis sets are designed such that a base set of *sp* functions is combined with correlation functions. The correlation-consistent basis set are written as (aug-)cc-pVXZ, where X =D, T, Q, 5, 6, … (D=double, T=triples, etc.). The 'cc-p', stands for 'correlation-consistent polarized' and the 'V' indicates they are valence-only basis sets, ‘aug’ is augmented versions of the preceding basis sets with added diffuse functions. These basis set include successively larger shells of polarization (correlating) functions (*d, f, g,* etc.). For the first and second-row atoms, the basis set are cc-pVXZ. For larger atoms, additional functions have turned out to be necessary; these are the cc-pV(X+d)Z basis sets. Even larger atoms may employ pseudopotential basis sets, cc-pVXZ-PP, or relativistic-contracted Douglas-Kroll basis sets, cc-pVXZ-DK.

The smallest member of this series and thus often the starting point for correlated calculations is the correlation consistent polarized double zeta basis set designated "cc-pVDZ".

2.2. Computational approaches to noncovalent interactions

2.2.1. Interaction energy

The interaction energy (E_{int}) of each investigated complex is determined by using the supermolecular approach as the difference in total energy between the complex and the sum of energies of the relevant monomers at the selected suitable level of theory.

$$E_{int} = E_{complex} - (E_{monomer\ 1} + E_{monomer\ 2} + \ldots)$$

The more negative interaction energy indicates the more stable complex formed, and *vice versa*. The supermolecular approach has an important disadvantage in that the final interaction energy is usually much smaller than the total energies from which it is calculated, and therefore contains a much larger relative uncertainty. In the case where energies are derived from quantum chemical calculations using finite atom-centered basis functions, basis set superposition

errors can also contribute some degree of artificial stabilization. The detail of basis set superposition errors is presented in later section.

2.2.2. Cooperativive energy

It is becoming increasingly apparent that cooperative interaction involving several molecules is an important component of intermolecular interactions. The cooperativity of hydrogen bond turns out to play a key role in controlling and regulating the processes occurring in living organisms. The importance of cooperativity in noncovalent interactions was reported in many works.[78,87,88,89]

To evaluate the cooperative effect existed in the ternary complexes, cooperativity energies are calculated as the difference between the complexation energy of the ternary system and sum of the complexation energy of its constituent binary systems. The positive cooperativity implies that the sum of at least two interactions is larger than the simple addition of the individual interactions. The equation[90]

$$E_{coop}=E_{int} - \sum\Delta E^2$$

where E_{int} term corresponds to the interaction energy of the considered complexes and ΔE^2 is energy of corresponding pairwise interactions.

Negative value of cooperative energy indicates that noncovalent interactions work cooperatively, strengthen each other and make the complex stronger, while a positive value indicates that these interactions work anti-cooperatively.

2.2.3. Basis set superposition error

In all systems treated in this work, molecules get closer and approach each other to form complexes by intermolecular interactions. This means the basis sets allocated to each of them are going to overlap. This overlapping gives electrons greater freedom to localize and can result in a reduction of the total electronic energy. This reduction in energy would not have occurred if the basis sets had been infinitely large. This energy reduction is therefore an artifact of working with limited basis sets. This problem is called the basis set superposition error (BSSE).

The interaction energy is calculated as followed

$$E_{\text{int}}(r_{AB}) = E_{AB}^{AB}(r_{AB}) - E_A^A - E_B^B \qquad (2.3)$$

where, at the right hand side of the equation, the subscript denotes the geometry of the system and the superscript the used basis sets. E_{int} denotes the interaction energy of the system. The energy of the separate atoms does not depend on the interatomic distance, while the basis set superposition error varies with the interatomic distance. The interaction energy in Eq. (2.3) is in need for a correction on the BSSE.

Boys and Bernardi introduced the counterpoise correction to correct for the BSSE.[91] In the counterpoise correction, the artificial stabilization is countered by letting the separate atoms improve their basis sets by borrowing functions of an empty basis set. To realize such an empty basis set, a ghost atom is used. The ghost atom has the basis set of the according atom, but no electrons to fill it. Performing this procedure for both atoms on the grid will correct for the BSSE. Hence, the interaction energy with counterpoise correction

$$E_{\text{int}}^{\text{CP}}(r_{AB}) = E_{AB}^{AB}(r_{AB}) - E_A^{AB}(r_{AB}) - E_B^{AB}(r_{AB}) \qquad (2.4)$$

Note that in Eq. 2.4 the energy of the separate atoms depends on a distance – the distance between the atom and the ghost atom.

2.2.5. Natural bond orbital theory

Natural bond orbital (NBO) methodology is intrinsically based on the quantum wave function ψ and its practical evaluation (to sufficient chemical accuracy) using modern computational technique. Unlike the conventional valence bond (VB) or molecular orbital (MO) viewpoints, NBO theory makes no assumption about the mathematical form of ψ. Instead, the NBO bonding picture is derived from variational, perturbative or DFT approximations of arbitrary form (based on chance) and accuracy, up to and including the exact ψ.

The concept of *natural* orbital was first introduced by Per-Olov Löwdin in 1955 to describe the unique set of orthonormal 1-electron functions.[92]

The NBOs are one of a sequence of natural localized orbital sets that include natural atomic (NAO), hybrid (NHO), and (semi-)localized molecular orbital (NLMO) sets, intermediate between basis AOs and canonical molecular orbitals

(MOs)

Input basis (NOs) → NAOs → NHOs → NBOs → NLMOs → MOs

❖ *Input basis (NOs)*

The input NOs are required to be orthonormal set by using the occupancy-weighted symmetric orthogonalization procedure. As originally introduced in Löwdin, the natural (spin) orbitals $\{\theta_i\}$ are the *eigen*-orbitals of one-electron density operator (γ_1) satisfying $\gamma_1\theta_i = n_i\theta_i$

Where n_i represents the population of the *eigen*-function θ_i for the one-electron density operator.

❖ *Natural atomic orbital (NAOs)*

NAOs $\{\theta_i^A\}$ are localized 1-center orbitals that can be described as the effective "natural orbitals of atom A" in the molecular environment. The NAOs incorporate two important physical effects that distinguish them from isolated-atom natural orbitals as well as from standard basis orbitals:

(i) The spatial diffuseness of NAOs is optimized for the *effective atomic charge* in the molecular environment (i.e., more contracted if A is somewhat cationic; more diffuse if A is somewhat anionic).

(ii) The outer fringes of NAOs incorporate the important nodal features due to *steric (Pauli) confinement* in the molecular environment (i.e., increasing oscillatory features and higher kinetic energy as neighboring NAOs begin to interpenetrate, preserving the interatomic orthogonality required by the Pauli exclusion principle).

❖ *Natural hybrid orbitals (NHOs)*

The natural hybrids are composed from a set of effective valence-shell atomic orbital (NAOs) $h_A = \sum_k a_k \theta_k^A$

❖ *Natural bond orbitals (NBOs)*

Natural Bond Orbitals (NBOs) are localized few-center orbitals ("few" meaning typically 1 or 2, but occasionally more) that describe the Lewis-like

molecular bonding pattern of electron pairs (or of individual electrons in the open-shell case) in optimally compact form. More precisely, NBOs are an orthonormal set of localized "maximum occupancy" orbitals whose leading $N/2$ members (or N members in the open-shell case) give the most accurate possible Lewis-like description of the total N-electron density.

The NBOs is formed directly from orthonormal NHOs $\{h_A\}$

$$\sigma_{AB} = c_A h_A + c_B h_B$$

However, the general transformation to NBOs also leads to orbitals that are unoccupied in the formal Lewis structure and that may be used to describe noncovalency effects. The most important of these are the antibonds σ^*_{AB}

$$\sigma^*_{AB} = c_B h_A - c_A h_B$$

❖ *Natural localized molecular orbitals (NLMOs)*

NLMOs $\{\omega_i\}$ can be described as *semi*-localized alternatives to the ordinary ("canonical") CMOs for representing the electron pairs of MO-type wave functions. Each NLMO ω_i closely resembles a "parent" NBO Ω_i (strictly localized) but captures the associated delocalizations needed to describe the density of a full electron pair, thereby becoming a valid (non-canonical) solution of the HF (or DFT-type) SCF equations. Compared to CMOs, the NLMOs are free from the superfluous constraints of overall symmetry adaptation. NLMOs therefore adopt the characteristic bonding pattern of a localized Lewis structure, averting the symmetry-imposed mixings (even between remote groups, beyond empirical van der Waals separation) that limit transferability and interpretability of CMOs.

❖ *Molecular orbitals (MOs) in NBO approach*

Types of orbitals in NBO analysis are given in Table 2.1.

Table 2.1**.** Characteristics of the common NBO types

NBO Type	centers	shell	L/NL	label
core c_A	1-c	core	L	CR
nonbonded (lone pair) n_A	1-c	valence	L	LP
bond Ω_{AB}	2-c	valence	L	BD
antibond Ω^*_{AB}	2-c	valence	NL	BD*
Rydberg r_A	1-c	Rydberg	NL	RY

Second-order perturbation theory

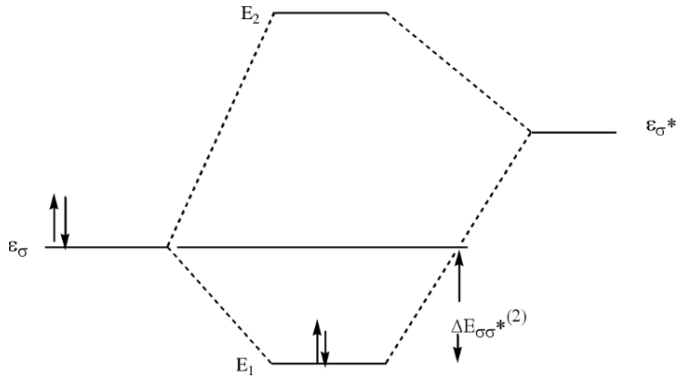

Figure 2.3. Perturbative donor-acceptor interaction, involving a filled orbital σ and an unfilled orbital σ*

The second-order perturbation energy is expressed by the following equation:

$$E_{ij}^{(2)} = -q_i \frac{\left\langle \varphi_i^{(0)} \middle| H \middle| \varphi_j^{(0)} \right\rangle^2}{\varepsilon_j^{(0)} - \varepsilon_i^{(0)}}$$

In this study, the NBO theory along with NBO 5.G program[93] was employed to quantitatively evaluate the charge transfer interactions between individual orbitals and the unit charges.[94]

2.2.4. Atoms in molecules theory

All properties of matter become apparent in the charge distribution, its topology that delineates atoms and the bonding between them. It is possible to define the structure of molecules quantum mechanically with the help of Bader's Quantum Theory of Atoms in Molecules (QTAIM).[95,96,97]

The AIM theory rests on analysing the variation from place to place in a molecule of the electron density function (electron probability function, charge density function, charge density), ρ.

$$\rho(x, y, z)dxdydz = \rho(x, y, z)dv$$

It is the probability of finding an electron in the infinitesimal volume dv centered on the point (x, y, z). This probability is the same as the charge in dv if we take the charge on an electron as unit of charge, hence the electron density function is also considered as the charge density.

Since nuclei of the atoms are the only source of positive charge, the electron

density has its maxima at or near the nuclei (attractors of electrons). The change in density between two attractors (*i.e.* two atoms) is described in terms of a gradient vector.

$$\nabla\rho = i\frac{\partial\rho}{\partial x} + j\frac{\partial\rho}{\partial y} + k\frac{\partial\rho}{\partial z}$$

Using the topology of electron density, QTAIM divides molecular space into atomic subspaces. Starting from a given point in space, one may move in infinitesimal steps along the direction of the gradient until an attractor is encountered. The part of space from which all gradient paths end up at the same nuclei is called the basin of atom (Figure 2.4). The border between two atomic basins identifying atoms in molecules is called zero flux surface. Once the molecular volume is divided up, the electron density is integrated within each of the atomic basins and the atomic charges, dipoles, and multipoles can be determined.

The zero flux surface in the gradient vector field of electron density is not crossed by any of the gradient vector $\nabla\rho(r)$ at any point.

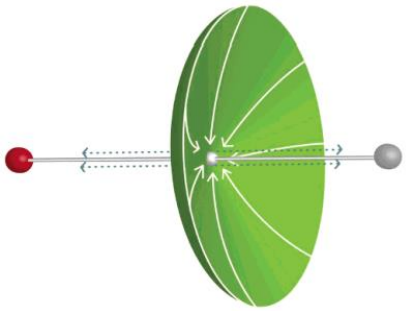

Figure 2.4. The separation between two atomic basins in HF molecule.

The points at which the density gradient ($\nabla\rho(r)$) has a zero value are called critical points (CPs). In QTAIM, the existence of CP defines whether a bond between two atoms exist or not. In detail,

$\nabla\rho(r) = 0$ at critical points and at ∞,

$\nabla\rho(r) \neq 0$ at all other points.

For the existence of CP, it does not bring any information about the nature of bonds. In order to define its nature, the analyses of the second derivatives of electron density ($\nabla^2\rho(r)$) are required. In three-dimensional space, there are nine

second derivatives which are arranged in a square matrix form, called Hessian matrix or simply Hessian.

$$\begin{pmatrix} \frac{\partial^2\rho(r)}{\partial x^2} & \frac{\partial^2\rho(r)}{\partial x\partial y} & \frac{\partial^2\rho(r)}{\partial x\partial z} \\ \frac{\partial^2\rho(r)}{\partial y\partial x} & \frac{\partial^2\rho(r)}{\partial y^2} & \frac{\partial^2\rho(r)}{\partial y\partial z} \\ \frac{\partial^2\rho(r)}{\partial z\partial x} & \frac{\partial^2\rho(r)}{\partial z\partial y} & \frac{\partial^2\rho(r)}{\partial z^2} \end{pmatrix}$$

The Hessian is real symmetric matrix, thus it can be diagonalized to be a diagonalized one. If λ_1, λ_2 and λ_3 are the eigenvalues of the Hessian matrix which represent curvature of the density with respect to the three principal axes *x'*, *y'*, *z'*, the Laplacian of the density is: $\nabla^2\rho(r) = \lambda_1 + \lambda_2 + \lambda_3$

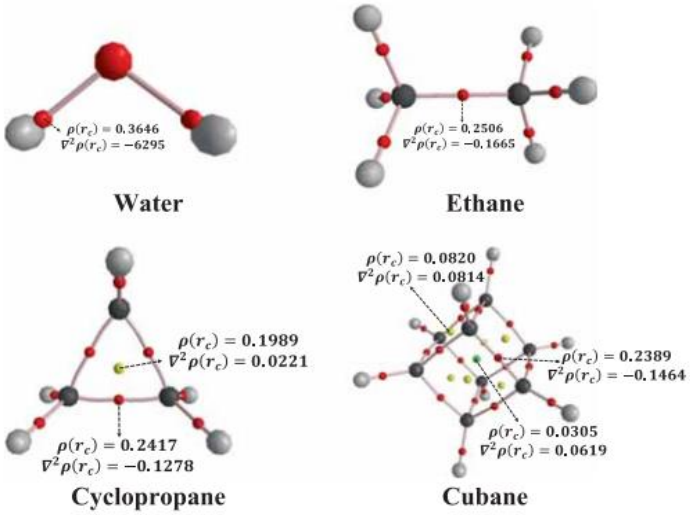

Figure 2.5. Molecular graph of H_2O, ethane, cyclopropane and cubane at MP2/6-311++G(d,p). (The red balls between bond are the bond critical points)

Mathematically, if $\nabla^2\rho(r) \geq 0$, the CP is a minimum and inversely, if $\nabla^2\rho(r) \leq 0$, the CP is a maximum. Thus, a positive value of Laplacian represents a local charge depletion and a negative value of Laplacian means local charge concentration. At BCP ($\nabla\rho(r)$=0), the sign of $\nabla^2\rho(r)$ provides information for nature of the bond. Specially, the negative value implies a covalent bond, while a positive one indicates an ionic bond or a van der Waals interactions.

The rank (ω), and signature (σ) are used to classified different types of CPs, which are symbolized as (ω,σ). Rank is the rank of Hessian matrix of $\nabla^2\rho(r)$ and is calculated by the number nonzero curvatures (λ). Signature is the algebraic sum of

the signs of curvatures. Where

Nucleus critical point (NCP): (3,-3)

Ring critical point (RCP): (3,+1)

Cage critical point (CCP): (3,3)

Bond critical point (BCP): (3,-1)

It is evident from literature that there are other important relationships between energetic topological parameters and the $\nabla^2\rho(r)$ at CPs. One of the important relationships is the local form of virial theorem:

$$\frac{1}{4}\nabla^2\rho(r) = 2G(r) + V(r)$$

$$\mathrm{H}(r) = G(r) + V(r)$$

To be more specific, the positive values of Laplacian ($\nabla^2\rho(r)$) and electron energy density ($H(r)$) imply that the kinetic electron energy density ($G(r)$) is greater than the potential electron energy density ($V(r)$) and hence such interactions are characterized as closed shell or noncovalent in nature. If $|V(r)|$ is one time more than the $G(r)$ then $\nabla^2\rho(r)$ is positive and $H(r)$ is negative. In this situation, the interaction is classified as partly covalent in nature.

2.2.6. Noncovalent index

NCIplot is an effective tool to detect noncovalent interactions in the real space based on electron density and reduced gradient density ($s(\rho(r))$).[98,99] The reduced density gradient is as follow:

$$s(\rho(r)) = \frac{1}{2(3\pi^2)^{1/3}} \frac{|\nabla\rho(r)|}{\rho(r)^{4/3}}$$

When a weak inter- or intramolecular interaction is present, there is a crucial change in the reduced gradient between the interacting atoms, producing density critical points between interacting fragments. Troughs appear in $s(\rho(r))$ associated with each critical point. The combination of s and ρ allows a rough partition of real space into bonding regions: high-s low-r corresponds to non-interacting density tails, low-s high-r to covalent bonds, and low-s low-r to noncovalent interactions.

To assign the origins of the troughs, further analysis of the electron density in these troughs is required. The electron density values within the troughs are an indicator of the interaction strength. However, both attractive and repulsive interactions appear in the same region of density and reduced gradient space. To distinguish them, the second derivatives of electron density are examined.

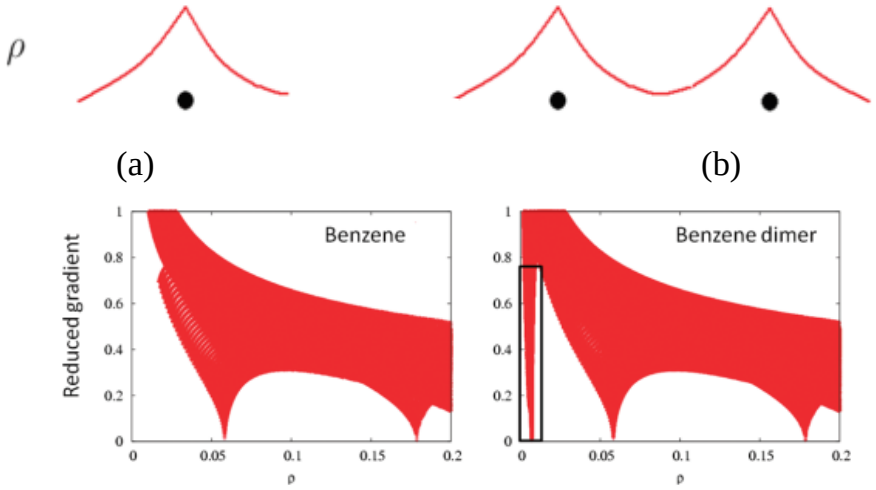

Figure 2.6. (ref. 99)

a) Representative behaviour of atomic density

b) Appearance of a $s(\rho(r))$ singularity when two atomic densities approach each other.

(c-d) Comparision of the reduced density behaviour for the benzen monomer and dimer

On the basis of the divergence theorem, the sign of the Laplacian of the electron density indicates whether the net gradient flux of electron density is entering ($\nabla^2\rho(r) < 0$) or leaving ($\nabla^2\rho(r) > 0$) an infinitesimal volume around a reference point. Therefore, the sign of $\nabla^2\rho(r)$ distinguishes the concentration and depletion of density at that point, relative to the surroundings.

The second ingredient of the NCI index is the classification of interactions as attractive or repulsive according to the sign of λ_2. This distinguishes bonding interactions, where the electron density is locally accumulated with respect to the plane perpendicular to the bond path ($\lambda_2 < 0$) from the non-bonding interactions or steric clashes ($\lambda_2 > 0$).

The value of sign(λ_2)$\rho(r)$ is used as an effective indicator to distinguish the interactions: sign(λ_2)$\rho(r)$ > 0 indicating a repulsive interaction (non-bonding) and sign(λ_2)$\rho(r)$ < 0 meaning an attractive interaction (bonding), and a value close to zero implying a very weak, van der Waals interaction.

2.2.7. Symmetry-adapted perturbation theory

Symmetry-adapted perturbation theory (SAPT) provides a means of directly computing the noncovalent interaction between two molecules, that is, the interaction energy is determined without computing the total energy of the monomers or dimer. In addition, SAPT provides a decomposition of the interaction energy into physically meaningful components, including electrostatic, exchange, induction, and dispersion terms.

The fundamental ideas of SAPT starts from unperturbed molecules (isolated monomers) and treats the interaction energy and wave function as small quantities resulting from the mutual perturbation of monomers by the Coulombic intermonomer interactions.[100]

First, the Schrödinger equation for isolated monomers A and B is solved:

$$H_X \psi_X = E_X \psi_X \text{ , } X = A \text{ or } B,$$

Where H_X, ψ_X and E_X are, respectively, the Hamiltonian, wave function, and energy of monomer *X*.

In the next step, these monomers are placed in the dimer configuration. The interactions between all electrons and nuclei in A and B are obeyed Coulomb's law. The sum of such Coulomb interaction terms is the intermolecular interaction operator denoted by V. The interaction energy is calculated by partitioning the total Hamiltonian into a term for each fragment and an inter-fragment interaction potential V. Then the Hamiltonian of dimer is:

$$H = H_A + H_B + V = H_0 + V$$

The solution of unperturbed system with the Hamiltonian H_0 is thus the product of the solution of a system contained two isolated monomers:

$$\psi^{(0)} = \psi_A \psi_B \text{ and } E^{(0)} = E_A + E_B$$

The effects of V can be accounted for using the standard Rayleigh-Schrödinger perturbation theory. The interaction energy is expressed as a sum of perturbation corrections.

$$E_{int} = E_{RS}^{(1)} + E_{RS}^{(2)} + ...$$

This conceptually simplest approach has several drawbacks, and the most important of them is that it does not predict the existence of van der Waals minima on PES. To solve this problem, a Pauli-correct wave function $A\Psi^{(0)}$ is introduced, where operator *A* is so-called anti-symmetrizer.

For unperturbed orbitals *a* and *b*:

$$A[a(1)b(2)] = a(1)b(2)-a(2)b(1)$$

Since $A\Psi^{(0)}$is not an eigenfunction of H_0, the Rayleigh-Schrödinger perturbation theory cannot be used anymore, so the symmetry-adapted perturbation theories are constructed to be able to use such an unperturbed function. There are many different versions of SAPT.

Many-body perturbation expansions for the interaction energy components:

- *Electrostatic energy (E_{elst})*

The first-order polarization energy represents the energy of the electrostatic (Coulombic) interaction of the monomers' charge distributions. For this reason, it is referred as the *electrostatic energy*.

$$E_{pol}^{(1)} = \langle \Psi_A \Psi_B | V \Psi_A \Psi_B \rangle$$

- *Induction energy (E_{ind})*

The induction energy is obtained when the sum-over-states is restricted to "singly excited" (in the molecular sense) eigenfunctions of H_0:

$$E_{ind}^{(2)} = E_{ind}^{(2)}(A) + E_{ind}^{(2)}(B)$$

Where

$$E_{ind}^{(2)}(A) = -\langle \Psi_A | \Omega_B \hat{R}_0^A \Omega_B | \Psi_A \rangle$$

And similarity for $E_{ind}^{(2)}(B)$. Ω_B denotes the operator of the electrostatic potential generated by the unperturbed monomer B. Specifically, the third-order induction energy $E_{ind}^{(3)}$ represents that part of $E_{pol}^{(3)}$ which can be obtained when the intermonomer electron correlation is completely neglected.

- *Dispersion energy (E_{disp})*

The second-order dispersion energy $E_{disp}^{(2)}$, is defined as the difference between the second-order polarization and induction energies:

$$E_{disp}^{(2)} = E_{pol}^{(2)} - E_{ind}^{(2)}$$
$$= -\left\langle \Psi_0 \middle| V\hat{R}_0^{AB}V \middle| \Psi_0 \right\rangle$$

In the third order of polarization theory, the intermolecular correlation contribution $E_{pol}^{(3)} - E_{ind}^{(3)}$ separates into two parts: the induction-dispersion energy $E_{ind-disp}^{(3)}$ and the third-order dispersion energy $E_{disp}^{(3)}$.

- *Exchange energy (E_{exch})*

All exchange terms in SAPT arise from the antisymmetrization of the wave functions of monomers A and B. Taking into account exchange of all possible electron pairs between the two monomers yields to complicated formulae. For this reason, exchange terms are often evaluated in the orbital overlap approximation, that can be interpreted as the exchange of a single electron pair between monomers.

$$E_{exch} = E_{exch}^{(10)} + E_{exch}^{(11)} + E_{exch}^{(12)}$$

2.3. Noncovalent interactions

Noncovalent interactions have a constitutive role in the science of intermolecular relationships. In nature, these interactions are the foundation of the life process itself, the ultimate function articulation, both mechanical and cognitive. In synthetic chemistry, interactions between rationally designed molecular subunits drive the assembly of nanoscopic aggregates with targeted functions.

Complexes containing noncovalent interactions are identified and characterized in isolation in the gas phase by rotational and vibrational

spectroscopy. The properties of these isolated complexes such as strength, geometry, *etc* are confirmed by the *ab initio* calculations.

2.3.1. Tetrel bond

The term tetrel bond (TtB) was coined recently to describe the noncovalent interactions involving group IV. The atoms of group IV act as the electrophilic site which seek for the nucleophile one of another molecule.[67] The carbon atom of CO_2 is an electrophilic center, forming tetrel bond with another component containing free electron pairs or π-electron of a Lewis base.

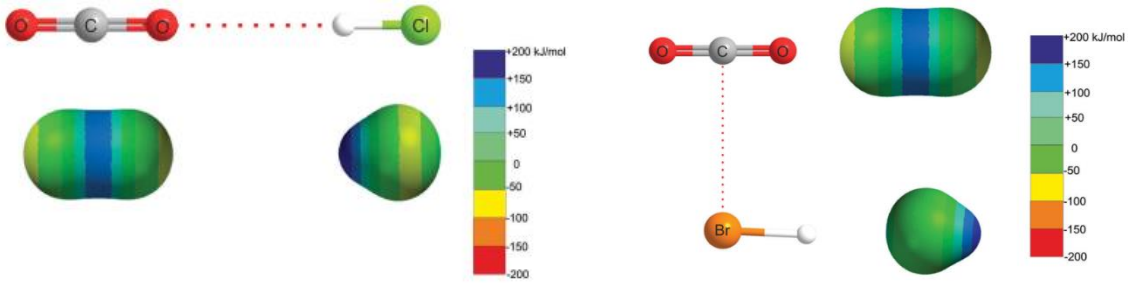

Complex of CO_2 with HCl Complexes of CO_2 with HBr

Figure 2.7. Difference in geometry of complexes CO_2-HCl and CO_2-HBr obtained from experimental spectroscopy

The term tetrel bond was first suggested by Frontera and co-workers recently in 2013.[101] Nevertheless, the first complex involving TtB was investigated in 1992 by Wittig and co-workers. It is the complexes of CO_2 and HBr, which is dramatically different from complexes of CO_2 with HF and HCl (Figure 2.7).[102] The O atoms of CO_2 is also a nucleophile region to interact with electron-deficient site of partner molecules. Indeed, the interactions of CO_2 with HF and HCl result in a linear configuration by $O_{CO2}\cdots H{-}F/Cl$ hydrogen bond.[103,104] However, going to HBr, the geometrical structure is stabilized by interactions of $C_{CO2}\cdots Br$ tetrel and $O\cdots H$ hydrogen bonds, as a ring.

The tetrel bond begins with the electronegative nonmetal C, then moves to semimetals Si and Ge, after which it includes the Sn and Pb metals. All of these atoms have been shown to be capable of engaging in a TtB, similar to other types including hydrogen bond, halogen bond, chalcogen bond, … Until now, the IUPAC

has not recommended the definition of tetrel bond. If the definition of tetrel bond parallels that of chalcogen bond, that is

A tetrel bond occurs when there is evidence of a net attractive interaction between an electrophilic region associated with a tetrel atom in a molecular entity and a nucleophilic region (e.g. a n-pair or p-pair of electrons) in another, or the same, molecular entity.

The tetrel bond stabilizing complexes formed involving CO_2 was concluded as the noncovalent bond.[67] Tetrel bonds are also reported to be comparable strength to hydrogen bonds and other σ-hole-based interactions, they are highly directional, and might serve as a new possible molecular linker.[101] The importance of TtBs in biology, particularly those involving C, was emphasized by a survey of protein structures[105] which placed emphasis on the CF_3 parallel of the methyl group. The authors stressed the importance of these bonds in such systems as the $NADP^+$-dependent isocitrate dehydrogenase enzyme and its interaction with an aspartate residue, as well as a triazine-based inhibitor of enasidenib. Calculations showed strong TBs between the CF_3 group and a variety of bases. Later surveys extended these TBs to the unsubstituted methyl group.

2.3.2. Hydrogen bond

Hydrogen bond (HB) is probably the most studied and analysed among noncovalent interactions. Its importance has been more comprehensively recognized when the presence of HBs involving C−H···O/N had been discovered in proteins, DNA double helix, RNA… It is operative in determining molecular conformation, molecular aggregation, and the function of a vast number of chemical systems ranging from inorganic to biological. In terms of modern concepts, the HB is understood as a very broad phenomenon, and it is accepted that there are open borders to other effects. Dissociation energies span more than two orders of magnitude (about 0.2 – 40 $kcal.mol^{-1}$). Within this range, the nature of the interaction is not constant, but it's electrostatic, covalent, and dispersion contributions vary in their relative weights. The HB has broad transition regions

that merge continuously with the covalent bond, the van der Waals interaction, the ionic interaction, and the cation-π interaction.

Definition of hydrogen bond according to IUPAC[106]

The hydrogen bond is an attractive interaction between a hydrogen atom from a molecule or a molecular fragment X–H in which X is more electronegative than H, and an atom or a group of atoms in the same or a different molecule, in which there is evidence of bond formation.

List of criteria for a hydrogen bond X–H···Y–Z:

- The forces involved in the formation of a hydrogen bond include those of an electrostatic origin, those arising from charge transfer between the donor and acceptor leading to partial covalent bond formation between H and Y, and those originating from dispersion.
- The atoms X and H are covalently bonded to one another and the X–H bond is polarized, the HY bond strength increasing with the increase in electronegativity of X.
- The X–HY angle is usually linear (180º) and the closer the angle is to 180º, the stronger is the hydrogen bond and the shorter is the HY distance.
- The length of the X–H bond usually increases on hydrogen bond formation leading to a red shift in the infrared X–H stretching frequency and an increase in the infrared absorption cross-section for the X–H stretching vibration.
- The greater the lengthening of the X–H bond in X–HY, the stronger is the HY bond.
- The X–H···Y–Z hydrogen bond leads to characteristic NMR signatures that typically include pronounced proton deshielding for H in X–H, through hydrogen bond spin–spin couplings between X and Y, and nuclear Overhauser enhancements.
- The Gibbs energy of formation for the hydrogen bond should be greater than the thermal energy of the system for the hydrogen bond to be detected experimentally.

Hydrogen bonds exist with a continuum of strengths. Nevertheless, it can be useful for practical reasons to introduce a classification, such as “weak”, “strong”, and possibly also “in between”. Following the system described by Jeffrey (1997),[107] HBs are called moderate if they resemble those between water molecules or in carbohydrates (one could also call them “normal”) and are associated with energies in the range 4-15 kcal.mol^{-1}. HBs with energies above and below this range are termed strong and weak, respectively.

A conventional hydrogen bond A−H···B or red-shifting hydrogen bond (RSHB) is accompanied by an elongation of A−H bond together with a decrease of its stretching vibrational frequency. Its origin is well-understood, that is an electrostatic interaction between H and B. However, in some systems, a hydrogen bond occurs to have opposite characteristics with RSHB including a shortening of A−H bond, increasing in its stretching vibrational frequency, so-called blue-shifting hydrogen bond (BSHB). BSHB has often been revealed in systems where a hydrogen atom bonded to a carbon atom forms a HB with either an electronegative atom or a region with an excess of electron density. BSHB has often been observed in systems where a hydrogen atom bonded to a carbon atom forms a hydrogen bond with either an electronegative atom or a region with an excess of electron density. A number of hypotheses and models have been proposed to explain the origin of both HB types.[108,109,110,111,112].

2.3.3. Halogen bond

The interest of halogen bond has surged because of the fact that this bond exists biological materials, like proteins, nucleic acid, and interactions of drug with biological objects.[113] Furthermore, X-bonds are found to be essential architectural elements in supramolecular systems, liquid crystal engineering, nanomaterial design and nanowire formation, and so on and so forth.[114,115] The widely range application of halogen bond leads to a great attention of both experimental and theoretical scientists. Definition of halogen bond according to IUPAC[116]

A halogen bond occurs when there is evidence of a net attractive interaction between an electrophilic region associated with a halogen atom in a molecular entity and a nucleophilic region in another, or the same, molecular entity.

A typical halogen bond is denoted by the three dots in R–X···Y. R–X is the halogen bond donor, X is any halogen atom with an electrophilic (electron-poor) region, and R is a group covalently bound to X. In some cases, X may be covalently bound to more than one group. Y is the halogen bond acceptor and is typically a molecular entity possessing at least one nucleophilic (electron-rich) region. Some common halogen bond donors and acceptors are itemized below. Some features that are useful as indications for the halogen bond, not necessarily exhaustive, are listed below. The greater the number of features satisfied, the more reliable the characterization of an interaction as a halogen bond is.

In a typical halogen-bonded complex R–X···Y:

• The interatomic distance between X and the appropriate nucleophilic atom of Y tends to be less than the sum of the van der Waals radii.

• The length of the R–X covalent bond usually increases relative to the unbonded R–X.

• The angle R–X···Y tends to be close to 180°.

• The halogen bond strength decreases as the electronegativity of X increases, and the electron-withdrawing ability of R decreases.

• The forces involved in the formation of the halogen bond are primarily electrostatic, but polarization, charge transfer, and dispersion contributions all play an important role.

• The analysis of the electron density topology usually shows a bond path (a “bond path” and a “bond critical point”.

• The infrared absorption and Raman scattering observables of both R–X and Y are affected by halogen bond formation; new vibrational modes associated with the formation of the X···Y bond are also observed.

• The UV–vis absorption bands of the halogen bond donor usually shift to shorter

wavelengths.

• The X···Y halogen bond usually affects the nuclear magnetic resonance observables of nuclei in both R–X and Y, both in solution and in the solid state.

• The binding energies of the peaks associated with X with the X-ray photoelectron spectrum of the complex shift to lower energies relative to unbonded X.

2.3.4. Chalcogen bond

The chalcogen bond has a venerable history. It appears to have been used for the first time in 1998 in a theory paper by Minyaev and Minkin who predicted O→chalcogen and N→chalcogen bonds in complexes such as $H_2CO \rightarrow SH_2$ of strength comparable to that of a strong HB.[117] Certainly by 2011 the term chalcogen bond was in common usage. An investigation of the Protein Data Bank revealed that S···O interactions are common in proteins, and they can play important roles in their functions, stability, and folding.[118] For instance, S···O and Se···O interactions were demonstrated that they stabilize the final molecular conformations of some thiazole and selenazole nucleosides possessing antitumor activity, and affect their biological activity and their binding to a target enzyme.[119]

Following the IUPAC Recommendation 2019,[120] the definition of chalcogen bond is written as:

Chalcogen bond (ChB) is the net attractive interaction between an electrophilic region associated with a chalcogen atom in a molecular entity and a nucleophilic region in another, or the same, molecular entity.

A typical chalcogen bond is denoted by the three dots in R–Ch···A, where Ch is the ChB donor, being any chalcogen atom (possibly hypervalent) having an electrophilic (electron-poor) region, R is the remainder of the molecular entity R–Ch containing the ChB donor, and A is the ChB acceptor and is typically a molecular entity possessing at least one nucleophilic (electron-rich) region. Chalcogen atoms can concurrently form one or more than one chalcogen bond. Chalcogen atoms of a molecular entity give rise to a variety of interactions with different electronic and geometric features. The term chalcogen bond must not be

used for interactions where the chalcogen (frequently oxygen) functions as a nucleophile.

2.4. Computational methods of the research

To achieve the objectives along with research contents specified above, we are going to use the quantum chemical methods available in the packages GAUSSIAN 09, AIM2000, NBO5.G, SAPT2012.2, Psi4, NCIplot … Suitable quantum-chemical methods including the molecular orbital theory (MO) and DFT methods with high basis sets will be utilized, depending on investigated systems. Besides, the software such as Molden, Gaussview, Origin and Excel will be employed to support for analysing calculated results. Research methodology and techniques appropriate for each issue are described in more detail as follows:

Calculating for geometry optimization, energy and infrared spectra will be carry out by using the Gaussian 09 suite of programs. Geometries and harmonic vibrational frequencies of the monomers and complexes are obtained by MP2 in combination with high basis sets 6-311++G(2d,2p). Harmonic vibrational frequencies are subsequently calculated to ensure that the optimized structures are local minima on the potential energy surfaces, to estimate zero-point energy and to identify red-shift and blue-shift of the formed HBs. The depth of the potential energy for the small complexes and isolated monomers is further examined by performing single point calculations at CCSD(T)/6-311++G(2d,2p) for small complexes to obtain more accurate energy while MP2/aug-cc-pVTZ is used in cases of larger complexes. In detail,

- Systems using MP2/aug-cc-pVTZ for single-point energy calculations:
  - Complexes of dimethyl sulfoxide with nCO_2 and nH_2O (n=1-2)
  - Complexes of acetone/thioacetone with nCO_2 and nH_2O (n=1-2)
  - Complexes of CH_3OCHX_2 with nCO_2 and/or nH_2O (n=1-2)
  - Complexes of dimethyl sulfide with nCO_2 (n=1-2)
  - Complexes of ethanol with nCO_2 (n=1-5)
- Systems using CCSD(T)/6–311++G(2d,2p) for single-point energy calculations:

- Complexes of methanol with CO_2 and/or H_2O
- Complexes of ethanethiol with CO_2 and/or H_2O

The interaction energy of each complex investigated is determined by using the supramolecular approach as the difference in total energies between the complex and the sum of energies of the relevant monomers at the selected suitable level of theory. The interaction energy is corrected by ZPE and BSSE, which is computed using the function counterpoise procedure of Boys and Bernardi.[91]

The AIM analyses at the MP2/6–311++G(2d,2p) level are applied to find the critical points and to calculate electron densities and their Laplacians. A topological analysis of the electron density will be carried out using the program package AIM2000 and QTAIM. [121] The energies of each hydrogen bond will be evaluated by the empirical Espinosa-Molins-Lecomte formula[122] based on the electron density distribution at the BCP of the hydrogen bonds.

NBO analysis represents one of the most frequently used tools for analysing noncovalent interactions. The GenNBO 5.G program will be used to perform the NBO calculations, which is extensively applied to investigate chemical essences of hydrogen bonds, and can provide information about natural hybrid orbitals, natural bond orbitals, natural population, occupancies in NBOs, hyperconjugation energies, rehybridization and repolarization. In the present study, NBO analysis is also performed at MP2/6-311++G(2d,2p) or ωB97XD/aug-cc-pVTZ to determine the changes of electron densities in anti-bonding orbitals, to identify directions of electron density transfer between monomers following complexation.

Furthermore, the total stabilization energy of the complex is decomposed into the different energy components including electrostatic, induction, exchange-repulsion and dispersion energies. The SAPT2+ approach with the consistent basis set is applied, which is calculated by the PSI4 packages. Additionally, the molecular electrostatic potential (MEP)[123] diagram of isolated monomers was evaluated at MP2/aug-cc-pVTZ. To further identify the noncovalent behaviours, intermolecular interactions were assessed with NCIplot at high level of theory.[98,99]

Chapter 3. RESULTS AND DISCUSSION

3.1. Interactions of dimethyl sulfoxide with nCO_2 and nH_2O (n=1-2)

This section is based on the results of Ref. 124.

3.1.1. Geometries, AIM analysis and stability of intermolecular complexes

The stable complexes of interactions of DMSO with nCO_2 and nH_2O (n=1-2) molecules are shown in Fig. 3.1. Intermolecular distances (Å) and intramolecular angles (degree) of the complexes derived from MP2/6-311++G(2d,2p) geometries are also displayed in Fig. 3.1, while selected parameters of BCPs corresponding to intermolecular interactions are collected in Tables A1a, A1b and A1c of *Appendix*.

Addition of either a CO_2 or a H_2O molecule into binary complexes to form relevant ternary complexes leads to the emergence of O···O interaction of CO_2···CO_2 in **TC-DMSO-1** and **TC-DMSO-2**, O−H···O interaction of H_2O···H_2O in **TH-DMSO-1**, **TH-DMSO-2** and **TH-DMSO-3**, and O···O interaction of CO_2···H_2O in **TCH-DMSO-2**. Besides, **TH-DMSO-3** possesses the O14−H15···S9 interaction as compared to the S9···O11 interaction in **DH-DMSO-3**. Remarkably, the complexes **TH-DMSO-1**, **TH-DMSO-2**, **TH-DMSO-3** and **TH-DMSO-5** of the DMSO···$2H_2O$ system found in this work were not reported in previous study of the cooperativity between red-shift and blue-shift HBs in DMSO aqueous solution.[125] All H···O(S), S···O, C···O and O···O contact distances are in the range of 1.81−2.84, 3.21, 2.68−2.84 and 3.20−3.25 Å, respectively, which in general are close to the sums of van der Waals radii of relevant atoms. This suggests the real existence of these intermolecular interactions., in which the existence of H6···O12 contact in **TC-DMSO-1** (2.84 Å), H2···O15 in **TC-DMSO-2** (2.76 Å) and O···O in **TC-DMSO-1, TC-DMSO-2** and **TCH-DMSO-1** (3.20−3.25 Å) may result from an additional cooperative contribution of the remaining interactions.

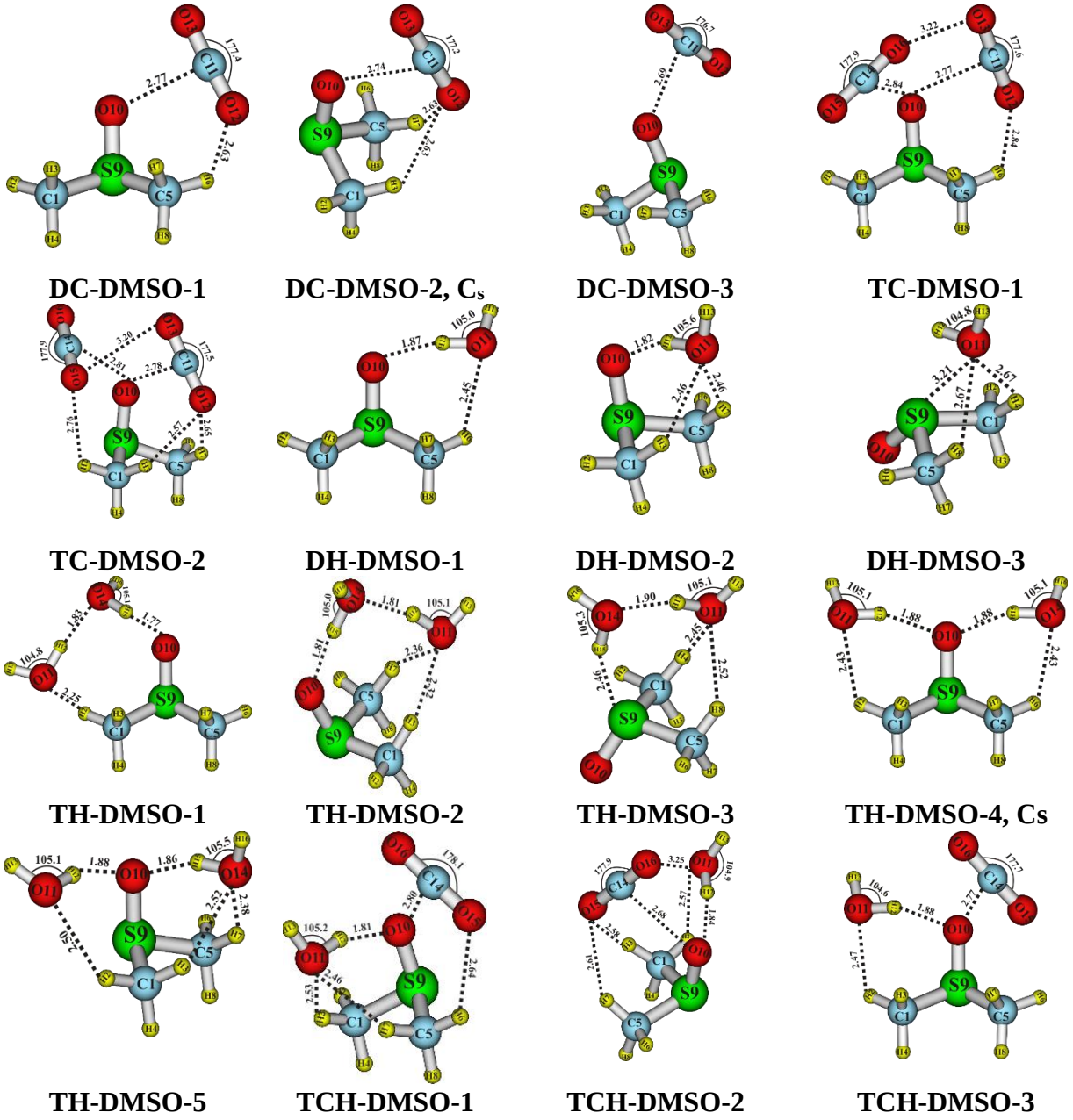

Figure 3.1. Geometries of stable complexes formed by interactions of DMSO with CO_2 and H_2O at MP2/6-311++G(2d,2p)

Further evidence for formation of intermolecular interactions in these complexes can be found in comparing variations of angles in CO_2 and H_2O molecules. Following complexation, a decrease of 2−3° for ∠OCO in CO_2 and an increase in 0.3−1.3° for ∠HOH in H_2O are indeed observed. Formation of intermolecular contacts is also confirmed by the presence of BCPs (red small balls surrounded by blue circle) shown in Fig. A1 of *Appendix*. The C···O distances of

2.77 Å in **DC-DMSO-1** and 2.69 Å in **DC-DMSO-3** are in line with those reported by Trung *et al.*[22] using the same theoretical method. The H12···O10 distances of 1.87 Å in **DH-DMSO-1**, 1.82 Å in **DH-DMSO-2** and 1.88 Å in **TH-DMSO-4** are also in good agreement with the work of Li *et al.* at the MP2/6-31++G(d,p) level (1.88, 1.83 and 1.87 Å respectively).[125] All values of $\rho(r)$ and $\nabla^2\rho(r)$ at the BCPs of H···O contacts located range from 0.004 to 0.035 au, and 0.017 to 0.117 au, respectively, except for the BCP of H15···O10 contact in **TH-DMSO** with a relatively high electron density of 0.038 au. They all fit within the criteria for formation of HB.[126] As a result, H···O(S) intermolecular contacts are considered as HBs. The positive values of both $\nabla^2\rho(r)$ (0.017−0.048 au) and $H(r)$ (0.0007−0.0014 au) for the C−H···O HBs at these BCPs confirm that these HBs are weak interaction. On the contrary, the O−H···O interactions are partly covalent in nature as indicated by $\nabla^2\rho(r) > 0$ and $H(r) \leq 0$, except for the O−H···O(S) HBs in **TH-DMSO-3** and **TH-DMSO-4** with values of $H(r) > 0$ (0−0.0008 au).

The S(O)···O and C···O intermolecular contacts are named as ChB and TtB, respectively. As shown in Table A1a-A1c, the positive values of both $\nabla^2\rho(r)$ (0.021−0.055 au) and $H(r)$ (0.0009−0.0014 au) for the S(O)···O and S=O···C interactions at these BCPs suggest that these intermolecular contacts are weak noncovalent interactions.[127,128,129]

There is an increase in electron density at the BCPs of the interactions in the order of O···O < C−H···O ≈ S···O < S=O···C < O−H···O(S) (*cf.* Tables A1a-c). Accordingly, the S=O···C TtB appears to play a more important role than the C−H···O HB and O···O ChB in stabilizing DMSO···1,2CO_2, while complexes of DMSO···1,2H_2O are mainly stabilized by O−H···O(S) HBs along with an additional role of C−H···O HB and S···O ChB. This observation will be confirmed by NBO analyses follows. In the case of DMSO···1CO_2···1H_2O, the magnitude of interactions contributing to their stability increases in the ordering going from O···O ChB to C−H···O HB to S=O···C TtB and finally to O−H···O HB. In an attempt to figure out a relationship between HB energies (E_{HB}) and their electron densities

($\rho(r)$) at BCPs of C(O)−H···O, a good linear correlation of E_{HB} and $\rho(r)$ is subsequently found (Fig. 3.2) as expressed in the following equation:

$$E_{HB}\ (\text{kJ.mol}^{-1}) = -1198.0\ \rho(r)\ (\text{au}) + 2.7\ (R^2 = 0.99) \qquad (3.1)$$

This indicates that the strength of HBs increases with increasing local electron density at BCPs of HBs.

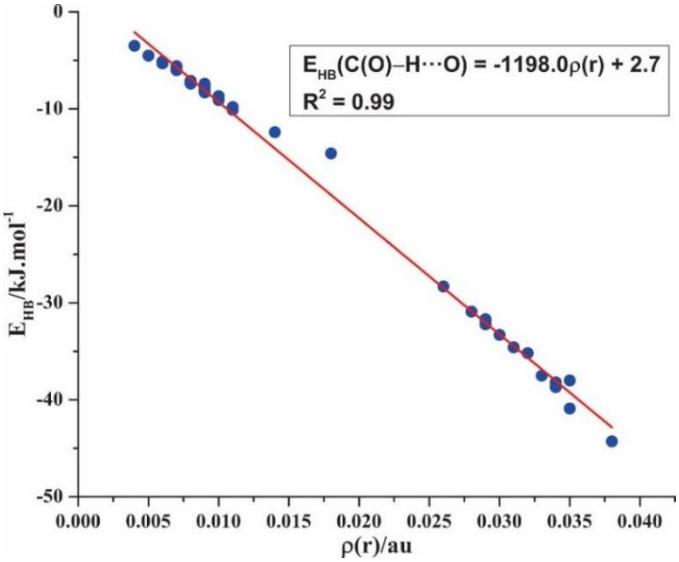

Figure 3.2. A linear correlation between individual E_{HB} and $\rho(r)$ values at BCPs

For the binary system DMSO···1CO_2, **DC-DMSO-2** with formation of two C−H···O HBs and one S=O···C TtB is compared to the existence of one C−H···O HB and one S=O···C TtB in **DC-DMSO-1,** and only one S=O···C TtB in **DC-DMSO-3**. The $\rho(r)$ values at BCPs of these contacts are approximate in magnitude (0.006 au for the C−H···O HBs and 0.012−0.014 au for the S=O···C TtBs), implying that it is possible to evaluate stabilization effect of these three complexes just by comparing the number of relevant interactions. Accordingly, we can predict that the stability of these complexes increases in going from **DC-DMSO-3** to **DC-DMSO-1** to **DC-DMSO-2**. In the case of DMSO···2CO_2, **TC-DMSO-2** is expected to be more stable than **TC-DMSO-1** as the E_{HB} values of three C−H···O HBs in **TC-DMSO-2** (from -4.5 to -5.9 kJ.mol^{-1}) are more negative than that of one C−H···O HB in **TC-DMSO-1** (-3.5 kJ.mol^{-1}) (*cf.* Table A1a). A decrease of electron density at BCPs and E_{HB} negative value of C(O)−H···O HBs in the ordering of **DH-DMSO-2** to **DH-DMSO-1** to **DH-DMSO-3** for DMSO···1H_2O (*cf.* Table A1b) implies that

the stability of the complexes tends to decrease along this trend.

Ternary complexes **TH-DMSO-1**, **TH-DMSO-2**, **TH-DMSO-4** and **TH-DMSO-5** with a presence of two O−H···O HBs are likely to be more stable than **TH-DMSO-3**, where only one O−H···O HB is involved. There is an increase in electron density at BCPs and the strength of O−H···O HBs in the ordering of **TH-DMSO-4** < **TH-DMSO-5** < **TH-DMSO-1** < **TH-DMSO-2** and **TH-DMSO-3** (*cf.* Table A1b). As shown in Fig. 3.1, there are three C−H···O HBs in **TH-DMSO-5** as compared to one C−H···O HB in **TH-DMSO-1**. These results suggest that the stability of DMSO···2H_2O ternary complexes increases in a sequence of **TH-DMSO-3** < **TH-DMSO-4** < **TH-DMSO-1** < **TH-DMSO-5** < **TH-DMSO-2**. An increase in both electron density and negative value of E_{HB} at the BCPs of O−H···O HB, in going from **TCH-DMSO-3** to **TCH-DMSO-2** to **TCH-DMSO-1** (*cf.* Table A1c), indicates an increase in the stability of complexes according to this ordering for ternary system DMSO···1CO_2···1H_2O.

As shown in Tables A1a-A1c, the stability of S=O···C TtBs and C−H···O HBs in DMSO···2CO_2 is decreased, except for C1(5)−H3(7)···O12 HBs in **TC-DMSO-2** as compared to **DC-DMSO-2**. In going from DMSO···1H_2O to the corresponding DMSO···2H_2O, there are increases in electron density and E_{HB} negative values at BCPs of C−H···O and O−H···O intermolecular contacts, except for C1−H2···O11 and C1−H3···O14 ones in **TH-DMSO-5**, O−H···O HBs in **TH-DMSO-4** and **TH-DMSO-5**. For DMSO···1CO_2···1H_2O, the stability of O−H···O HBs in **TCH-DMSO-1** and **TCH-DMSO-2** is enhanced while it is decreased in **TCH-DMSO-3**. In summary, the stability of most of interactions is enhanced in DMSO···2H_2O, while it is reduced in both DMSO···2CO_2 and DMSO···1CO_2···1H_2O upon the formation of ternary complexes.

3.1.2. Interaction and cooperative energies and energy component

Interaction and cooperative energies of complexes determined at the CCSD(T)/6-311++G(2d,2p)//MP2/6-311++G(2d,2p) level are summarized in Table 3.1. All interaction energies evaluated for both binary and ternary systems are

significantly negative, in the range between -9 to -52 kJ.mol^{-1} with both ZPE and BSSE corrections, indicating that the obtained complexes are relatively stable on potential energy surface. Interaction and cooperative energies listed in Table 3.1 show a similar varying trend in estimating strength of complexes without and with BSSE correction. The contribution of BSSE is important, about 23-34% in the interaction energy. Therefore, interaction and cooperative energy values corrected for both ZPE and BSSE corrections are used in the following discussion.

Table 3.1. Interaction energy and cooperative energy of complexes of DMSO with CO_2 and/or H_2O at CCSD(T)/6-311++G(2d,2p)//MP2/6-311++G(2d,2p), kJ.mol^{-1}

Complex	E_{int}	Complex	E_{int}	E_{coop}
DC-DMSO-1	-17.7(-12.5)	**TC-DMSO-1**	-35.8(-23.7)	-1.4(-1.4)
DC-DMSO-2	-19.2(-13.3)	**TC-DMSO-2**	-39.0(-25.6)	-1.3(-1.0)
DC-DMSO-3	-14.5(-9.5)	**TH-DMSO-1**	-60.6(-46.6)	-19.6(-20.3)
DH-DMSO-1	-29.9(-22.8)	**TH-DMSO-2**	-67.1(-51.7)	-22.1(-22.7)
DH-DMSO-2	-35.6(-27.1)	**TH-DMSO-3**	-39.4(-28.5)	-12.2(-13.1)
DH-DMSO-3	-13.2(-9.2)	**TH-DMSO-4**	-58.2(-44.2)	-9.8(-10.3)
		TH-DMSO-5	-62.6(-47.4)	-9.0(-9.5)
		TCH-DMSO-1	-54.0(-39.0)	-5.2(-5.4)
		TCH-DMSO-2	-51.2(-36.4)	-5.4(-5.5)
		TCH-DMSO-3	-46.9(-34.3)	-4.6(-5.2)

Calculated energies for DMSO···1H_2O (from -9 to -27 kJ.mol^{-1}) are more negative than that for DMSO···1CO_2 (from -10 to -13 kJ.mol^{-1}), showing that DMSO interacts with H_2O more strongly than with CO_2. Interaction energy of -52 kJ.mol^{-1} for the most stable complex of DMSO···2H_2O (**TH-DMSO-2**) is more negative than that for DMSO···1CO_2···1H_2O (**TCH-DMSO-1**) by 13 kJ.mol^{-1} and DMSO···2CO_2 (**TC-DMSO-2**) by 26 kJ.mol^{-1}, indicating that the interaction of DMSO with 2H_2O is stronger than that of DMSO with 1CO_2+1H_2O and with 2CO_2. Interaction energies for DMSO···2H_2O and DMSO···2CO_2 are more negative than those compared to corresponding binary systems by 1−43 kJ.mol^{-1} and 10−16 kJ.mol^{-1}. In addition, the complexes of DMSO···1CO_2···1H_2O are also found to be more stable than DMSO···1H_2O and DMSO···1CO_2 by 7−30 kJ.mol^{-1} and 21−29 kJ.mol^{-1}, respectively. Thus, addition of CO_2 and H_2O molecules into binary

complexes leads to an increase in stability of ternary complexes, in which the increasing magnitude is larger for the addition of H_2O than that for CO_2 counterpart.

The SAPT2+ analysis is used to evaluate the contributions of different energy components to the total stabilization energy of complexes. Obtained results are shown in Fig. A2 of *Appendix*. Contribution of electrostatic term is larger for DMSO···1H_2O (44−49%) than for DMSO···1CO_2 (38−40%), whereas contribution of the induction and dispersion terms into the stability is reversed. This can be understood by the existence of O−H···O HB with a high electrostatic characteristic playing a significant role in DMSO···1H_2O, as compared to the S=O···C TtB in DMSO···1CO_2 as mentioned earlier.

As shown in Table 3.1, a decrease of complex stability is observed in the ordering of **DC-DMSO-2** > **DC-DMSO-1** > **DC-DMSO-3** for DMSO···1CO_2 and **DH-DMSO-2** > **DH-DMSO-1** > **DH-DMSO-3** for DMSO···1H_2O. Interaction energy of **DC-DMSO-1** (-13 kJ.mol^{-1}, CCSD(T)/6-311++G(2p,2d)//MP2/6-311++G(2d,2p)) is close to the value previously reported by Trung *et al.*[22] at a higher level CCSD(T)/6-311++G(3df,2pd) but with the same geometry MP2/6-311++G(2d,2p) (-14.5 kJ.mol^{-1}) and Wallen *et al.*[9] at MP2/aug-cc-pVDZ//MP2/6-31+G(d) level (-14.3 kJ.mol^{-1}). Interaction energies of -23 kJ.mol^{-1} for **DH-DMSO-1** and -27 kJ.mol^{-1} for **DH-DMSO-2** obtained in this work are also in line with those given by Li *et al.*[125] (MP2/6-31++G(d,p)) namely -24.8 and -28.3 kJ.mol^{-1}, respectively. In the ternary system DMSO···2CO_2, **TC-DMSO-1** is found to be ~2 kJ.mol^{-1} less stable than **TC-DMSO-2**.

For ternary system DMSO···2H_2O, the complex strength is enhanced in the sequence of **TH-DMSO-3** < **TH-DMSO-4** < **TH-DMSO-1** < **TH-DMSO-5** < **TH-DMSO-2** (*cf.* Table 3.1). Complex **TH-DMSO-2** is more stable than the most stable one by 4 kJ.mol^{-1} (MP2/6-31++G(d,p)) which is reported by Li by *et al.*[125] Interaction energy (-69 kJ.mol^{-1}) for DMSO···3H_2O obtained at the MP2/6-31G(d,p) level by Hobza *et al.*[130] is *ca.* 17 kJ.mol^{-1} more stable than that for DMSO···2H_2O (**TH-DMSO-2)** in the present work, suggesting that addition of water molecules

into DMSO system can be an efficient way of increasing the stability of complexes, leading to a DMSO solvent stabilization. For DMSO···1CO_2···1H_2O, **TCH-DMSO-1** is the most stable, which is *ca.* 3 and 5 kJ.mol^{-1} more negative than **TCH-DMSO-2** and **TCH-DMSO-3**. These results on stability of complexes are thus consistent with the afore mentioned discussion in terms of structural and AIM analyses.

To evaluate the cooperativity of relevant interactions in ternary systems, cooperative energies are calculated and given in Table 3.1. Significantly negative values of E_{coop} from -1 to -23 kJ.mol^{-1} imply that interactions in ternary systems work in concert with each other to enhance the overall complex stabilization. The increase in negative E_{coop} values in going from DMSO···2CO_2 to DMSO···1CO_2···1H_2O and to DMSO···2H_2O is consistent with increase of interaction energy negative values in these systems. Thus, cooperative energies are more negative for DMSO···2H_2O than for DMSO···2CO_2 by 9−22 kJ.mol^{-1} and DMSO···1CO_2···1H_2O by 5−18 kJ.mol^{-1}. This implies a good correlation between both cooperative and interaction energies of the investigated systems. The cooperative capacity of interactions in DMSO···2CO_2 is quite weak, as reflected in cooperative energies of only from -1.0 to -1.4 kJ.mol^{-1}, whereas a strong cooperativity of interactions in DMSO···2H_2O is observed. This can be explained by a stronger cooperativity of O−H···O HBs in DMSO···2H_2O in comparison to S=O···C TtBs in DMSO···2CO_2.

Calculated energies due to a cooperativity in **TH-DMSO-1**, **TH-DMSO-2** and **TH-DMSO-3** are from -13 to -23 kJ.mol^{-1}, which are *ca.* 3−14 kJ.mol^{-1} more negative than in **TH-DMSO-4** and **TH-DMSO-5**. Cooperative energy of **TCH-DMSO-2** is also found to be more slightly negative than that of **TCH-DMSO-1** and **TCH-DMSO-3** by *ca.* 0.1 and 0.3 kJ.mol^{-1} respectively. As a result, the presence of O−H···O HB in H_2O···H_2O of **TH-DMSO-1**, **TH-DMSO-2** and **TH-DMSO-3** and O···O ChB in CO_2···H_2O of **TCH-DMSO-2** results in an increase in cooperative capacity. From structural perspective and cooperative effect analysis, the cooperativity of interactions likely emerges to be stronger for ring structure than for

open counterparts.

3.1.3. Bonding vibrational modes and NBO analysis

To clarify characteristics of the bonds involving in intermolecular interactions upon complexation, the bond stretching vibrational frequencies and an NBO analysis for the complexes and relevant monomers are performed at the MP2/6-311++G(2d,2p) level.

Table 3.2. The second-order perturbation energy ($kJ.mol^{-1}$) for transfers in complexes of DMSO with nCO_2 and nH_2O (n=1-2)

Complex	Type	$E^{(2)}$	**Complex**	Type	$E^{(2)}$
DC-DMSO-1	n(O12)→σ*(C5−H6)	1.7	**TH-DMSO-3**	n(O11)→σ*(C1−H4)	5.3
	n(O10)→π* (C11=O13)	12.0		n(O11)→σ*(C5−H8)	4.4
DC-DMSO-2	n(O12)→σ*(C1−H3)	2.3		n(S9)→σ*(O14−H15)	21.8
	n(O12)→σ*(C5−H7)	2.3		n(O14)→σ*(O11−H12)	36.3
	n(O10)→π*(C11=O13)	10.9	**TH-DMSO-4**	n(O11)→σ*(C1−H2)	3.2
DC-DMSO-3	n(O10)→π*(C11=O13)	15.8		n(O14)→σ*(C5−H6)	3.2
TC-DMSO-1	n(O12)→σ*(C5−H6)	0.7		n(O10)→σ*(O11−H12)	45.2
	n(O10)→π*(C11=O13)	12.3		n(O10)→σ*(O14−H15)	45.2
	n(O10)→π*(C14=O16)	9.7	**TH-DMSO-5**	n(O11)→σ*(C1−H2)	2.9
	π(C14=O16)→π*(C11=O13)	0.8		n(O14)→σ*(C1−H3)	3.4
TC-DMSO-2	n(O12)→σ*(C1−H3)	2.8		n(O14)→σ*(C5−H7)	4.6
	n(O12)→σ*(C5−H7)	2.2		n(O10)→σ*(O11−H12)	51.0
	n(O15)→σ*(C1−H2)	0.3		n(O10)→σ*(O14−H15)	46.9
	n(O10)→π*(C11=O13)	9.8	**TCH-DMSO-1**	n(O11)→σ*(C1−H3)	3.4
	n(O10)→π*(C14=O16)	9.1		n(O11)→σ*(C5−H7)	3.7
	π(C14=O15)→π*(C11=O13)	0.8		n(O15)→σ*(C5−H6)	1.3
DH-DMSO-1	n(O11)→σ*(C5−H6)	2.9		n(O10)→σ*(O11−H12)	62.9
	n(O10)→σ*(O11−H12)	50.0		n(O10)→π*(C14=O16)	6.5
DH-DMSO-2	n(O11)→σ*(C1−H3)	3.8	**TCH-DMSO-2**	n(O11)→σ*(C1−H2)	1.2
	n(O11)→σ*(C5−H7)	3.8		n(O15)→σ*(C1−H3)	2.6
	n(O10)→σ*(O11−H12)	60.5		n(O15)→σ*(C5−H7)	2.6
DH-DMSO-3	n(O11)→σ*(C1−H4)	1.3		n(O10)→σ*(O11−H12)	54.7
	n(O11)→σ*(C5−H8)	1.3		n(O10)→π*(C14=O16)	6.7
	n(S9)→σ*(O11−H12)	1.5		n(O11)→π*(C14=O16)	1.5
	n(O11)→π*(S9=O10)	0.3	**TCH-DMSO-3**	n(O11)→σ*(C1−H2)	2.8
TH-DMSO-1	n(O11)→σ*(C1−H2)	14.2		n(O10)→σ*(O11−H12)	47.6
	n(O10)→σ*(O14−H15)	78.7		n(O10)→π*(C14=O16)	12.3
	n(O14)→σ*(O11−H12)	57.7	*n: nonbonded (lone-pair) orbital*		
TH-DMSO-2	n(O11)→σ*(C1−H3)	9.5	*π: π-bond*		
	n(O11)→σ*(C5−H7)	8.3	*σ*: anti σ-bond*		
	n(O10)→σ*(O14−H15)	106.9	*π*: anti π-bond*		
	n(O14)→σ*(O11−H12)	63.1			

The second-order perturbation energy ($E^{(2)}$) for intermolecular interactions

are given in Table 3.2 while directions of electron density transfer (EDT), changes in C(O)−H bond lengths (Δr) along with its stretching frequencies (Δν), and the factors causing the red and blue shift of the C(O)−H bonds in HBs are collected in Tables 3.3a-c.

Obviously, there are various trends of electron density transfer between DMSO with CO_2 and H_2O. The positive EDT values of DMSO (from 0.004 to 0.041 electron) show an electron transfer from DMSO to CO_2 and H_2O. EDT values of H_2O (from -0.002 to -0.028 electron) are more negative than that of CO_2 (from -0.002 to -0.006 electron) indicating a stronger electron transfer from DMSO to H_2O as compared to that from DMSO to CO_2.

The existence of C−H···O HB, O−H···O HB and S=O···C TtB in the complexes is confirmed here by means of EDT from n(O) to σ*(C−H), n(O) to σ*(O−H) and n(O) to π*(C=O) with the $E^{(2)}$ values of 0.3−14 kJ.mol^{-1}, 36−107 kJ.mol^{-1} and 6−16 kJ.mol^{-1}, respectively. The presence of S···O ChB in **DH-DMSO-3** is resulted from EDT of both from n(S) to σ*(O−H) (1.5−1.6 kJ.mol^{-1}). The existence of O···O ChB in **TC-DMSO-1** and **TC-DMSO-2** is identified on the basis of the EDT from π(C=O) to π^*(C=O) between two CO_2 molecules with quite small $E^{(2)}$ value of 0.8 kJ.mol^{-1}, while electron density transfer from n(O) of H_2O to π*(C=O) of CO_2 (1.5 kJ.mol^{-1}) results in the formation of O···O chalcogen bond in **TCH-DMSO-2**.

The calculated $E^{(2)}$ values are larger for n(O)→π*(C=O) than for n(O)→σ*(C−H) by 6−16 kJ.mol^{-1}, and π(C=O)→π*(C=O) by 8−15 kJ.mol^{-1} in DMSO···1,2CO_2, corroborating the fact that the S=O···C TtB plays a significant role in stabilizing this system. The larger $E^{(2)}$ for n(O) → σ*(O−H) (36−107 kJ.mol^{-1}) as compared to n(S)→σ*(O−H) (21.8 kJ.mol^{-1}), n(O)→σ*(C−H) (1−14 kJ.mol^{-1}) and n(O)→π*(S=O) (0.3−0.6 kJ.mol^{-1}) in DMSO···1,2H_2O reaffirms a pivotal contribution of the O−H···O HB to the overall strength of these complexes. For ternary system DMSO···1CO_2···1H_2O, the role of interactions contributing to the stability of this system decreases in the ordering of O−H···O HB to S=O···C TtB to

C−H···O HB and finally to O···O ChB. Thus, the $E^{(2)}$ values for n(O)→σ*(O−H) ranging from 48 to 63 kJ.mol^{-1} are much larger than that for n(O)→π*(C=O) (7−12 kJ.mol^{-1}), n(O)→σ*(C−H) (1−4 kJ.mol^{-1}) and n(O)→π*(C=O) (1.5 kJ.mol^{-1}).

Table 3.3a. Selected results of vibrational and NBO analyses for interaction of DMSO with nCO_2 (n=1-2)

Complex	EDT	Hydrogen bond	Δr (Å)	Δν (cm^{-1})	Δσ* (C(O)−H) (e)	Δ%s (C(O)) (%)
DC-DMSO-1	0.005[a)] -0.005[b)]	C5−H6···O12	-0.0034	35.0	0.0003	0.34
DC-DMSO-2	0.004[a)]	C1−H3···O12	-0.0037	38.4	-0.0005	0.43
	-0.004[b)]	C5−H7···O12	-0.0037	38.4	-0.0005	0.43
TC-DMSO-1	0.010[a)] -0.006[b)] -0.004[c)]	C5−H6···O12	-0.0030	29.3	0	0.15
TC-DMSO-2	0.006[a)]	C1−H2···O15	-0.0031	30.5	0	0.12
	-0.004[b)]	C1−H3···O12	-0.0040	42.5	-0.0004	0.47
	-0.002[c)]	C5−H7···O12	-0.0037	39.5	-0.0007	0.45

[a),b),c)] For charge of DMSO, CO_2, CO_2 , respectively.

Following complexation, C−H bond lengths are shortened by *ca.* 0.0014−0.0040 Å and accompanied by an increase in its stretching frequency of 8−45 cm^{-1}, while an elongation of O−H bond length by 0.0084−0.0223 Å and a decrease of its corresponding stretching frequency within the range of 167−438 cm^{-1} are observed as compared to those in the relevant monomers. The C−H···O HBs in the complexes thus belong to the blue-shifting HB type, while the O−H···O(S) HBs are red-shifting. The largest blue-shift of C−H bond is observed in C5−H7···O15 bond of **TCH-DMSO-2**, while the most significant red-shift of O−H stretching frequency is obtained in O14−H15···O10 bond of **TH-DMSO-2**. In addition, a good linear correlation between the changes of the C(O)−H stretching frequencies and its bond distance is observed according to equations:

$$\Delta\nu(\text{C−H})\ (\text{cm}^{-1}) = -12258.0\Delta r(\text{C−H})\ (\text{Å}) - 5.6\ (R^2 = 0.95) \quad (3.2),$$

and

$$\Delta\nu(\text{O−H})\ (\text{cm}^{-1}) = -19823.0\Delta r(\text{O−H})\ (\text{Å}) - 1.3\ (R^2 = 0.99) \quad (3.3)$$

as represented in Fig. A3 and A4 of *Appendix*.

The negative slope and high correlation coefficients show a strong inverse correlation between changes of C(O)−H bond distances and their corresponding stretching frequencies upon complexation. A stronger linear correlation between the change of O−H stretching frequency and its bond length is found as compared to the C−H counterpart's.

Table 3.3b. Selected results of vibrational and NBO analyses for interaction of DMSO with nH_2O (n=1-2)

Complex	EDT	Hydrogen bond	Δr (Å)	Δν (cm^{-1})	Δσ* (C(O)−H) (e)	Δ%s (C(O)) (%)
DH-DMSO-1	0.021[a)]	C5−H6···O11	-0.0028	29.7	0.0004	0.77
	-0.021[b)]	O11−H12···O10	0.0132	-261.5	0.0208	3.16
DH-DMSO-2	0.026[a)]	C1−H3···O11	-0.0033	33.9	-0.0006	0.94
	-0.026[b)]	C5−H7···O11	-0.0033	34.3	-0.0006	0.94
		O11−H12···O10	0.0172	-347.6	0.0284	3.52
DH-DMSO-3	0.006[a)]	C1−H4···O11	-0.0036	38.7	-0.0006	0.47
	-0.006[b)]	C5−H8···O11	-0.0036	40.7	-0.0006	0.47
TH-DMSO-1	0.025[a)]	C1−H2···O11	-0.0014	8.4	0.0048	1.52
	-0.019[b)]	O14−H15···O10	0.0196	-382.2	0.0292	4.19
	-0.006[c)]	O11−H12···O14	0.0152	-300.3	0.0239	3.72
TH-DMSO-2	0.025[a)]	C1−H3···O11	-0.0032	33.2	0.0010	1.44
	-0.007[b)]	C5−H7···O11	-0.0031	30.5	0.0015	1.39
	-0.018[c)]	O14−H15···O10	0.0223	-438.4	0.0337	4.32
		O11−H12···O14	0.0168	-331.9	0.0263	3.93
TH-DMSO-3	0.026[a)]	C1−H4···O11	-0.0030	32.9	0.0003	0.88
	-0.012[b)]	C5−H8···O11	-0.0029	32.8	0.0004	0.79
	-0.014[c)]	O14−H15···S9	0.0084	-167.1	0.0153	2.17
		O11−H12···O14	0.0107	-206.6	0.0223	3.01
TH-DMSO-4	0.036[a)]	C1−H2···O11	-0.0030	31.8	0.0005	0.87
	-0.018[b)]	C5−H6···O14	-0.0030	31.8	0.0005	0.87
	-0.018[c)]	O11−H12···O10	0.0122	-241.5	0.0187	3.03
		O14−H15···O10	0.0122	-241.5	0.0187	3.03
TH-DMSO-5	0.041[a)]	C1−H2···O11	-0.0024	25.7	0.0003	0.56
	-0.021[b)]	C1−H3···O14	-0.0033	34.4	-0.0008	0.73
	-0.020[c)]	C5−H7···O14	-0.0036	38.4	-0.0007	1.07
		O11−H12···O10	0.0121	-244.4	0.0205	3.07
		O14−H15···O10	0.0150	-302.9	0.0246	3.25

[a),b),c)] For charge of DMSO, H_2O, H_2O, respectively

In going from a binary to corresponding ternary systems, a different change is noticed in the magnitude of stretching frequency blue and red shifts of C−H and O−H bonds in the C(O)−H···O HBs. Thus, the magnitude of C−H blue shift in

C−H···O HBs decreases by *ca.* 1−21 cm^{-1}, except for C−H bonds including C1(5)−H3(7)···O12 in **TC-DMSO-2**, C1(5)−H2(6)···O11(14) in **TH-DMSO-4**, C1(5)−H3(7)···O14 in **TH-DMSO-5**, C1−H2···O11 and C5−H7···O15 in **TCH-DMSO-2** with a slight increase of 1−6 cm^{-1} in the stretching frequency compared to the corresponding HBs in the binary complexes. On the contrary, a much larger red shift by *ca.* 9−121 cm^{-1} of O-H stretching frequencies in the O−H···O HBs is obtained, except for a decrease of red shift level by ca. 9−45 cm^{-1} of O−H bonds in the O−H···O HBs in **TH-DMSO-4, TH-DMSO-5, TCH-DMSO-1** and **TCH-DMSO-3**. Consequently, the cooperative effect in ternary complexes induces various trends for changes in stretching frequencies of the C−H or O−H involved in HBs, generally an enhancement in the magnitude of O−H stretching frequency red shift in most O−H···O HBs but causes a reverse trend on the blue shift of C−H stretching frequency of a majority of the C−H···O HBs.

Table 3.3c. Selected results of vibrational and NBO analyses (MP2/6-311++G(2d,2p)) for interaction of DMSO with CO_2 and H_2O

Complex	EDT	Hydrogen bond	Δr (Å)	Δν (cm^{-1})	Δσ* (C(O)−H) (e)	Δ%s (C(O)) (%)
TCH-DMSO-1	0.030[a)] -0.004[b)] -0.026[c)]	C1−H3···O11	-0.0032	32.4	-0.0008	0.83
		C5−H7···O11	-0.0031	32.3	-0.0008	0.82
		C5−H6···O15	-0.0033	33.7	-0.0003	0.72
		O11−H12···O10	0.0166	-338.6	0.0219	3.16
TCH-DMSO-2	0.025[a)] -0.004[b)] -0.021[c)]	C1−H2···O11	-0.0039	41.3	0	0.43
		C1−H3···O15	-0.0030	32.0	-0.0008	0.47
		C5−H7···O15	-0.0040	44.5	-0.0008	0.50
		O11−H12···O10	0.0135	-270.9	0.0226	3.25
TCH-DMSO-3	0.030[a)] -0.004[b)] -0.026[c)]	C1−H2···O11	-0.0025	27.3	-0.0003	0.63
		O11−H12···O10	0.0123	-243.2	0.0293	3.54

[a),b),c)] For charge of DMSO, CO_2, H_2O, respectively

Results listed in Tables 3.3a-c show that a contraction of C−H bond and a blue shift of its stretching frequency in the C−H···O HBs are in general accompanied by a decrease of population in the σ*(C−H) orbital, and an increase of *s*-character percentage of C(H) orbital. However, a contraction of the C−H bond being concomitant with its stretching frequency blue shift in the C5−H6···O12 in

DC-DMSO-1, C5−H6···O11 in **DH-DMSO-1**, C1−H2···O11 in **TH-DMSO-1**, C1(5)−H3(7)···O11 in **TH-DMSO-2**, C1(5)−H4(8)···O11 in **TH-DMSO-3**, C1(5)−H2(6)···O11(14) in **TH-DMSO-4**, and C1−H2···O11 in **TH-DMSO-5** is governed by an increase of *s*-character percentage of C(H) atom overcoming an increase of population in the σ*(C−H) orbital. Besides, there are increases in *s*-character of O(H) atoms and electronic population of σ*(O−H) orbitals for all complexes (*cf.* Tables 3.3b and 3.3c). Accordingly, an elongation of the O−H bond length and a red shift of its stretching frequency arise from an increase in electron population of σ*(O−H) orbitals, which overcomes an increase in the *s*-character of O(H) hybrid orbital upon complexation.

3.1.4. Remarks

Interactions between DMSO with CO_2 and H_2O molecules were investigated at using high level *ab initio* methods. Addition of H_2O or CO_2 molecules into binary complexes leads to an increase in the stability of the resulting ternary complexes. It is remarkable that a greater cooperativity of relevant interactions in DMSO···$2H_2O$ (from -9.5 to -22.7 kJ.mol^{-1}) are observed, as compared to those in DMSO···$1CO_2$···$1H_2O$ (from -5.2 to -5.5 kJ.mol^{-1}) and DMSO···$2CO_2$ (from -1.0 to -1.4 kJ.mol^{-1}).

In going from a binary to corresponding ternary systems, the stability of most interactions in DMSO···$2H_2O$ is enhanced, whereas it is decreased in DMSO···$2CO_2$ and DMSO···$1CO_2$···$1H_2O$. The stability of DMSO···$1,2CO_2$ complexes is contributed by the crucial role of the S=O···C TtB and an additional cooperation of the C−H···O HB and O···O ChB, while the O−H···O HB plays a more important role than other weak interactions in stabilizing DMSO···$1,2H_2O$ and DMSO···$1CO_2$···$1H_2O$.

The water molecule plays different roles in both types of HB, namely a proton-donor in the O−H···O(S) red-shifting HB, and a proton-acceptor in the C−H···O blue-shifting HB. In general, the magnitude of the red shift in O−H stretching frequency of O−H···O bond is enhanced, whereas the extent in stretching

frequency blue shift of the C−H bond in the C−H···O bonds is weakened when a cooperativity happens.

3.2. Interactions of acetone/thioacetone with nCO_2 and nH_2O

This section is based on the results of Ref. 131.

3.2.1. Geometric structures

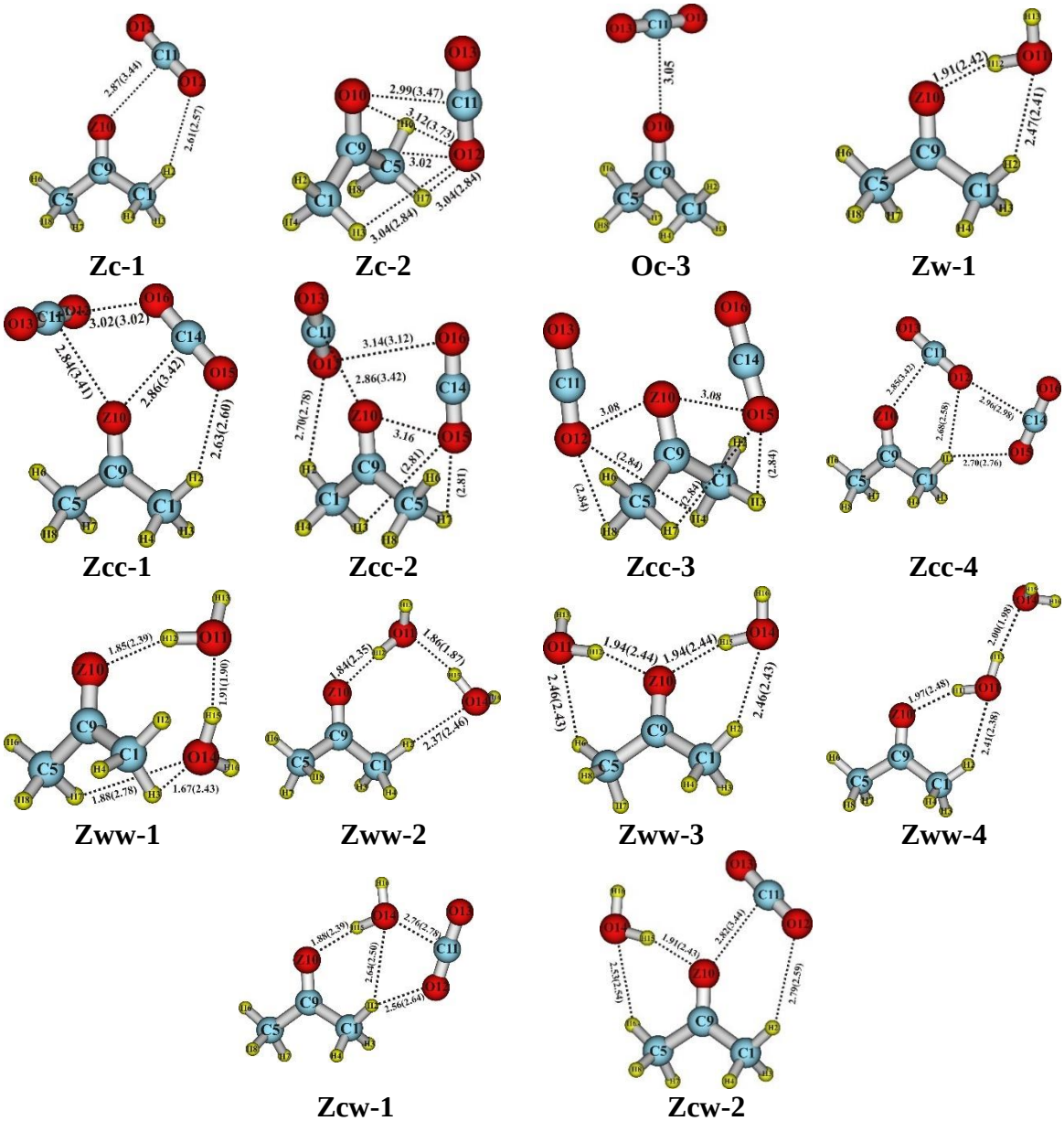

Figure 3.3. Stable structures of complexes formed by interactions of $(CH_3)_2CZ$ with CO_2 and H_2O (Z=O, S) (values in parentheses are for complexes of $(CH_3)_2CS$)

The stable complexes formed by interactions of $(CH_3)_2CZ$ (denoted for acz) with CO_2 and H_2O are presented in Fig. 3.3 (Z = O, S; c and w are denoted for CO_2

and H_2O, respectively). Obviously, CO_2 and H_2O guest molecules prefer to locate around the >C=O/S groups. The first evidence for the formation of intermolecular interactions is that all the O···O(S), C···O(S), C–H···O and O–H···O(S) contact distances are shorter than sums of van der Waals radii of relevant atoms (*cf.* Fig. 3.3). The existence of intermolecular interactions is also confirmed by BCPs in topological geometries obtained from AIM analysis at MP2/6-311++G(2d,2p). Selected parameters at BCPs including $\rho(r)$, $\nabla^2\rho(r)$ and $H(r)$ of the C···O(S), O···O(S) and C/O–H···O(S) interactions are presented in Table A3 and A4 of *Appendix*. The calculated values of $\rho(r)$ at BCPs of these intermolecular interactions lie in the range of 0.004-0.030 au and positive values of $\nabla^2\rho(r)$ and $H(r)$ (*cf.* Table A2 and A3) suggest that they are weakly noncovalent interactions.[132]

In present work, three types of aco···CO_2 geometries are observed as previously investigated, in which **Oc-1** was reported as global minimum with the cooperativity of C···O TtB and C–H···O HB, as typical or conventional structure.[15,40,43,44,45,48,133] The **Oc-2** were introduced by Altarsha *et al.*[44] as non-conventional one, with slipped-parallel geometry, similar to the structure of $(CO_2)_2$ dimer and carbonyl-carbonyl interactions.[134,135] It is noteworthy that in case of acs complexes, the non-conventional geometry **Sc-2** is also found, however, the T-shape one is not observed on the potential surface. This absence is probably explained by the decreasing negative charge from O to S atom, which cause the electrostatic nature of C···O/S TtB. In particular, the oxygen atom of aco is assigned a net charge of -0.546 e; while sulfur atom of acs displays a positive charge with +0.074 e at MP2/6-311++G(2d,2p). Remarkably, the all obtained $2CO_2$ complexes are based on the **Zc-1** or **Zc-2** structures. This geometric trend shows the high stability of both conventional and non-conventional structures of aco and even acs complexes. The chalcogen interaction is absent in aco···$1CO_2$ complexes, but it exists in aco···$2CO_2$ ones as noted in previous work,[136] supporting its potential role in the larger complexes with more coordination of CO_2.

As presented in Fig. 3.3, complexes with the attendance of $1,2H_2O$ are

mainly characterized by two types of HBs including O–H···O/S and C–H···O. Three in four $2H_2O$ complexes exist mutual interactions of three isolated components, while the **Zww-4** exhibits the linear interactions. Indeed, **Zww-4** seems to be formed by the O–H···O/S and C–H···O HBs between aco/acs host molecule and $(H_2O)_2$ cluster.[137] Two H_2O molecules in **Zww-1** are lying in a perpendicular planar and associate with host molecule *via* HBs. In **Zww-2**, H_2O molecules are located in one side of the host molecule but they are established in two different sides in **Zww-3**. The coexistence of C···O/S TtBs and O–H···O/S HBs is found in the combinations of aco/acs and CO_2 and H_2O. In **Zcw-1**, three molecules form a cycle structure *via* O–H···O/S, C···O and C–H···O associations. The location of H_2O and CO_2 in two sides of host molecules leads to the formation of **Zcw-2**.

3.2.2. Stability and cooperativity

The interaction energies and cooperative energies corrected both ZPE and BSSE of studied complexes at CCSD(T)/6-311++G(2d,2p)//MP2/6-311++G(2d,2p) are gathered in Table 3.4. The difference of interaction energies for three aco/acs···$1CO_2$ structures is quite small. **Oc-1** is defined as the energetically preferred structure of aco···CO_2 system, in well agreement with previous studies for carbonyl compounds.[9,43,45,48,40,44,133] It supports the additional stabilizing role of C–H···O HB existed in **Oc-1** as compared to others. The stability of acs···$1CO_2$ complexes is increased in order **Sc-2** < **Sc-1**. This trend indicates that the structures of aco/acs with $1CO_2$ favor the tetrel-bonded model than slipped-parallel and T-shape ones. Nevertheless, the **Zc-2** is also found to be comparable with **Zc-1** by a small magnitude 0.1-0.2 kcal.mol^{-1}. This result confirms again the importance of **Zc-2** non-conventional structure relative to **Zc-1** conventional one as previously reported[44] not only for aco system, but also for acs one, which is detected the first time in this work.

Going to ternary system, **Occ-1** is assumed to be the global minimum with E_{int} value of -4.4 kcal.mol^{-1}. The **Occ-2** was reported before as the most stable complex at MP2/aug-cc-pVTZ,[45] but in this work, it is slightly less negative than

Occ-1 by around 0.2 kcal.mol^{-1} at CCSD(T)/6-311++G(2d,2p). Furthermore, this result was supported by experimental infrared spectra and theoretical calculations at CO_2 pressure of 18 MPa.[133] For acs···2CO_2 system, **Scc-2** is the most favorable structure and more stable than **Scc-1, Scc-3** and **Scc-4** by 0.6-0.7 kcal.mol^{-1}. This different trend between 2CO_2 structures supports the more significant role of the non-conventional geometry in acs complexes. It is probably resulted from the weaken of TtBs when going from C···O to C···S and naturally, it takes C–H···O and O···O interactions into account to become more important in acs···2CO_2 complexes.

Table 3.4. Interaction energy and cooperative energy of complexes of aco/acs and 1,2CO_2 and/or 1,2H_2O at CCSD(T)/6-311++G(2d,2p)//MP2/6-311++G(2d,2p)

Complex	E_{int}	E_{coop}	Complex	E_{int}	E_{coop}
Zc-1	-2.0(-1.5)	_	**Zcw-1**	-6.4(-5.2)	-1.8(-1.6)
Zc-2	-1.8(-1.4)	_	**Zcw-2**	-5.9(-4.1)	-1.0(-0.9)
Oc-3	-1.9	_	**Zww-1**	-8.6(-6.8)	-3.9 (-3.4)
Zw-1	-3.7(-2.7)	_	**Zww-2**	-8.1(-6.6)	-3.9(-3.2)
Zcc-1	-4.4(-2.7)	-0.2(0.1)	**Zww-3**	-7.0(-4.9)	-2.8(-1.5)
Zcc-2	-4.2(-3.4)	-0.3(-0.2)	**Zww-4**	-5.4(-4.6)	-1.2(-1.2)
Zcc-3	-3.8(-2.8)	-0.3(1.0)			
Zcc-4	-3.2(-2.7)	-0.4(-0.2)			

The values in parentheses for acs with CO_2 and H_2O
All energies in kcal.mol^{-1}, corrected for both BSSE and ZPE

The typical contacts in aco···1,2CO2 complexes are C···O TtB with a cooperative additional contribution of C−H···O HB, as reported previously.[9,44,45,48] AIM results also give the same observation that the acs···1,2CO_2 complexes seem be loosely packed and balanced by multiple weak interactions because of the approximation of $\rho(r)$ values at BCPs of intermolecular interactions. The $\rho(r)$ values of C···S contact are remarkably lower than those of C···O one, while other interactions are mostly unchanged (*cf.* Table A2 and A3 of *Appendix*). This result is in line with the previous study that the C···S contact is less stable than that of the C···O one in R-CHO(S)···CO_2 (R = F, Cl, Br, H, CH_3) complexes.[42] The decreasing strength of TtBs from C···O to C···S is suitable for the higher stability of aco relative to acs complexes, indicating a crucial role of TtB in stabilizing complexes.

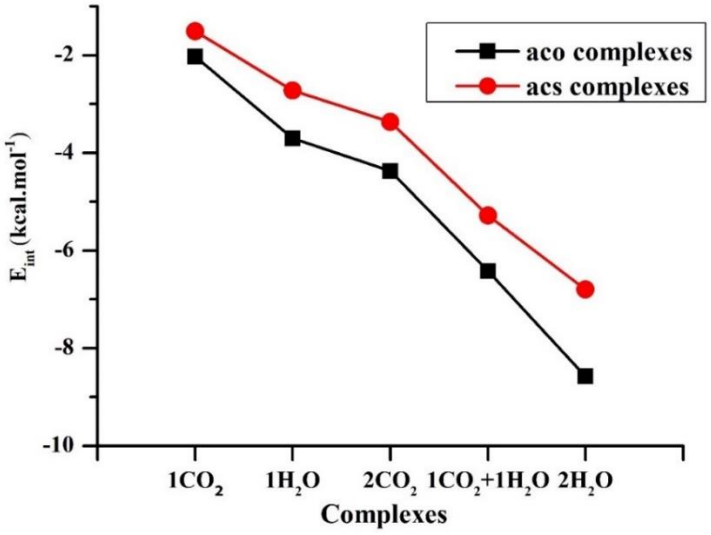

Figure 3.4. The correlation in interaction energies of the most energetically favorable structures in six systems at CCSD(T)/6-311++G(2d,2p)//MP2/6-311++G(2d,2p)

The interaction energy of -3.7 kcal.mol^{-1} of **Ow-1** is completely fitted with result G2M method[138] and more negative than that of **Sw-1** by around 1 kcal.mol^{-1}. The stability of $2H_2O$ complexes is decreasingly ordered as **Zww-1** > **Zww-2** > **Zww-3** > **Zww-4** (**Z** = **O**, **S**). The **Oww-1** with E_{int} of -8.6 kcal.mol^{-1} has been reported for the first time to be the most stable structure of aco···$2H_2O$ instead of **Oww-2** in the Liao's work.[138] From **Zw-1** to **Zww-1**, the binding energy is remarkably increased by 4.9 kcal.mol^{-1} for **Z=O** and 4.1 kcal.mol^{-1} for **Z=S**. For acz···CO_2···H_2O system, the more negative E_{int} of 1 kcal.mol^{-1} indicates that **Zcw-1** is more stable than **Zcw-2**. The obtained results show that all energetically preferred complexes belong to the cyclic geometries in which sub-molecules interact mutual. This gives evidence that cyclic structures reinforce the stability upon complexation. It is expected an existence of positive cooperativity between intermolecular interactions in aco/acs ternary complexes. Similar to $1,2CO_2$ systems, the aco···$1,2H_2O$ and aco···$1CO_2$···$1H_2O$ complexes are also found to be more stable than the corresponding derivatives of acs. This observation is clarified on the basis of obtained results from AIM analysis. The E_{HB} values of O–H···O HBs are significantly more negative than those of O–H···S ones, implying a stronger strength of the former compared to the later HBs. The electron densities at BCPs of

these interactions also have the same trend, indicating a good linear correlation of E_{HB} and $\rho(r)$ in aco and acs complexes (*cf.* Fig. A5). Moreover, individual energies of O–H···O/S HBs are incredibly more negative than those of C–H···O HBs, indicating the main contribution of O–H···O/S HBs to the stability of H_2O complexes. The correlation in stabilities of global minimum structures is represented in Fig. 3.4.

There is a great similarity in energetic behaviour of aco and acs complexes when both of them interact with CO_2 and/or H_2O guest molecules. The stability of aco complexes is typically larger than that of acs ones by 0.5-2.0 kcal.mol^{-1}. This implies that the interactions of aco with CO_2 and/or H_2O are more thermodynamically favorable than those of acs in gas phase. An addition of one H_2O molecule into aco/acs···CO_2/H_2O binary complexes leads to an enhancement of binding energy by 3.7-4.9 kcal.mol^{-1} while a less binding energy increase of 1.9-2.7 kcal.mol^{-1} is estimated in adding of one CO_2 molecule into these binary complexes. As a result, the addition of H_2O is favored than that of CO_2 in stabilizing studied complexes.

In order to clarify the solvent-solvent interactions, we performed calculations for $(CO_2)_n$ and $(H_2O)_n$ (n = 2, 3) at the same level with those for complexes of aco/acs. The most stable structures and their interaction energies were collected in Fig. A6 and Table A4 of *Appendix*, in well agreement with previous works.[135,137] The interaction energies of $(CO_2)_2$ and $(CO_2)_3$ at CCSD(T)/6-311++G(2d,2p)//MP2/6-311++G(2d,2p) are *ca.* -1.2 and -3.6 kcal.mol^{-1}, respectively. Both of them are less negative than those of corresponding complexes of aco but they are comparable with values of acs with 1,2CO_2. It indicates that carbon dioxide has stronger interaction with carbonyls as compared to thiocarbonyls and carbon dioxide. The present interactions energies are -2.2 and -8.1 kcal.mol^{-1} for $(H_2O)_2$ dimer and $(H_2O)_3$ trimer, respectively. Accordingly, the aco···H_2O interaction is predicted to be stronger than solvent-solvent interaction between H_2O

molecules. However, in case of acs, binary complex with H_2O is more stable than $(H_2O)_2$, while the ternary one with $2H_2O$ is less stable than $(H_2O)_3$.

To generalize the trends on interaction capacity and predominant interactions of complexes between organic compounds and $1,2CO_2$ and/or $1,2H_2O$, results of previous studies and this work are summarized in Table 3.5a-b.

Table 3.5a. Concise summary of interactions between some organic compounds and CO_2

Complexes	Level of theory	E_{int}* ($kJ.mol^{-1}$)	Dominant interaction	Source
DMSO···$1CO_2$ DMSO···$2CO_2$	CCSD(T)/6-311++G(2d,2p) **	-13.5 -27.1	Tetrel bond n(O)→π*(C=O)	This work
aco···$1CO_2$ aco···$2CO_2$	CCSD(T)/6-311++G(2d,2p) **	-8.4 -18.4	Tetrel bond n(O)→π*(C=O)	This work
acs···$1CO_2$ acs···$2CO_2$	CCSD(T)/6-311++G(2d,2p) **	-6.3 -14.2	*Interactions contribute nearly equal*	This work
CH_3OCH_3···$1CO_2$ CH_3OCH_3···$2CO_2$	MP2/aug-cc-pVTZ **	-13.3 -19.9	Tetrel bond n(O)→π*(C=O)	This work
$CH_3OCH(CH_3)_2$···$1CO_2$ $CH_3OCH(CH_3)_2$···$2CO_2$	MP2/aug-cc-pVTZ **	-15.1 -22.5	Tetrel bond n(O)→π*(C=O)	This work
CH_3OCHX_2···$1CO_2$ CH_3OCHX_2···$2CO_2$ (X = F, Cl, Br)	MP2/aug-cc-pVTZ **	-10.7→ -11.9 -18.1 →-25.0	Tetrel bond n(O)→π*(C=O)	This work
CH_3SCH_3···$1CO_2$ CH_3SCH_3···$2CO_2$	MP2/aug-cc-pVTZ **	-9.9 -15.2	Tetrel bond n(S)→π*(C=O)	This work
RCHO···$1CO_2$ (R=H, CH_3)	CCSD(T)/6-311++G(2d,2p) **	-1.5 (R=H) -1.9 (R=CH_3)	Tetrel bond n(O)→π*(C=O)	This work (Geometries from Ref 40,44)
XCH=CHX···$1CO_2$ (X = H, F, Cl, Br)	CCSD(T)/aug-cc-pVTZ **	≈-2.0	Tetrel bond and HB n(X)→π*(C=O) n(O)→σ*(C–H)	145
CH_3OH···$1CO_2$	CCSD(T)/6-311++G(2d,2p) **	-9.4	Tetrel bond n(O)→π*(C=O)	This work
C_2H_5OH···$1CO_2$ C_2H_5OH···$2CO_2$	MP2/aug-cc-pVTZ **	-11.4 -23.9	Tetrel bond n(O)→π*(C=O)	This work
C_2H_5SH···$1CO_2$	CCSD(T)/6-311++G(2d,2p) **	-6.1	Tetrel bond n(S)→π*(C=O)	This work
C_2H_6···$1CO_2$	MP2/6-311+g(2d,p)	-2.9	-	58
$CH_3(S=S)CHX_2$···$1CO_2$ (X = H, CH_3, F, Cl, Br)	MP2/aug-cc-pVTZ **	≈-3.5	Tetrel bond n(S)→π*(C=O)	22

*All values are corrected both ZPE and BSSE

** Geometries optimized at MP2/6-311++G(2d,2p)

Table 3.5b. Concise summary of interactions of organic compounds and H_2O (and CO_2)

Complexes	Level of theory	E_{int}* ($kJ.mol^{-1}$)	Dominant interaction	Source
DMSO···$1H_2O$ DMSO···$2H_2O$	CCSD(T)/6-311++G(2d,2p)**	-27.1 -51.7	O–H···O HB n(O)→ σ*(O–H)	This work
aco···$1H_2O$ aco···$2H_2O$	CCSD(T)/6-311++G(2d,2p)**	-15.5 -36.0	O–H···O HB n(O)→ σ*(O–H)	This work
acs···$1H_2O$ acs···$2H_2O$	CCSD(T)/6-311++G(2d,2p)**	-11.3 -28.5	O–H···S HB n(S)→ σ*(O–H)	This work
CH_3OCH_3···$1H_2O$ CH_3OCH_3···$2H_2O$	MP2/aug-cc-pVTZ **	-16.0 -37.2	O–H···O HB n(O)→ σ*(O–H)	This work
$CH_3OCH(CH_3)_2$···$1H_2O$ $CH_3OCH(CH_3)_2$···$2H_2O$	MP2/aug-cc-pVTZ**	-19.3 -41.8	O–H···O HB n(O)→ σ*(O–H)	This work
CH_3OCHX_2···$1H_2O$ CH_3OCHX_2···$2H_2O$	MP2/aug-cc-pVTZ **	-10.1→-10.6 -32.4→-34.1	C–H···O HB n(C)→ σ*(O–H)	This work
CH3OH···$1H_2O$	CCSD(T)/6-311++G(2d,2p) **	-12.6	O–H···O HB n(O)→ σ*(O–H)	This work
C_2H_5SH···$1H_2O$	CCSD(T)/6-311++G(2d,2p) **	-9.8	O–H···S HB n(S)→ σ*(O–H)	This work
DMSO···$1CO_2$···$1H_2O$	CCSD(T)/6-311++G(2d,2p)**	-39.0	O–H···O HB n(O)→ σ*(O–H)	This work
aco···$1CO_2$···$1H_2O$	CCSD(T)/6-311++G(2d,2p)**	-26.8	O–H···O HB n(O)→ σ*(O–H)	This work
acs···$1CO_2$···$1H_2O$	CCSD(T)/6-311++G(2d,2p)**	-21.6	O–H···S HB n(S)→ σ*(O–H)	This work
CH3OH···$1CO_2$···$1H_2O$	CCSD(T)/6-311++G(2d,2p) **	-25.3	O–H···O HB n(O)→ σ*(O–H)	This work
C_2H_5SH···$1CO_2$···$1H_2O$	CCSD(T)/6-311++G(2d,2p) **	-21.3	O–H···S HB n(S)→ σ*(O–H)	This work

*All values are corrected both ZPE and BSSE

** Geometries optimized at MP2/6-311++G(2d,2p)

Clearly, the interaction capacity of CO_2 with functionalized compounds is higher than that with hydrocarbons or even with their halogen derivatives. Accordingly, dimethyl sulfoxide, acetone, dimethyl ether is considered to be more effective than ethanol, methanol, ethanthiol, acetaldehyde, formaldehyde, thioacetone, halogen derivatives of ethylene and finally, ethane in aiming of carbon dioxide capture. Another importance achievement found in Table 3.5a-b is the general trend to determine the primary interactions for binary/ternary systems with only CO_2/H_2O or simultaneous CO_2+H_2O. The complexes with CO_2 are mainly

determined by C···O/S TtB typed n(O/S)→π*(C=O) (with exception of hydrocarbons and thioacetone complexes). The presence of H_2O in complexes regularly produces strong O–H···O/S HBs to strengthen the corresponding complexes. The O–H···O/S HBs are particularly efficient to reinforce other interactions.

a) Acetone complexes

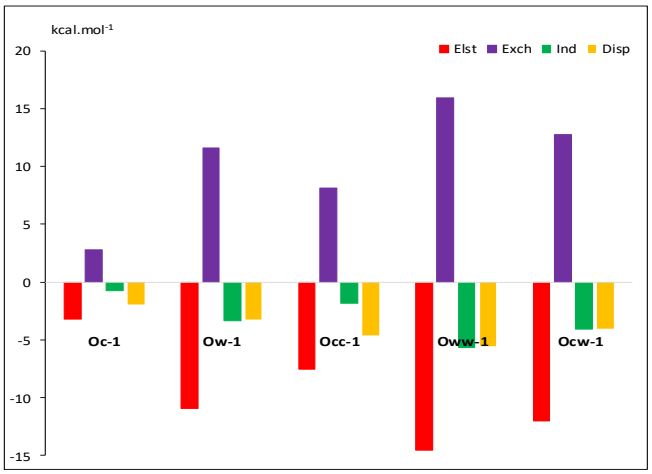

b) Thioacetone complexes

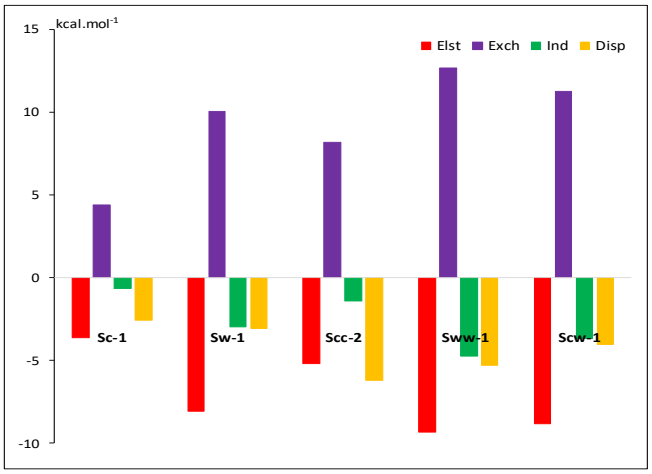

Figure 3.5. SAPT2+ decompositions of the most stable complexes into physically energetic terms: electrostatic (Elst), exchange (Exch), induction (Ind) and dispersion (Disp) at aug-cc-pVDZ basis set

To solve the differences in complex stability, the molecular electrostatic potentials of isolated monomers at MP2/aug-cc-pVTZ level are illustrated in Fig. A7 of *Appendix*. The change in electrostatic potential energy from negative to positive is described by different color from red < orange < yellow < green < blue. It shows a more negative electrostatic potential of O site in comparison with that of

S site. Besides, C and H atoms of CO_2 and H_2O located at blue regions show the positive charge or the absence of electrons. This result it is a well explanation for the larger stability of aco relative to acs complexes when intermolecular interactions are based solely on attractive electrostatic consideration. Indeed, the SAPT2+ decomposition of interaction energy shows the largest contribution of electrostatic component into complex stability (*cf.* Fig. 3.5). The contribution of electrostatic terms considerably increases from binary to ternary complexes, especially with the presence of H_2O. This evidence supports for the larger magnitude in stability of complexes with H_2O presence as compared to CO_2 one. In short, the solubility of aco and acs in co-solvent of $scCO_2$ and water is expected to be higher than that in sole $scCO_2$ solvent.

Weak interactions can affect mutual to strengthen the stability of ternary complexes, which is qualitatively examined *via* cooperative energies (*cf.* Table 3.4). The negative values of E_{coop} are in consistent with the expectation of positive cooperative effect in ternary systems. The cooperative energies of aco complexes are more negative than the corresponding ones of acs by 0.1-1.3 kcal.mol^{-1}. Namely, the most negative values of E_{coop} belong to **Zww-1** complexes (-3.9 and -3.4 kcal.mol^{-1} for **Oww-1** and **Sww-1**, respectively) while those in $2CO_2$ systems are really small and even get positive value in **Scc-1** and **Scc-3**. Furthermore, the enhancement in strength of interactions from binary to ternary complexes obtained from the changes of $\rho(r)$ and E_{HB} affirms the positive cooperative effect between interactions in complex stabilization. The trend of calculated cooperative energies is consistent with that of interaction energies of investigated systems. This positive behaviour of cooperativity is also observed in DMSO···$2CO_2$ and DMSO···$2H_2O$ complexes with the cooperative energies of -0.3 and -5.4 kcal.mol^{-1}, respectively.[124] It implies that the O−H···O HBs in $2H_2O$ complexes with a high electrostatic characteristic give a stronger cooperativity in comparison to C···O(S) in $2CO_2$ ones. Thus, an addition of H_2O as compared to CO_2 molecule to binary complexes gives rise to a larger increase of positive cooperativity which leads to an enhancement of

stability of ternary complexes.

3.2.3. NBO analysis, and hydrogen bonds

In order to evaluate the charge-transfer effect, the EDT and the $E^{(2)}$ are executed at *w*B97X-D/6-311++G(2d,2p) level of theory (Table A5 and A6). The overlap orbitals describing the primary orbital interactions of the most stable binary complexes are plotted in Fig. A8. The positive EDT values of aco and acs units in the most favorable complexes implies that electron transfers taking place from aco/acs to CO_2 and/or H_2O. The EDT magnitude is quite small for complexes relevant CO_2, however, it becomes significantly larger in H_2O complexes. This suggests a stronger electron transfer from aco/acs to H_2O relative to CO_2.

For **Oc-1** and **Occ-1** complexes, the $E^{(2)}$ values of Lp(O)→π*(C=O) transfers (1.4-1.5 kcal.mol^{-1}) are marginally higher than those of remaining interactions (0.2-0.7 kcal.mol^{-1}) including π(C=O)→π*(C=O) and Lp(O)→σ*(C–H). Consequently, the primary orbital interaction in aco···1,2CO_2 systems is the donation of Lp(O) into π*(C=O) of CO_2 (*cf.* Fig. A8 of *Appendix*). For **Sc-1** and **Scc-2** complexes, $E^{(2)}$ values of Lp(S)→π*(C=O) interactions range from 0.9 to 1.0 kcal.mol^{-1}, in competition with those of Lp(O)→σ*(C–H). It is well consistent with the AIM results that in acs···1,2CO_2 systems, both S···C=O TtB and C–H···O HB determine the stability of complexes. From binary to ternary complexes, the second-order energies of these interactions change insignificant, consistent with the quite slight positive cooperativity between them.

Tables A5 and A6 also point out the Lp(O/S)→σ*(O–H) and Lp(O)→σ*(C–H) processes represented for the O–H···O/S and C–H···O HBs orbital interactions. The $E^{(2)}$ values of the O–H···O/S HBs are roughly 10.1 kcal.mol^{-1} in **Ow-1** and 9.6 kcal.mol^{-1} in **Sw-1**. Both of them are remarkably larger than those of C–H···O HBs (0.8-0.9 kcal.mol^{-1}), affirming the considerable strength of the O–H···O/S relative to C–H···O HBs. For acz···2H_2O ternary systems, the dominant role of O–H···O/S HBs is also observed. Thus, the $E^{(2)}$ values of Lp(O/S)→σ*(O–H) interaction range from 6.7 to 13.5 kcal.mol^{-1} while the

Lp(O)→σ*(C–H) transfer is considerably weaker, with the $E^{(2)}$ values of 0.1-1.3 kcal.mol^{-1}. From **Zw-1** to **Zww-1**, the charge-transfer energies of Lp(O/S)→σ*(O–H) intermolecular interactions are increased by 0.5-1.0 kcal.mol^{-1}. For **Zcw-1**, it exits both of Lp(O/S)→σ*(O–H) and Lp(O/S)→π*(C=O) orbital interactions, in which the $E^{(2)}$ values of the formers are incredibly higher than those of the laters by 9.7-11.0 kcal.mol^{-1}, indicating the dominant charge-transfer contribution of the O–H···O/S HBs as compared to C=O···O/S TtB. Combined to other complexes from Table 3.5a-b, it is predicted a general trend to determine the primary interactions for binary/ternary systems with only CO_2/H_2O or simultaneous CO_2+H_2O. The C···O/S tetel bond typed n(O/S)→π*(C=O) is found to determine the stability of complexes containing 1,2 CO_2. Whereas, the presence of H_2O in complexes regularly produces strong O–H···O/S HBs to strengthen the corresponding complexes. The O–H···O/S HBs are particularly efficient to reinforce other interactions.

Table 3.6 provides the changes in X–H bond lengths (Δr(X–H)) and its stretching frequency (Δν(X–H)) for typical HBs in examined complexes in comparison with relevant monomers. Upon complexation, all O–H bonds involving O–H···O are elongated by 4.1-14.1 mÅ and red-shifted within 62.3-271.9 cm^{-1}. Accordingly, they are determined as red-shifting HBs. In addition, an elongation of O-H bond length and a decrease of its corresponding stretching frequency in aco systems are generally much more than those in acs ones, implying a stronger red-shift magnitude of O–H stretching frequencies in the formers following complexation. Nevertheless, the obtained results indicate that the changes of C–H bond length and its concomitant stretching frequency are quite slight. For complexes involving CO_2, the compression of 0.1-0.7 mÅ and the blue-shift in stretching frequency of 1.1-17.9 cm^{-1} in C–H bonds involving HBs are observed as shown in Table 3.6, indicating characteristics of the blue-shifting HB. In going from 1,2CO_2 to 1,2H_2O systems, the distance changes of C–H bonds involving C–H···O

HBs are increased, and their stretching frequencies are red-shift with a small magnitude. This is evident that the blue-shift characteristic of C–H in C–H···O HB changes to red-shift one by the effect of H_2O addition.

Table 3.6. Changes of bond length (Δr(X-H), in mÅ) and stretching frequency (Δν(X-H), in cm^{-1}) of C-H and O-H bonds involved in hydrogen bond

Complex	Bond	Δr(X-H)	Δν(X-H)	Complex	Bond	Δr(X-H)	Δν(X-H)
Zc-1	C1-H2	-0.2(-0.1)	5.8(6.2)	**Zww-2**	C1-H2	0.9(-0.8)	-5.3(19.4)
Sc-2	C1-H3	(-0.1)	(3.3)		O11-H12	14.1(12.7)	-271.9(-259.2)
	C5-H7	(-0.1)	(3.3)		O14-H15	12.5(11.1)	-247.3(-220.2)
Zw-1	C1-H2	0.2(-0.3)	1.9(10.6)	**Zww-3**	C1-H2	0.2(0)	2.4(6.4)
	O11-H12	10.0(8.9)	-200.1(-187.5)		C5-H6	0. 2(0)	2.4(6.4)
Zcc-1	C1-H2	-0.2(0)	5.6(5.2)		O11-H12	8.6(7.6)	-172.7(-160.4)
Zcc-2	C1-H2	-0.1(-0.2)	3.8(4.7)		O14-H15	8.6(7.6)	-172.7(-160.4)
	C1-H3	(0.3)	(1.1)	**Zww-4**	C1-H2	0.2(0.1)	2.4(5.4)
	C5-H7	(-0.3)	(6.3)		O11-H12	7.3(6.2)	-147.3(-139.0)
Zcc-3	C1-H3	(0.1)	(2.3)		O11-H13	5.2(6.3)	-109.9(-126.5)
	C1-H4	(0.1)	(2.3)	**Zcw-1**	C1-H2	-0.3(-1.0)	10.5(21.8)
	C5-H7	(0.1)	(2.3)		O14-H15	11.4(10.2)	-230.6(-216.0)
	C5-H8	(0.1)	(2.3)	**Zcw-2**	C1-H2	0.4(0)	0(6.7)
Zcc-4	C1-H2	-0.6(-0.7)	13.2(17.9)		C5-H6	0.2(0)	1.0(5.2)
Zww-1	C1-H3	0.6(0.5)	1.0(1.8)		O14-H15	9.2(8.5)	-185.4(-178.4)
	C5-H7	-2.2(-0.8)	28.1(14.8)				
	O11-H12	13.6(10.1)	-240.0(-204.9)				
	O14-H15	11.7(11.0)	-226.1(-211.7)				

Values in parenthesis for acs complexes

Results listed in Table A7 show that the s-character percentage of O atom and σ-antibonding orbital electron density of O–H bonds are increased upon complexation. In the context, an O-H elongation, and its red-shift of stretching frequency are determined by an increase of population in the σ*(O-H) orbital (0.0109-0.0235 au for aco and 0.0160-0.0319 au for acs derivatives) overcoming an increase in *s*-character of O hybridized atom. An increase of %*s* character in C atom determines the C–H distance contraction and causes the blue-shift of C–H stretching frequency in complexes involving CO_2.

3.2.4. Remarks

The quantum calculations on interactions of acetone/thioacetone with CO_2 and/or H_2O establish general trends in geometric structures, stability and properties of formed complexes. All structures are primarily supported by TtB or O–H···O/S

HB, and the non-conventional complexes are found for not only aco but also acs system. An addition of H_2O or CO_2 molecule into binary complexes leads to an increase in the stability of the corresponding ternary ones, and it is larger for the H_2O than CO_2 addition. A larger positive cooperativity is also found in case of H_2O relative to CO_2 addition. The solubility of aco and acs in $scCO_2$ with the presence of water as cosolvent is promising to be better than that that in pure $scCO_2$.

Remarkably, the complexes of CO_2 and/or H_2O with aco are more stable than those with acs, and the larger positive cooperativity of ternary complexes is estimated in the aco relative to acs systems. It is found that the stabilities of considered complexes are contributed mainly by electrostatic energy. The complexes of $1,2CO_2$ with aco are primarily stabilized by C···O TtBs while those with acs are balanced by multiple weak interactions. For complexes relevant H_2O, the O–H···O/S dominating C–H···O HB plays a decisive role in stabilizing the complexes.

All O−H···O HBs in the systems investigated belong to red-shifting HBs, which is caused by an increase of electron occupation of σ*(O−H) antibonding orbital overcoming an increase of s-character of O hybridized atom. A contraction of C−H bond length and an increase of its stretching frequency in the C−H···O HB in CO_2 complexes are apparently governed by an increase of *s*-character percentage in C−hybridized atom.

3.3. Interactions of methanol with CO_2 and H_2O

This section is based on the results of Ref. 139.

3.3.1. Structures and AIM analysis

Stable structures formed by interactions of CH_3OH with CO_2 and H_2O, and selected geometric parameters are presented in Fig. 3.6, denoted by **DX-Met-n** and **TCH-Met-n**, where **D**, **T** represent dimers and trimers, respectively; **X = C**, **H** (C for CO_2, H for H_2O); **n** = **1**, **2**, **3**, … are ordinal numbers of isomers. The selected characteristics at BCPs of intermolecular interactions are also listed in Table 3.7.

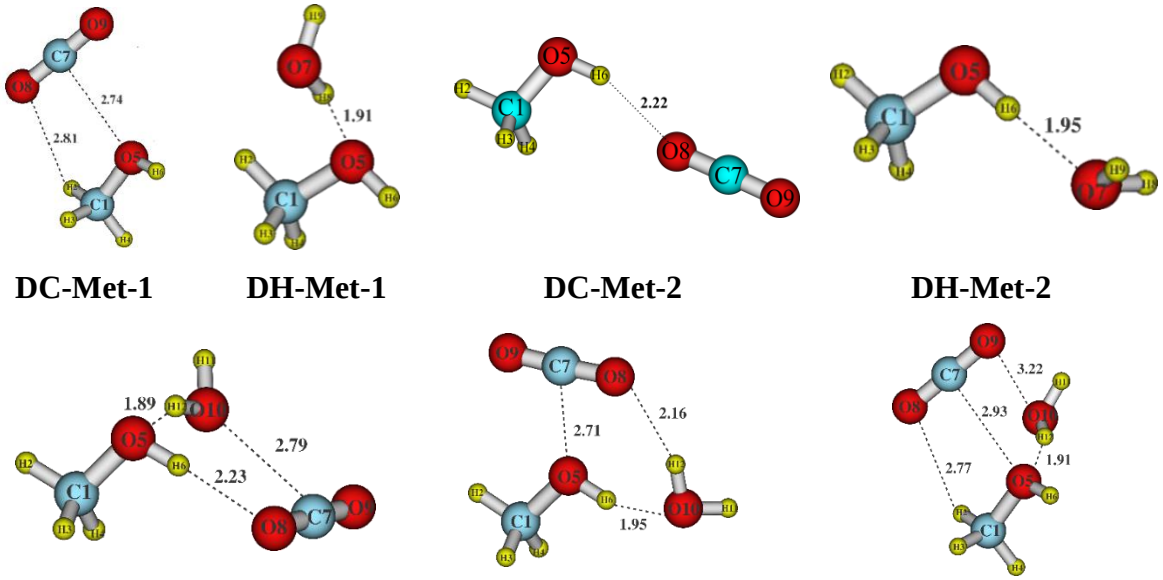

Figure 3.6. Stable geometries of complexes formed by interaction of CH_3OH with CO_2 and H_2O at MP2/6-311++G(2d,2p) (all intermolecular distances in Å)

Data in the Fig. 3.6 show that the intermolecular distances between O and C, O and H are in the ranges of 2.71-2.93 Å and 1.91-2.81 Å, respectively; and most of them are smaller than the sum of van der Waals radii of the two relevant atoms (3.22 Å for O···C contact and 2.72 Å for O···H one). This result supports for the presence of O···C=O TtBs and O−H···O hydrogen ones upon complexation. In contrast, the C1−H2···O8 distances in **DC-Met-1** and **TCH-Met-3** are larger than the sums of van der Waals radii of the two isolated atoms. The existence of these C−H···O HBs, however, would be proved from AIM and NBO analyses. In four stable structures of binary complexes, CO_2 or H_2O guest molecule are located around the -OH group of CH_3OH host molecule. While **DC-Met-1** is stabilized by O···C=O TtB and C−H···O HB, **DH-Met-1** is obtained by the formation of O−H···O HB. Both **DC-Met-2** and **DH-Met-2** complexes are strengthened by O−H···O HBs involving -OH group of methanol and O atom of CO_2 or H_2O molecule. The obtained geometrical parameters are in good agreement with the previous studies for $CH_3OH\cdots CO_2$ and $CH_3OH\cdots H_2O$ heterodimers.[40,140,141] The intermolecular interactions in three stable structures of the $CH_3OH\cdots CO_2\cdots H_2O$ system are

mutually associated which is described by the presence of ring critical points from AIM topologies. Also, an O···O ChB is found in **TCH-Met-3** geometry.

Table 3.7. Selected parameters at the BCPs of intermolecular contacts in complexes of methanol with CO_2 and/or H_2O at MP2/6-311++G(2d,2p)

Complex	**Contact**	$\rho(r)$ (au)	$\nabla^2(\rho(r))$ (au)	$H(r)$ (au)	E_{HB} (kJ.mol^{-1})
DC-Met-1	O5···C7=O8	0.0118	0.051	0.0016	-
DC-Met-2	O5−H6···O8	0.0108	0.046	0.0012	-10.3
DH-Met-1	O7−H8···O5	0.0267	0.091	0.0005	-28.7
DH-Met-2	O5−H6···O7	0.0239	0.083	0.0009	-24.9
TCH-Met-1	O10−H12···O5	0.0290	0.096	-0.0002	-31.9
	O5−H6···O8	0.0121	0.047	0.0015	-11.5
	O10···C7=O8	0.0107	0.045	0.0015	-
TCH-Met-2	O5−H6···O10	0.0244	0.088	0.0009	-26.3
	O10−H12···O8	0.0128	0.052	0.0019	-12.3
	O5···C7=O	0.0131	0.053	0.0014	-
TCH-Met-3	O10−H12···O5	0.0257	0.092	0.0009	-28.0
	O5···C7=O8	0.0083	0.035	0.0013	-
	C1−H2···O8	0.0056	0.022	0.0009	-4.8
	C7=O9···O10	0.0067	0.027	0.0010	-

From Table 3.7, all the values of $\rho(r)$ and $\nabla^2\rho(r)$ at BCPs of interactions are in the ranges of 0.006-0.029 au and 0.022-0.096 au, respectively; and most of H(r) values at BCPs are positive (0.0005-0.0019 au). These results indicate that most of them are noncovalent weak interactions.[132] It is interesting that the O−H···O HB in **TCH-Met-1** (with the highest values of $\rho(r)$ and E_{HB}) behaves a slightly negative total electron energy density implying a small covalent part in nature. From optimized structures in Fig. 3.6, it is distinguished three types of O−H···O HBs: O−H···O_m, O−H···O_w and O−H···O_c in which O_m, O_w and O_c are denoted for oxygen atom of CH_3OH, H_2O and CO_2, respectively. Based on $\rho(r)$ and E_{HB} negative values, it is predicted that the stability of these interactions decreases in order of O−H···O_m > O−H···O_w > O−H···O_c, which is in good agreement with Fileti *et al.*[140] Indeed, the $\rho(r)$ at BCP and E_{HB} values of O−H···O_m are in the ranges of 0.026-0.029 au and 28.0-31.9 kJ.mol^{-1}, respectively; which are slightly higher than those of O−H···O_w (0.023-0.024 au, 24.3-26.3 kJ.mol^{-1}) and considerably higher than

O−H···O_c (0.012-0.013 au, 11.5-12.3 kJ.mol^{-1}). It is also proved *via* distances of intermolecular contacts, while the lengths of H···O_m contact range from 1.89 to 1.91 Å, the distances of H···O_w/O_c are higher and in the range of 1.95-2.23 Å. Considered to the remaining interactions, the $\rho(r)$ values of 0.008-0.013 au for O_m/O_c···C=O TtBs are smaller than those for C−H···O HBs (0.004-0.006 au) and O···O ChBs (0.007 au). In short, the strength of intermolecular interactions in the examined complexes are predicted to decrease in order of O−H···O_m > O−H···O_w > O−H···O_c > O_m/O_c···C=O > O···O ≈ C−H···O.

Based on obtained strengths of intermolecular interactions above, the stability of binary and ternary complexes could be revealed. Particularly, the stability of CH_3OH···CO_2 and CH_3OH···H_2O could be sorted increasingly as **DC-Met-2** < **DC-Met-1** and **DH-Met-2** < **DH-Met-1**, respectively. For ternary complexes, **TCH-Met-1** and **TCH-Met-2** are mainly stabilized by two O−H···O HBs while **TCH-Met-3** only exists one O−H···O HB. Comparision to electron density at BCPs of intermolecular interactions, it is supported that the stability of CH_3OH···CO_2···H_2O complexes decreases in going from **TCH-Met-1**, **TCH-Met-2** to **TCH-Met-3**. In addition, in cases of CH_3OH···H_2O and CH_3OH···CO_2···H_2O systems, the O−H···O_m HBs formed by -OH of H_2O and oxygen of CH_3OH dominate the remaining interactions in determining the stability of these complexes. In a word, the CH_3OH···CO_2 complex is mainly stabilized by the O···C=O TtB while the O−H···O HB strengthens the complex involving H_2O.

3.3.2. Interaction and cooperative energies

Table 3.8 illustrates the interaction and cooperative energies with both ZPE and BSSE corrections of complexes at CCSD(T)/6-311++G(2d,2p) using optimized geometries at MP2/6-311++G(2d,2p). For binary complexes, the interaction energy of **DC-Met-1** is *ca.* 5.5 kJ.mol^{-1} more negative than that of **DC-Met-2**, implying that **DC-Met-1** is the most stable structure of CH_3OH···CO_2. The interaction energy with ZPE and BSSE of **DH-Met-1** is *ca.* -12.6 kJ.mol^{-1} and slightly negative than that of **DH-Met-2** by 1.5 kJ.mol^{-1} leading to the preference of **DH-Met-1** geometry

compared to **DH-Met-2** one in $CH_3OH\cdots H_2O$ system. In both **DC-Met-1** and **DH-Met-1** structures, CH_3OH subunit plays a role as an electron donor or Lewis base while it acts as an electron acceptor in **DC-Met-2** and **DH-Met-2**. From these observations, it is predicted that when CH_3OH interacts with CO_2 or H_2O guest molecules, it tends to be a Lewis base. This could be understood by evaluating proton affinity (PA) at oxygen site in relevant monomers. Thus, at the CCSD(T)/aug-cc-pVTZ level of theory, the obtained PA of O sites in CH_3OH, H_2O and CO_2 are 720.00, 653.41 and 611.72 $kJ.mol^{-1}$, respectively. The decreasing order of PA values at O sites from CH_3OH to H_2O and finally to CO_2 indicates that CH_3OH are stronger Lewis base in comparison with H_2O and CO_2. Moreover, it can be seen that the $CH_3OH\cdots CO_2$ complexes is less stable than the $CH_3OH\cdots H_2O$ ones, which indicates a better interaction of CH_3OH host molecule with H_2O as compared to CO_2 guest molecule. For $CH_3OH\cdots CO_2\cdots H_2O$ system, the complex strength is enhanced in the sequence of **TCH-Met-3** < **TCH-Met-2** ≈ **TCH-Met-1** (*cf.* Table 3.8). The calculated data from energetic analysis is in good agreement with AIM results. Remarkably, interaction energy of ternary complexes is much more negative than binary ones by 12.7-24.5 $kJ.mol^{-1}$, suggesting that the addition of a CO_2 or H_2O molecule into dimers leads to an increase in the stability of the formed trimers, in which the increasing magnitude is higher for the adding of H_2O than the CO_2 counterpart.

Table 3.8. Interaction energy and cooperative energy of complexes formed by interactions between CH_3OH with CO_2 and/or H_2O at CCSD(T)/6-311++G(2d,2p)//MP2/6-311++G(2d,2p) ($kJ.mol^{-1}$)

Complex	E_{int}	Complex	E_{int}	E_{coop}
DC-Met-1	-9.4	**TCH-Met-1**	-25.3	-8.9
DC-Met-2	-3.9	**TCH-Met-2**	-25.3	-8.7
DH-Met-1	-12.6	**TCH-Met-3**	-21.1	-3.8
DH-Met-2	-11.1			

To evaluate the cooperativity of intermolecular interactions, we also calculated the cooperative energy of ternary complexes, as shown in Table 3.23. It can be seen that all values of E_{coop} of ternary complexes are negative in ranging

from -3.8 to -8.9 kJ.mol^{-1}, indicating that the formed interactions work in concert and enhance the complex stability. The cooperative effect is stronger for **TCH-Met-1** and **TCH-Met-2** compared to the remaining complex by about 5 kJ.mol^{-1}. The absolute values of E_{coop} are decreased in consistent with the decreasing order of complex stability which implies a high correlation between cooperative energy and the strength of complexes.

3.3.3. Vibrational and NBO analyses

The NBO analysis is performed at the MP2/6-311++G(2d,2p) level of theory. The charge of CH_3OH subunits, electron transfer processes and the E_{inter} are collected in Table 3.9.

Table 3.9. Changes of bond length (Δr) and corresponding stretching frequency (Δν) of C(O)−H bonds involved in HBs along with selected parameters at MP2/6-311++G(2d,2p)

Complex	**Charge** [a] (e)	**Delocalization**	$\mathbf{E^{(2)}}$ (kJ.mol^{-1})	**Δr** (Å)	**Δν** (cm^{-1})	**Δσ*** (e)	**Δ%s** (%)
DC-Met-1	0.004	n(O5)→π*(C7=O8)	8.20	-	-	-	-
		n(O8)→σ*(C1−H2)	0.54	0.0005	4.5	-0.0003	0.11
DC-Met-2	-0.001	n(O8)→σ*(O5−H6)	3.81	0.0004	4.9	0.0010	0.70
DH-Met-1	0.019	n(O5)→σ*(O7−H8)	37.37	0.0089	-180.3	0.0167	2.79
DH-Met-2	-0.015	n(O7)→σ*(O5−H6)	33.44	0.0058	-107.2	0.0116	2.57
TCH-Met-1	0.023	n(O5)→σ*(O10−H12)	42.55	0.0114	-233.0	0.0210	3.07
		n(O8)→σ*(O5−H6)	4.56	0.0033	-41.9	0.0012	0.77
		n(O10)→π*(C7=O8)	7.44	-	-	-	-
TCH-Met-2	-0.013	n(O_w)→σ*(O5−H6)	30.47	0.0073	-134.1	0.0120	2.66
		n(O_c)→σ*(O10−H12)	11.33	0.0043	-63.4	0.0025	1.22
		n(O5)→π*(C7=O8)	7.27	-	-	-	-
TCH-Met-3	0.018	n(O5)→σ*(O10−H12)	32.44	0.0082	-162.7	0.0145	2.52
		n(O5)→π*(C7=O8)	3.76	-	-	-	-
		n(O9)→σ*(C1−H2)	0.42	-0.0008	15.8	-0.0017	0.47
		n(O10)→π*(C7=O9)	2.55	-	-	-	-

[a] charge of CH_3OH subunit

Charges of CH_3OH components are positive for the three most stable complexes (**DC-Met-1**, **DH-Met-1** and **TCH-Met-1**). This result shows that electron density is transferred from CH_3OH host molecule to CO_2 or H_2O guest molecule. The existence of electron transfer processes from n(O) orbitals to σ*(X−H) (X=C, O) and π*(C=O) antibonding orbitals is the evidence for the

X−H···O HBs and O···C=O TtBs. The presence of n(O8)→σ*(C1−H2) in **DC-Met-1** and its small $E^{(2)}$ value (0.54 kJ.mol^{-1}) indicates for the formation of an additional C−H···O HB in this complex which is not observed from AIM topological analysis. For $CH_3OH···CO_2$ system, the $E^{(2)}$ of n(O5)→π*(C7=O8) in **DC-Met-1** is higher than that of n(O8)→σ*(O5−H6) in **DC-Met-2** by *ca.* 4.39 kJ.mol^{-1}, indicating that the stability of **DC-Met-1** is larger than **DC-Met-2** and the O···C=O TtB plays a decisive role in stabilization of $CH_3OH···CO_2$ complexes. For complexes involving H_2O such as $CH_3OH···H_2O$ and $CH_3OH···CO_2···H_2O$, $E^{(2)}$ values of n(O)→σ*(O−H) are remarkably higher than those of the remaining interactions. These results show a considerable role of the O−H···O HB in stabilizing the complexes.

The changes of the O(C)−H bond lengths (Δr) and its stretching vibrational frequency (Δν) and the factors causing the red/blue shifting of HBs are also gathered in Table 3.9. Most O−H bond lengths increase with an amount of 0.00043-0.0144 Å and a stretching frequency decrease of 41.9–233.0 cm^{-1} as compared to relevant monomers, implying that the O−H···O contacts belong to the red-shifting HBs, except for the O−H bond in **DC-Met-2**. The C−H···O contact in **TCH-Met-3** is characterized as blue-shifting HB because the C−H bond length is contracted by 0.0008 Å and accompanied by a stretching frequency increase of 15.8 cm^{-1} in comparison with those in isolated monomer. As shown in Table 3.26, an elongation of O(C)−H bond length and a decrease of its corresponding stretching frequency are determined by an increase in the electron density at the σ*(O(C)−H) orbital. By contrast, a contraction of C–H bond length and an increase in its stretching vibrational frequency in **TCH-Met-3** is determined by a decrease of the σ*(C–H) electron density and an enhancement of s-character of C(O) hybrid orbital upon complexation.

3.3.4. Remarks

The obtained results show that $CH_3OH···CO_2$ is less stable than $CH_3OH···H_2O$, indicating the stronger interaction of CH_3OH with H_2O compared to CO_2. It is found that the stability of the binary complexes decreases in the ordering

of **DH-Met-1** > **DH-Met-2** > **DC-Met-1** > **DC-Met-2**. For ternary complexes, the addition of a CO_2 or H_2O guest molecule into binary structures leads to an increase in the stability of complexes and the stability of ternary systems decreases from **TCH-Met-1** ≈ **TCH-Met-2** > **TCH-Met-3**. While the $CH_3OH\cdots CO_2$ complex is stabilized by the O=C···O TtB, the O–H···O HB plays a primary role in the stabilization of complexes involving H_2O. Remarkably, there is a large cooperativity (ranging from 3.8 to 8.9 kJ.mol^{-1}) between various types of HBs and TtBs in stabilizing the ternary complexes. The vibrational and NBO results demonstrate that the O−H···O and C−H···O contacts in examined complexes generally belong to the red-shifting HB, except for the C1−H2···O9 in **TCH-Met-3** which belongs to the blue-shifting HB.

3.4. Interactions of ethanethiol with CO_2 and H_2O

This section is based on the results of Ref. 142.

3.4.1. Structure, stability and cooperativity

Three model systems formed by interactions of C_2H_5SH with CO_2 and H_2O at the MP2/6-311++G(2d,2p) level induce stable complexes with different geometric shapes, as shown in Fig. 3.7.

For binary complexes, **DC-thiol-1** structure is formed by C···S electron donor-acceptor interaction and C−H···O hydrogen interaction which is quite consistent with the results reported for $C_2H_5OH\cdots 1CO_2$.[12,13] For $C_2H_5SH\cdots 1H_2O$, geometry of **DH-thiol-2** is also found in the study reported by M. Kieninger *et al.*[143] It is noteworthy that there is no theoretical and experimental study on $C_2H_5SH\cdots 1CO_2\cdots 1H_2O$ system. The interaction energies and cooperative energies of examined complexes are summarized in Table 3.10.

All interaction energies of the examined complexes are negative, indicating that the obtained complexes are stable in gas phase. Interaction energies of ternary complexes range from -10.5 to -21.3 kJ.mol^{-1} with ZPE and BSSE corrections and more negative than those of binary complexes by *ca.* 8.6–15.2 kJ.mol^{-1} for $C_2H_5SH\cdots 1CO_2$ and 7.5–11.5 kJ.mol^{-1} for $C_2H_5SH\cdots 1H_2O$. This result indicates that

the addition of one CO_2 or H_2O guest molecule into binary complexes leads to a considerable increase in the stability of complexes.

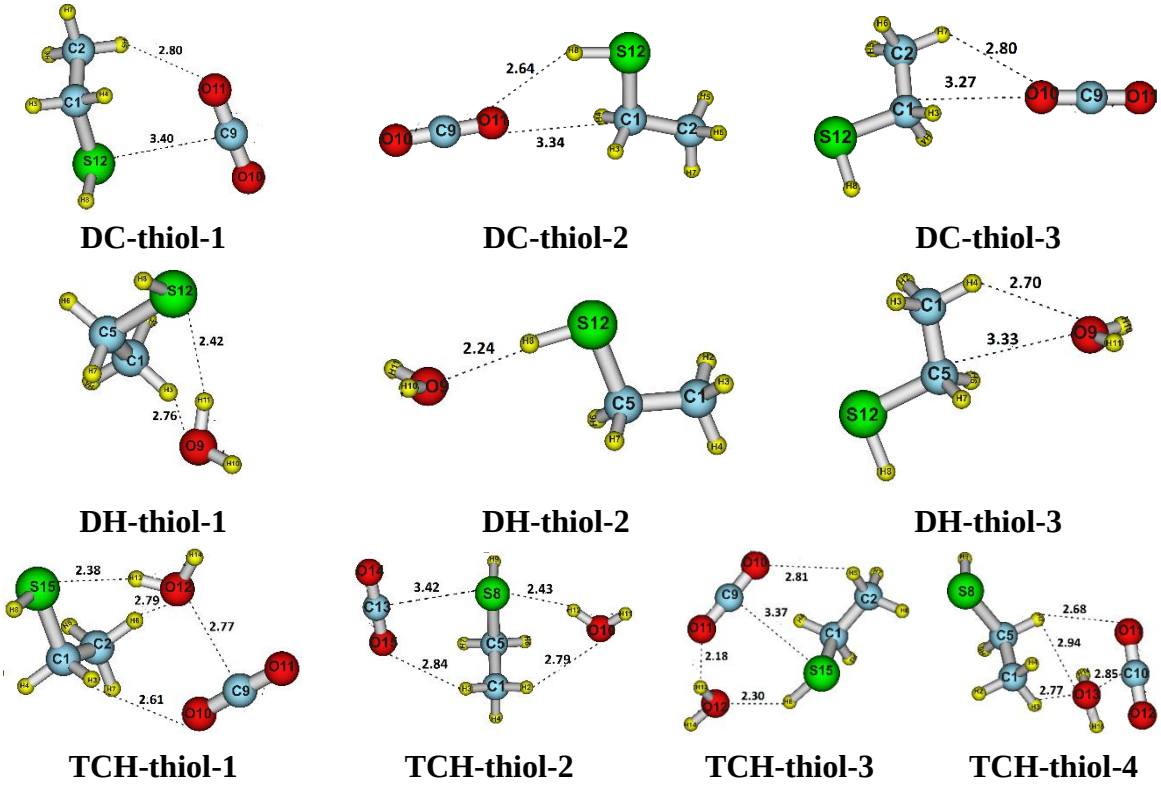

Figure 3.7. Stable geometries of complexes formed by interactions of C_2H_5SH with CO_2 and H_2O at MP2/6-311++G(2d,2p)

Some selected characteristics of BCPs of interactions formed are listed in Table 3.11. It can be seen that the **DC-thiol-1** is more stable than **DC-thiol-2** and **DC-thiol-3** complexes by *ca*. 3.5 and 4.2 kJ.mol^{-1}, respectively. This observation could be explained by the significant contribution of S···C=O TtB in **DC-thiol-1**, combined to AIM characteristics. When the guest molecule goes from CO_2 to H_2O, the **DH-thiol-1** complex is more stable than the **DH-thiol-2** and **DH-3** complexes by *ca.* 6.0 and 6.8 kJ.mol^{-1}, respectively. Table 3.11 indicates that **DH-thiol-1** exists O−H···S strong HB (E_{HB} value is -15.8 kJ.mol^{-1}) while other HBs in the remaining complexes are weaker (based on values of $\rho(r)$ and E_{HB}). Thus, in $C_2H_5SH\cdots1H_2O$, O−H···S HB plays a main role in strengthen the stability of complexes. The stability of ternary complexes increases in order: **TCH-thiol-4 < TCH-thiol-3 < TCH-thiol-2 < TCH-thiol-1**. Similar to $C_2H_5SH\cdots1H_2O$, **TCH-thiol-1** and **TCH-thiol-2**

complexes contain the O−H···S HB with the dramatically larger $\rho(r)$ values, meaning that the O−H···S HB determines the stability of $C_2H_5SH\cdots1CO_2\cdots1H_2O$ system. Notably, the stabilities of three sets of models are sorted in order: **DC-thiol** < **DH-thiol** < **TCH-thiol**. In a word, C···S TtB determines the stability of $C_2H_5SH\cdots1CO_2$, which is in good agreement with the result of C_2H_5OH reported by McGuire *et al*.[150] Nevertheless, for the stability of complexes involved H_2O, the O−H···S HB plays a main role while the C−H···O and C···O act as complementary roles. The cooperative energies with ZPE and BSSE corrections of trimers are also listed in Table 3.10. These values are quite negative, from around -2.2 to -6.4 kJ.mol^{-1}, indicating that formed intermolecular interactions work in concert together and enhance the stability of ternary complexes. The absolute values of E_{coop} decrease in the order of **TCH-thiol-1** > **TCH-thiol-3** > **TCH-thiol-2 > TCH-thiol-4** and are consistent with the decreasing order in the interaction capacity of ternary complexes.

Table 3.10. Interaction energy and cooperative energy of complexes between C_2H_5SH and CO_2 and/or H_2O at CCSD(T)/6-311++G(2d,2p)//MP2/6-311++G(2d,2p), (kJ.mol^{-1})

Dimer	E_{int}	Dimer	E_{int}	Trimer	E_{int}	E_{coop}
DC-thiol-1	-6.1	**DH-thiol-1**	-9.8	**TCH-thiol-1**	-21.3	-6.4
DC-thiol-2	-2.6	**DH-thiol-2**	-3.8	**TCH-thiol-2**	-15.8	-3.3
DC-thiol-3	-1.9	**DH-thiol-3**	-3.0	**TCH-thiol-3**	-14.5	-4.0
				TCH-thiol-4	-10.5	-2.2

We now discuss in more details the role and nature of intermolecular interactions formed between monomers. All H···O(S) and C···O intermolecular distances are in the range of 2.24−2.99 Å and 2.77−3.33 Å (Fig. 3.6), respectively, which are shorter to sums of Van der Waals radii of the relevant atoms (being 2.72 Å, 3.00 Å and 3.22 Å for H···O, H···S and C···O corresponding contacts). Moreover, the topographies of studied complexes obtained from AIM calculation have the existence of BCPs between two relevant atoms. These evidences support for the formation of intermolecular interactions in examined complexes: C···O, S···C=O tetrel interactions and C–H···O, S–H···O, O–H···O(S) hydrogen bonding contacts.

Table 3.11. Selected parameters at the BCPs of intermolecular contacts of complexes between C_2H_5SH and CO_2 and/or H_2O at MP2/6-311++G(2d,2p)

Complex	Contacts	$\rho(r)$ (au)	$\nabla^2\rho(r)$ (au)	$H(r)$ (au)	E_{HB} (kJ.mol^{-1})
DC-thiol-1	C9=O11···S12	0.007	0.025	0.0011	-
	C2−H5···O11	0.005	0.021	0.0008	-4.6
DC-thiol-2	C1···O11	0.004	0.017	0.0010	-
	S12–H8···O11	0.006	0.022	0.0009	-4.8
DC-thiol-3	C1···O10	0.004	0.020	0.0011	-
	C2−H7···O10	0.004	0.017	0.0007	-3.8
DH-thiol-1	O9−H11···S12	0.018	0.046	-0.0002	-15.8
	C1−H3···O9	0.005	0.020	0.0007	-4.7
DH-thiol-2	S12–H8···O9	0.014	0.047	0.0013	-12.1
DH-thiol-3	C1−H4···O9	0.006	0.021	0.0007	-5.2
	C5···O9	0.004	0.019	0.0010	-
TCH-thiol-1	O12−H13···S15	0.020	0.047	-0.0007	-17.4
	C1−H3···O10	0.007	0.023	0.0008	-5.6
	C2−H6···O12	0.005	0.019	0.0007	-4.4
	C9···O12	0.011	0.047	0.0017	-
TCH-thiol-2	O10−H12···S8	0.018	0.046	-0.0001	-15.3
	C1−H2···O10	0.005	0.020	0.0007	-4.5
	C1−H3···O15	0.004	0.017	0.0007	-3.7
	C13···S8	0.009	0.022	0.0007	-
TCH-thiol-3	S15−H8···O12	0.013	0.044	0.0013	-11.2
	O12−H13···O11	0.012	0.051	0.0018	-11.9
	C2−H5···O10	0.005	0.017	0.0007	-3.8
	C9···S15	0.007	0.026	0.0013	-
TCH-thiol-4	C1−H3···O13	0.006	0.019	0.0006	-4.7
	C5−H7···O13	0.004	0.018	0.0008	-3.7
	C5−H7···O11	0.006	0.021	0.0007	-5.0
	C10···O13	0.010	0.041	0.0015	-

Table 3.11 shows that the electron density $\rho(r)$, $\nabla^2\rho(r)$ and $H(r)$ at BCPs of intermolecular contacts are in the range: 0.004–0.020 au, 0.017–0.051 au and 0.0006–0.0018 au, respectively, almost obtained values fall within the limitation criteria for the formation of noncovalent weak interactions.[132] Besides, the slightly negative values of H(r) (from -0.0007 to -0.0002 au) at BCPs of O–H···S contacts in **DH-thiol-1** and **TCH-thiol-1** indicate that they are partially covalent in nature. For binary complexes, $\rho(r)$ values of tetrel interactions increase in order: C···O < C···S

while these values in ternary complexes follow an inverse trend. Thus, C···S TtB contribute a larger role to stability of dimers compared to C···O associations. The values of $\rho(r)$ at BCPs of HBs increase in order: C−H···O < O−H···O ≈ S–H···O < O–H···S. The magnitude in strength of HBs is also shown by values of E_{HB}. The O–H···S, O–H···O and S–H···O are observed as strong HBs with absolute values of E_{HB} in the range from 11.2 to 17.4 kJ.mol^{-1}. On comparison between **TCH-thiol-1** and **TCH-thiol-2**, $\rho(r)$ and E_{HB} of HBs O−H···S in **TCH-thiol-1** are slightly higher than corresponding values of **TCH-thiol-2** indicating the contribution of O−H···S in **TCH-thiol-1** is larger than in **TCH-thiol-2**.

Going from dimers to trimers, we analyse the characteristic of interactions in the most stable complexes of the three systems. By looking at the values of $\rho(r)$ and E_{HB}, it appears a slight upward pattern in the strength of C−H···O, O−H···S upon complexation. In **DC-thiol-1** and **DH-thiol-1**, the electron density of C−H···O and O−H···S are 0.05 and 0.09 au and the individual energy of them are around -4.0 and -15.8 kJ.mol^{-1}, respectively. These values increase slightly in **TCH-thiol-1**. The C···S TtB in **DC-thiol-1** is replaced by C···O contact in **TCH-thiol-1** with the larger value of $\rho(r)$. These results prove again that the cooperativity among the subunits contacts in $C_2H_5SH\cdots CO_2\cdots H_2O$ complex leads to a slight increase in stability of interactions. From this, it can be affirmed that the larger cooperative capacity is, the more stable complex is.

3.4.2. Vibrational and NBO analyses

Stretching vibrational frequency and NBO analysis for the complexes and relevant monomers are performed at the MP2/6-311++G(2d,2p) to gain more thorough insight into the origin and cooperativity of interactions in the complexes. The EDT, electron transfer process and the E_{inter} are collected in Table 3.12. The existence of electron transfer processes from n(O), n(S) orbitals to σ*(X−H) (X=C, O, S) anti-bonding orbitals and from n(O), n(S) orbitals to σ*(C−S), σ*(C−C), π*(C=O) anti-bonding orbitals proves again the formation X−H···O(S) HBs and >C=O···O(S) TtB in complexes mentioned above.

Table 3.12. EDT and $E^{(2)}$ of intermolecular interactions of complexes between C_2H_5SH and CO_2 and/or H_2O at MP2/6-311++G(2d,2p) level

Complex	EDT	Delocalization	$E^{(2)}$ kJ.mol^{-1}
DC-thiol-1	0.0040[a)]	n(S12)→π*(C9=O10)	5.1
		n(O11)→σ*(C2−H5)	0.5
DC-thiol-2	-0.0007[a)]	n(O11)→σ*(S12−H8)	1.4
		n(O11)→σ*(C1−C2)	0.3
DC-thiol-3	-0.0006[a)]	n(O10)→σ*(C1−S12)	0.5
		n(O10)→σ*(C2−H7)	0.5
DH-thiol-1	0.0160[a)]	n(S12)→σ*(O9−H11)	29.5
		n(O9)→σ*(C1−H3)	0.7
DH-thiol-2	-0.0050[a)]	n(O9)→σ*(S12−H8)	15.9
DH-thiol-3	-0.0015[a)]	n(O9)→σ*(C1−H4)	1.4
		n(O9)→σ*(C5−S12)	0.6
TCH-thiol-1	0.0200[a)]	n(S15) → σ*(O12−H13)	37.5
	-0.0020[b)]	n(O12) → π*(C9=O11)	7.0
	-0.0180[c)]	n(O10) → σ*(C1−H3)	1.7
		n(O12) → σ*(C2−H6)	0.8
TCH-thiol-2	0.0170[a)]	n(S8) → σ*(O10−H12)	27.6
	-0.0030[b)]	n(S8) → π*(C13=O14)	4.4
	-0.0140[c)]	n(O10) → σ*(C1−H2)	0.7
		n(O15) → σ*(C1−H3)	0.2
TCH-thiol-3	0.0018[a)]	n(O12) → σ*(S15−H8)	9.3
	-0.0032[b)]	n(O11) →σ*(O12−H13)	7.5
	0.0014[c)]	n(S15) → π*(C9=O10)	5.2
		n(O10) → σ*(C2−H5)	0.3
TCH-thiol-4	-0.0016[a)]	n(O13) →π*(C10=O11)	6.4
	-0.0020[b)]	n(O13) → σ*(C1−H3)	0.9
	0.0036[c)]	n(O11) → σ*(C5−H7)	0.6
		n(O13) → σ*(C5−H7)	0.3

[a)], [b)] and [c)] denote for charge of C_2H_5SH, CO_2 and H_2O, respectively
n: nonbonded (lone-pair) orbital, σ: anti σ-bond, π*: anti π-bond*

In detail, E_{inter} values of n(O)→σ*(C−S), n(S)→π*(C=O), n(O)→π*(C=O) processes are in the range of 0.5−0.6 kJ.mol^{-1}, 4.4−5.2 kJ.mol^{-1}, 6.4−7.0 kJ.mol^{-1}, respectively. Besides, these values for HBs change with a large amplitude from 0.2 to 37.5 kJ.mol^{-1}. The positive EDT values of C_2H_5SH in **DC-thiol-1**, **DH-thiol-1**, and **TCH-thiol-1** which are the most stable complexes for three systems imply that an amount of electron transfers from the host molecule to the guest molecules in which C_2H_5SH acts as electron donor while CO_2 and H_2O prefer to be electron

acceptors. The inverse role of these molecules is observed in the remaining complexes. In $C_2H_5SH\cdots CO_2$, the $E_{inter}(n(S)\rightarrow\pi^*(C=O))$ value is significantly larger than that of remaining interactions by around 5.1 kJ.mol^{-1}. This confirms again the primary role of S···C=O tetrel interaction in this system.

For complexes involving H_2O, the $E^{(2)}(n(S)\rightarrow\sigma^*(O-H))$ values are in the range of 27.6–37.5 kJ.mol^{-1}, while these values of other interactions are significantly lower (0.2–9.3 kJ.mol^{-1}). In particular, the second-order perturbation energies of $n(O11)\rightarrow\sigma^*(O12-H13)$ and $n(O9)\rightarrow\sigma^*(S12-H8)$ are around 7.5 kJ.mol^{-1} and 9.3-15.9 kJ.mol^{-1}, respectively. The C−H···O interactions are observed as weak HBs with $E^{(2)}$ to be considerably lower, from 0.2 to 1.7 kJ.mol^{-1}. These values describe the strength of HBs increasing in the ordering: C−H···O < O−H···O < S−H···O < O−H···S. This result proves again the crucial role of O−H···S into the stability of complexes involving H_2O. Moreover, as can be seen from Table 3.30, from structure of binary to ternary complexes, the strength of TtB and HBs increase slightly. This observation affirms the cooperation between intermolecular interactions enhancing the stability of ternary complexes.

The changes in X-H bond lengths (Δr(X-H)), stretching frequency ($\Delta\nu$(X-H)), electron population in σ^*(X-H) (X= C, O, S), s-character percentage of X(H) orbitals in each HB (Δ%s(X)) for complexes in comparison with relevant monomers are shown in Table 3.12. The C−H bond lengths are shortened by 0.04−1.18 mÅ and accompanied by stretching frequency increases of 2.02−21.62 cm^{-1}, whereas an elongation of O−H bond length by 2.73−9.56 mÅ and a decrease of its corresponding stretching frequency from 43.76 to 200.31 cm^{-1} are observed as compared to those in the relevant monomers. These results indicate that the C−H···O interaction in the complexes belongs to the blue-shifting HB, while the O−H···O(S) HBs are red-shifting ones. The S−H···O contact in **DC-thiol-2** is characterized as blue-shifting HB because the S−H bond length is contracted by 0.34 mÅ and its stretching frequency increase of 7.3 cm^{-1} in comparison with those in C_2H_5SH. Nevertheless, it is interesting that in **DH-thiol-2** and **TCH-thiol-3**, an

elongation of S−H bond lengths (2.36−2.85 mÅ) and a decrease of its corresponding stretching frequency (18.37−24.97 cm^{-1}) are observed with respect to relevant monomer. These results demonstrate that the S−H···O HBs in complexes involved H_2O (**DH-thiol-2** and **TCH-thiol-3**) are red-shifted which is in good agreement with the report by M. Kieninger *et al.*[143] The O-H distance elongation and its red frequency shift are increased going from **DH-thiol-1** to **TCH-thiol-1**. Consequently, the cooperation between intermolecular interactions leads to an increase in red-shifting magnitude of O−H···S HB.

Table 3.13. Selected results of vibrational and NBO analyses for interaction of C_2H_5SH with CO_2 and H_2O

Complex	**Hydrogen bond**	**Δr(X-H) (mÅ)**	**Δν(X-H) (cm^{-1})**	**Δσ*(X-H) (e)**	**Δ%s(X) (%)**
DC-thiol-1	C2−H5···O11	-0.37	6.20	0.0002	0.14
DC-thiol-2	S12–H8···O11	-0.34	7.30	0.0007	0.17
DC-thiol-3	C2−H7···O10	-0.46	8.08	0.0003	0.12
DH-thiol-1	O9−H11···S12	7.92	-165.61	0.0181	2.07
	C1−H3···O9	-0.74	11.66	-0.0004	0.39
DH-thiol-2	S12–H8···O9	2.85	-24.97	0.0066	1.22
DH-thiol-3	C1−H4···O9	-1.03	15.98	0.0003	0.37
TCH-thiol-1	O12−H13···S15	9.56	-200.31	0.0227	2.66
	C1−H3···O10	-1.01	21.62	-0.0015	0.53
	C2−H6···O12	-0.52	8.74	-0.0001	0.33
TCH-thiol-2	O10−H12···S8	7.46	-155.86	0.0167	1.97
	C1−H2···O10	-0.60	9.96	-0.0003	0.36
	C1−−H3···O15	-0.04	2.02	0.0001	0.11
TCH-thiol-3	O12−H13···O11	2.73	-43.76	0.0027	1.04
	S15−H8···O12	2.36	-18.37	0.0045	0.91
	C2−H5···O10	-0.24	4.40	0.0003	0.13
TCH-thiol-4	C1−H3···O13	-0.47	10.29	0.0008	0.29
	C5−H7···O13	-1.18	18.89	-0.0006	0.35
	C5−H7···O11	-1.18	18.89	-0.0006	0.35

Following complexation, a slight increase of 0.12−0.53% in the s-character of C−H hybrid orbital is observed for all blue-shifting HBs with respect to relevant monomers. In addition, electron density of the σ*(C−H) antibonding orbitals fluctuates slightly in the range of -0.0015 to 0.0008 e. This observation

demonstrates that a contraction of X−H bond length and an increase in its stretching frequency result from an enhancement of s-character of X(H) atom. However, a considerable rise of 0.0027–0.0227 e in population of σ*(X−H) orbital causes an elongation of X-H (X= O, S) bond length and its red shift of vibrational frequency following complexation.

3.4.3. Remarks

Stable structures obtained from interactions between C_2H_5SH host molecule and CO_2, H_2O guest molecules were investigated using MP2/6-311++G(2d,2p). The interaction energies calculated at CCSD(T)/6-311++G(2d,2p)//MP2/6-311++G(2d,2p) range widely from -1.9 kJ.mol^{-1} to -21.3 kJ.mol^{-1}, in which $C_2H_5SH\cdots1CO_2\cdots1H_2O$ is more stable than $C_2H_5SH\cdots1CO_2$ and $C_2H_5SH\cdots1H_2O$ by 8.4 - 9.7 kJ.mol^{-1} and 6.0 - 11.5 kJ.mol^{-1}, respectively. Accordingly, the addition of CO_2 or H_2O guest molecule into binary complexes leads to an upward trend in stability of complexes, in which it is larger for the adding of H_2O than of CO_2. The stability of $C_2H_5SH\cdots1CO_2$ is due to the crucial role of the >C=O···S TtB and an additional cooperation from C−H···O HBs. In other word, $C_2H_5SH\cdots1H_2O$ and $C_2H_5SH\cdots1CO_2\cdots1H_2O$ are significantly stabilized by O−H···S strong hydrogen bonded interaction and a complementary of C−H···O, O−H···O interactions. Generally, all C−H···O interactions are characterized as blue-shifting HBs while O−H···S interactions belong to red-shifting HBs. Remarkably, the behaviour of S−H···O HB depends on the guest molecule. Their character changes from blue to red shift when the guest molecule goes from CO_2 to H_2O.

3.5. Interactions of CH_3OCHX_2 with nCO_2 and nH_2O (X=H, F, Cl, Br, CH_3; n=1-2)

The total electronic energies and BSSE were calculated at MP2/aug-cc-pVTZ with geometries obtained at MP2/6-311++G(2d,2p).

3.5.1. Interactions of CH_3OCHX_2 with $1CO_2$ (X = H, F, Cl, Br, CH_3)

This section is based on the results of Ref. 144.

Two stable structures formed by interactions of CH_3OCHX_2 (X = H, F, Cl,

Br, CH_3) with CO_2 are presented in Fig. 3.8, denoted by **DC1-DME-X** and **DC2-DME-X** where **X =** H, F, Cl, Br, CH_3.

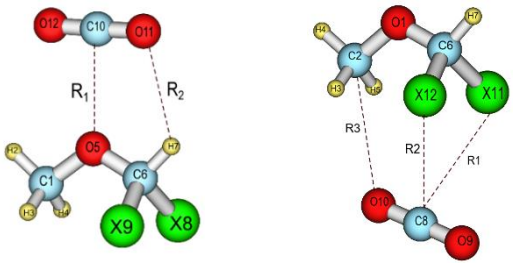

DC1-DME **DC2-DME**

Figure 3.8. Stable structures of $CH_3OCHX_2\cdots 1CO_2$ complexes at MP2/6-311++G(2d,2p)

The $CH_3OCHX_2\cdots 1CO_2$ complexes are stabilized by intermolecular contacts including C···O, C–H···O and X···O (X = F, Cl, Br) interactions. For **DC1-DME** complexes, all C···O distances are in the range of 2.66-2.75 Å, considerably shorter than sum of van der Waals radii of two relevant atoms (3.22 Å). This gives the first evidence for the formation of C···O TtB. The symmetry of **DC2-DME-H** is C_{2V} and consistent with result of previous study.[47] The O···H distances in **DC1-DME-Cl** and **DC1-DME-Br** are 2.69 Å and 2.72 Å, respectively. These values are shorter than or very close to sum of van der Waals radii of relevant atoms (2.72 Å) while those in the remaining complexes are longer ranging from 2.78 Å to 2.96 Å. For **DC2-DME**, all C···F/Cl/Br distances range from 3.00 to 3.60 Å, slightly shorter or close to the sum of van der Waals radii of two corresponding atoms (3.17-3.55 Å), indicating the formation of C···X (X=F, Cl, Br) interactions.

Table 3.14. Intermolecular distances (Å) of $CH_3OCHX_2\cdots 1CO_2$ complexes

	X	**H**	**F**	**Cl**	**Br**	**CH_3**
DC1-DME	R_1	2.69	2.75	2.73	2.73	2.66
	R_2	2.96	2.85	2.72	2.69	2.78
	X	**H**	**F**	**Cl**	**Br**	**CH_3**
DC2-DME	R_1	3.10	3.00	3.47	3.60	-
	R_2	3.20	3.00	3.47	3.60	-
	R_3	3.09	3.40	3.38	3.36	-

The interaction energies corrected ZPE+BSSE of studied complexes at MP2/aug-cc-pVTZ//MP2/6-311++G(2d,2p) are summarized in Table 3.15. In

general, all values of the interaction energies are negative, indicating that the reactions between CH_3OCHX_2 and $1CO_2$ are favorable thermodynamics. Indeed, the interaction energies range from -2.8 kJ.mol^{-1} to -15.1 kJ.mol^{-1}. The correlation in interaction energies **DC1-DME** and **DC2-DME** structures are described in Fig. 3.9.

Table 3.15. Interaction energies corrected ZPE+BSSE of complexes $CH_3OCHX_2\cdots1CO_2$

	E_{int}		E_{int}
DC1-DME-H	-13.3	**D2-DME-H**	-2.8
DC1-DME-F	-10.7	**D2-DME-F**	-8.1
DC1-DME-Cl	-11.7	**D2-DME-Cl**	-9.8
DC1-DME-Br	-11.9	**D2-DME-Br**	-10.4
DC1-DME-CH$_3$	-15.1		

All values are in kJ.mol^{-1}

With the same substituents, the interaction energies of **DC1-DME** complexes are more negative than those of **DC2-DME**, implying that the former geometries are energetic-favored than the later ones. Thus, CO_2 counterpart favors to locate around O atom of DME to form the stable structures. For **DC1-DME** system, ΔE^* has negative value ranging from -10.7 kJ.mol^{-1} to -15.1 kJ.mol^{-1} and its magnitude increases in order of substituents: **F < Cl < Br < H < CH$_3$**, indicating that the strength of complexes also increases in this order. Furthermore, **DC1-DME-H** complex represents an interaction energy of -13.3 kJ.mol^{-1}, in well agreement with the value of -13.7 kJ.mol^{-1} at CCSD(T)/aug-cc-pVTZ//MP2/aug-cc-pVTZ.[40] Moreover, Ginderen *et al.*[47] also reported **DC1-DME-H** as the global minimum structure of $CH_3OCH_3\cdots CO_2$ system with an interaction energy (without BSSE) of -15.58 kJ.mol^{-1}, completely consistent with the calculated value of -15.7 kJ.mol^{-1} in this work (with only ZPE correction). The substitution of two H atoms by two halogens leads to a decrease in the strength of $CH_3OCHX_2\cdots1CO_2$ complex by 1.4-2.6 kJ.mol^{-1} while that of two methyl groups leads to an enhancement of 1.8 kJ.mol^{-1} in complexation energy. The effect of substituents on the complex stability is consistent with the results of halogenated- and methyl- substitutions on complexes of acetone and CO_2.[43]

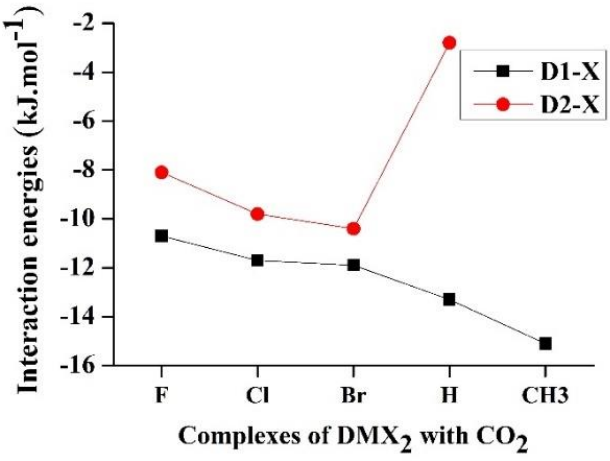

Figure 3.9. The difference in interaction energies (with ZPE and BSSE) of $CH_3OCHX_2\cdots 1CO_2$ complexes

For **DC2-DME** complexes, the stability of di-halogenated derivatives is significantly higher than that of DME which increases in order: **DC2-DME-H** < **DC2-DME-F** < **DC2-DME-Cl** < **DC2-DME-Br**. From geometric structure of **DC2-DME** complexes, they are stabilized by two C···X TtB and an additional cooperation of the C−H···O HBs, except **DC2-DME-H** with only two weak HBs. The fact is that the electronegativity decreases from F *via* Cl to Br. Therefore, the C···X TtBs (X = F, Cl, Br) existed in **DC2-DME** complexes are predicted to be electrostatic in nature.

The interaction capacity of CO_2 with CH_3OCHX_2 are significantly stronger than that of C_2H_6, C_2H_4 and CH_3SCH_3 by 7.7-12.1, 8.4-10.2 and 0.8-5.2 kJ.mol^{-1}; respectively.[58,145,146] Moreover, for the same halogenated-substitution, the complexes of CO_2 and CH_3OCHX_2 are also more stable than the corresponding XHC=CHX ones by 4.1-4.5 kJ.mol^{-1}.[145] Therefore, CH_3OCHX_2 is predicted to be an effective functional group in aiming of CO_2 capture.

SAPT2+ analysis for **DC1** complexes is performed to better understand the nature and role of each energetic component into the total stabilization energy of $CH_3OCHX_2\cdots 1CO_2$ complexes. The contribution percentages of different energetic components including electrostatic, induction and dispersion of **DC1-DME** energetic-favored complexes are described in Fig. 3.10.

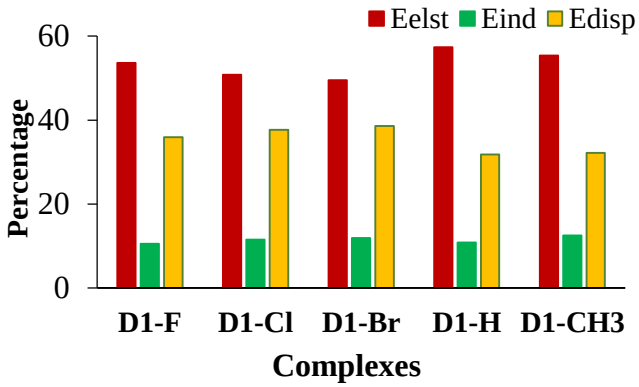

Figure 3.10. Contributions (%) of physical energetic terms

It is showed that the attractive electrostatic term mainly contributed to the stabilization of $CH_3OCHX_2\cdots 1CO_2$ system as compared to dispersion and induction ones. In particularly, the contribution of electrostatic attraction component ranges from 49.5% to 57.4%, considerably larger than that of two remaining counterparts, which is roughly 31.8%-38.6% for dispersion and 10.5%-12.5% for induction one. For the halogenated-substituted derivatives, the percentage of attractive electrostatic term is decreased in going from -F *via* -Cl to -Br, while that of dispersion is slightly increased in this order. The interaction energies taken from SAPT2+ approach are estimated from -13.2 $kJ.mol^{-1}$ to -18.0 $kJ.mol^{-1}$, which the magnitude increases in order F < Cl < Br < H < CH_3 and consistent with those derived from supramolecular theory.

For **DC2-DME** complexes, the contributions of electrostatic, induction and dispersion terms are about 18.4-42.1%, 8.3-19.1% and 41.6-62.4%, respectively. Going from **DC1-DME** to **DC2-DME**, there is a change of the main contribution component, which is going from electrostatic to dispersion one, respectively.

The molecular graphs of $CH_3OCHX_2\cdots 1CO_2$ complexes according to AIM approach are shown in Fig. A9 in *Appendix* (Red points denote the BCPs). The existence of BCPs between the contacts of the two molecules demonstrates the formation of intermolecular interactions. The selected features at BCPs of intermolecular interactions are collected in Table 3.16. In general, the electron density, Laplacian and total electron energy density at BCPs of all interactions

formed are in the range of 0.0032-0.0144 au, 0.0128-0.0589 au and 0.0007-0.0020 au, respectively; indicating that they are weakly noncovalent interactions.[132]

The proton affinity at O site and deprotonated enthalpy of the C−H involved C−H···O HB of isolated monomers are summarized in Table A8 to further investigate the effect of substituents.

Table 3.16. Selected parameters (au) of $CH_3OCHX_2\cdots 1CO_2$ complexes (X = H, F, Cl, Br, CH_3)

Complex	Contact	$\rho(r)$ au	$\nabla^2\rho(r)$ au	$H(r)$ au
DC1-DME-H	O1···C8	0.0135	0.0589	0.0020
DC1-DME-F	O1···C8	0.0117	0.0527	0.0020
DC1-DME-Cl	O1···C6	0.0121	0.0540	0.0020
	C4−H6···O7	0.0056	0.0247	0.0011
DC1-DME-Br	O1···C8	0.0121	0.0538	0.0020
	C2−H3···O10	0.0060	0.0255	0.0011
DC1-DME-CH_3	O1···C8	0.0144	0.0614	0.0019
DC2-DME-H	C2−H11···O10	0.0038	0.0155	0.0010
	C4−H7···O9	0.0032	0.0128	0.0007
DC2-DME-F	F11(12)···O10	0.0058	0.0306	0.0017
	C2···O10	0.0042	0.0177	0.0010
DC2-DME-Cl	Cl11(12)···O10	0.0049	0.0183	0.0009
	O10···C2	0.0045	0.0191	0.0011
DC2-DME-Br	Br11(12)···O10	0.0049	0.0169	0.0008
	C2−H3···O10	0.0046	0.0198	0.0011

For **DC1-DME** complexes, the $\rho(r)$ values at BCPs of O···C TtBs are enhanced in order of **DC1-DME-F** < **DC1-DME-Cl** ≈ **DC1-DME-Br** < **DC1-DME-H** < **DC1-DME-CH_3**. This means that the O···C TtB becomes stronger in **DC1-DME-CH_3** and weaker in halogenated derivatives, as compared to that in $CH_3OCH_3\cdots 1CO_2$ complex. This change is explained based on the gas phase basicity at the O site increases as followed: CH_3OCHF_2 < CH_3OCHCl_2 < CH_3OCHBr_2 < CH_3OCH_3 < $CH_3OCH(CH_3)_2$ (*cf.* Table A8). Furthermore, the DPE values of isolated monomers show that the polarization of the C−H bond increases in the sequence CH_3 ≈ H < F < Cl < Br. This result is confirmed by the existence of

C−H···O HB in **DC1-DME-Cl/Br** and no HB formed in the remaining complexes. Taking into account the strength of C−H···O HB, its $\rho(r)$ value at BCP in **DC1-DME-Br** is slightly higher than that in **DC1-DME-Cl**. Combined AIM results and energetic parameters, $CH_3OCHX_2\cdots 1CO_2$ complexes are mainly stabilized by the C···O TtB and an additional role of C−H···O HB. Regarding **DC2-DME** complexes, it is existed the O··· F/Cl/Br interactions in which are slightly reinforced from Br *via* Cl to F. These interactions are predicted to be electrostatic in nature due to the electronegativity of halogenated atoms also decreases in the same order.

The substitution of halogen and methyl group leads to a significant change in the strength of intermolecular interactions and stability of complexes. It is explained by the electron withdrawing effect of halogenated groups, which causes a decrease electron density at O site and the largest decrement belongs to F-substituted derivative, followed by -Cl and finally, by -Br one. In contrast, the presence of $-CH_3$ groups instead of -H atoms results in a slight enhancement of the electron density at the O site as compared to CH_3OCH_3.

The charge transfer and the formation of intermolecular orbital interactions upon complexation are examined at MP2/6-311++G(2d,2p). The EDT (m*e*) and $E^{(2)}$ ($kJ.mol^{-1}$) are gathered in Table 3.17. The EDT values of CH_3OCHX_2 are positive in range of 0.4-6.0 m*e*, implying that electron density transfers from DME and its derivatives to CO_2 monomer. The EDT value of the halogenated-substituted complexes is smaller than that of the remaining ones due to the electron withdrawing effect of halogen atoms.

Generally, the second-order energies of interactions in **DC1-DME** complexes are considerably higher than those in **DC2-DME** ones supporting that $CH_3OCHX_2\cdots 1CO_2$ complexes favor **DC1-DME** geometry. The $E^{(2)}$ values of Lp(O)→π*(C=O) delocalization in **DC1-DME** complexes range from -8.6 to -12.5 $kJ.mol^{-1}$, significantly larger than those of Lp(O)→σ*(C−H) by 8.3-11.5 $kJ.mol^{-1}$. This result confirms the dominant role of the former interactions as compared to the later. For **DC2-DME** complexes, the $E^{(2)}$ of Lp(X)→π*(C=O) (X = F, Cl, Br) is

roughly 1.5−1.8 kJ.mol^{-1}, which is the main interactions of these complexes.

Table 3.17. EDT and $E^{(2)}$ for $CH_3OCHX_2\cdots 1CO_2$ complexes at MP2/6-311++G(2d,2p) level of theory

Complex	EDT*	Orbital interaction	$E^{(2)}$ kJ.mol^{-1}
DC1-DME-H	6.0	Lp(O1)→π*(C8=O9)	11.3
DC1-DME-F	2.7	Lp(O1)→π*(C8=O9)	8.6
		Lp(O10)→σ*(C2−H3)	1.0
DC1-DME-Cl	2.3	Lp(O1)→π*(C6=O8)	8.8
		Lp(O7)→σ*(C4−H5)	0.7
DC1-DME-Br	1.9	Lp(O1)→π*(C8=O9)	8.7
		Lp(O10)→σ*(C2−H3)	0.5
DC1-DME-CH$_3$	4.5	Lp(O1)→π*(C8=O10)	12.5
		Lp(O10)→σ*(C2−H3)	0.3
DC2-DME-H	0.4	σ(C2−H12)→π*(C8=O10)	0.2
DC2-DME-F	3.1	Lp(F11)→π*(C8=O9)	1.8
		Lp(F12)→ π*(C8=O9)	1.8
		Lp(O10)→σ*(C2−H4)	0.3
DC2-DME-Cl	3.4	Lp(Cl11)→π*(C8=O9)	1.8
		Lp(Cl12)→π*(C8=O9)	1.8
		Lp(O10)→σ*(C2−H3)	0.2
		Lp(O10)→σ*(C2−H5)	0.2
DC2-DME-Br	3.2	Lp(Br11)→π*(C8=O9)	1.7
		Lp(Br12)→π*(C8=O9)	1.7
		Lp(O10)→σ*(C2−H3)	0.5
		Lp(O10)→σ*(C2−H5)	0.3

***** the EDT values of CH_3OCHX_2 monomer

3.5.2. Interactions of CH_3OCHX_2 with $2CO_2$ (X = H, F, Cl, Br, CH_3)

The stable structures of complexes $CH_3OCHX_2\cdots 2CO_2$ are presented in Fig. 3.11 (denoted as **TC-DME-X**). The predicted structures of complexes $CH_3OCHX_2\cdots 2CO_2$ are built by adding one CO_2 molecule to the lowest structures on PES of $CH_3OCHX_2\cdots 1CO_2$. The topological geometries and selected parameters of BCPs corresponding to intermolecular interactions are collected in Fig. A9 and Table A9 of *Appendix*, respectively.

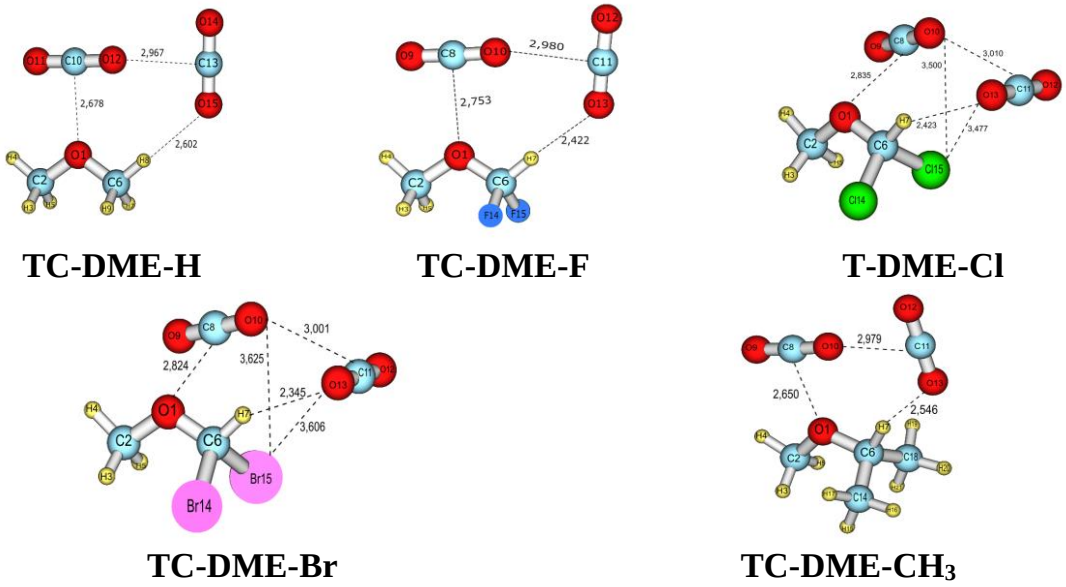

Figure 3.11. Stable structures of complexes $CH_3OCHX_2\cdots 2CO_2$

The addition of CO_2 molecule into binary complexes leads to the rearrangement of geometries, where three molecules interact mutual creating a ring or a cage. The O1···C8(10) TtB still remains its dominant role in all stable complexes due to the highest values of $\rho(r)$ at BCPs. The appearance of new TtB between two CO_2 molecules is predicted to strengthen the ternary complexes. From the topological graph of these complexes, it is observed the existence of BCPs between Cl/Br atom of CH_3OCHX_2 (X = Cl, Br) and O one of CO_2 which is not found in the remaining complexes. The $\rho(r)$ values at BCP of O1···C8(10) TtB are lower in case of **TC-DME-F/Cl/Br** and higher in complex **TC-DME-CH$_3$** in comparison with those of **TC-DME-H**. It is consistent with the results of binary complexes $CH_3OCHX_2\cdots 1CO_2$ that the O1···C8(10) TtB becomes weaker in halogenated derivatives and stronger in CH_3-substituent complexes. The interaction energy and cooperative energy of complexes $CH_3OCHX_2\cdots 2CO_2$ are given in Table 3.18 to investigate their stability.

The interaction energy corrected ZPE+BSSE of $CH_3OCHX_2\cdots 2CO_2$ are negative and range from -18.1 to -25.0 kJ.mol^{-1}. Similar to previous systems, the stability of ternary complexes $CH_3OCHX_2\cdots 2CO_2$ is found to be more stable than

that of binary ones $CH_3OCHX_2\cdots 1CO_2$ about 6-13 kJ.mol^{-1}. The stability of $CH_3OCHX_2\cdots 2CO_2$ increases in order of F < H < CH_3 < Cl < Br, which is different with the binary complexes. It is due to the formation of Cl/Br···C=O interactions in **TC-DME-Cl** and **TC-DME-Br** strengthens the complex stability.

Table 3.18. Interaction energy and cooperative energy of complexes $CH_3OCHX_2\cdots 2CO_2$ at MP2/aug-cc-pVTZ//MP2/6-311++G(2d,2p) (X = H, F, Cl, Br, CH_3)

Complex	$\mathbf{E_{int}}$	$\mathbf{E_{coop}}$
TC-DME-H	-19.9	-3.3
TC-DME-F	-18.1	-2.6
TC-DME-Cl	-23.9	-1.2
TC-DME-Br	-25.0	-1.0
TC-DME-CH_3	-22.5	-3.7

The cooperative energies of all complexes are estimated to range from -1.0 đến -3.7 kJ.mol^{-1}, indicating a slightly positive cooperativity between these noncovalent interactions. The E_{coop} of complexes **TC-DME-H** and **TC-DME-CH_3** is negative of -3.1 and -3.7 kJ.mol^{-1}, respectively, however, that of the halogen-derivatives is quite small which ranges from -1.0 to -2.6 kJ.mol^{-1}.

The electron density transfer and second-order perturbation energy for intermolecular interactions are given in Table 3.19. The positive EDT values of CH_3CHX_2 monomer (from 0.0003 to 0.0054 electron) show an electron transfer from CH_3CHX_2 to CO_2. The existence of C···O TtB, C−H···O HB and Cl/Br···C=O is confirmed here by means of delocalization from n(O) to π*(C10=O11), σ*(C−H) and from n(Cl/Br) to π*(C=O), respectively.

The prominent role of O1···C8(10) TtB is confirmed again by its $E^{(2)}$ value in all of ternary complexes. In particular, the $E^{(2)}$ of n(O1)→π*(C=O) delocalization ranges from 4.2 to 11.8 kJ.mol^{-1}, while that value of n(O)→σ*(C6−H7) and n(O10/O13)→π*(C=O) is significantly lower, about 0.5-6.4 and 1.9-3.4 kJ.mol^{-1}, respectively. For complexes **TC-DME-Cl/Br**, the second-order energy of n(Cl/Br)→π*(C=O) is almost equal and is estimated of 1.3-2.6 kJ.mol^{-1}. The higher stability of **TC-DME-Br** is explained by the stronger O1···C8(10) TtB as compared

to **TC-DME-Cl**.

Table 3.19. EDT and $E^{(2)}$ for $CH_3OCHX_2\cdots 2CO_2$ complexes at MP2/6-311++G(2d,2p) level of theory

Complex	**EDT/e**	**Delocalization**	**$E^{(2)}$/kJ.mol^{-1}**
TC-DME-H	0.0054[(a)]	n(O1) → π*(C10=O11)	11.8
	-0.0061[(b)]	n(O12) → π*(C13=O14)	2.0
	0.0007[(c)]	n(O15) → σ*(C6−H8)	2.8
TC-DME-F	0.0003[(a)]	n(O1) → π*(C8=O9)	8.4
	-0.0025[(b)]	n(O10) → π*(C11=O12)	1.9
	0.0022[(c)]	n(O10) → σ*(C6−H7)	0.5
		n(O13) → σ*(C6−H7)	6.4
TC-DME-Cl	0.0041[(a)]	n(O1) → π*(C8=O9)	6.9
	-0.0037[(b)]	n(O10) → π*(C11=O12)	3.2
	-0.0004[(c)]	n(O10) → σ*(C6−Cl14)	0.8
		n(O13) → σ*(C6−H7)	3.6
		n(Cl15) → π*(C11=O12)	2.6
		n(Cl15) → π*(C8=O9)	1.3
TC-DME-Br	0.0032[(a)]	n(O1) → π*(C8=O9)	7.1
	-0.0036[(b)]	n(O10) → π*(C11=O12)	3.2
	0.0004[(c)]	n(O10) → σ*(C6−Br14)	0.9
		n(O13) → σ*(C6−H7)	4.4
		n(Br15) → π*(C11=O12)	2.5
		n(Br15) → π*(C8=O9)	1.3
TC-DME-CH_3	0.0030[(a)]	n(O1) → π*(C8=O9)	4.2
	-0.0045[(b)]	n(O1) → π*(C8=O10)	3.4
	0.0015[(c)]	n(O10) → π*(C11=O12)	1.9
		n(O13) → σ*(C6−H7)	3.5

3.5.3. Interactions of CH_3OCHX_2 with nH_2O (X = H, F, Cl, Br, CH_3; n=1-2)

The minimum structures of complexes $CH_3OCHX_2\cdots nH_2O$ (n=1-2) in PES are presented in Fig. 3.12 (denoted as **DH-DME-X** for n=1 and **TH-DME-X** for n=2). The molecular graphs of $CH_3OCHX_2\cdots nH_2O$ complexes according to AIM approach are shown in Fig. A10 in *Appendix*. The properties of some BCPs taken from AIM analysis are gathered in Table 3.20.

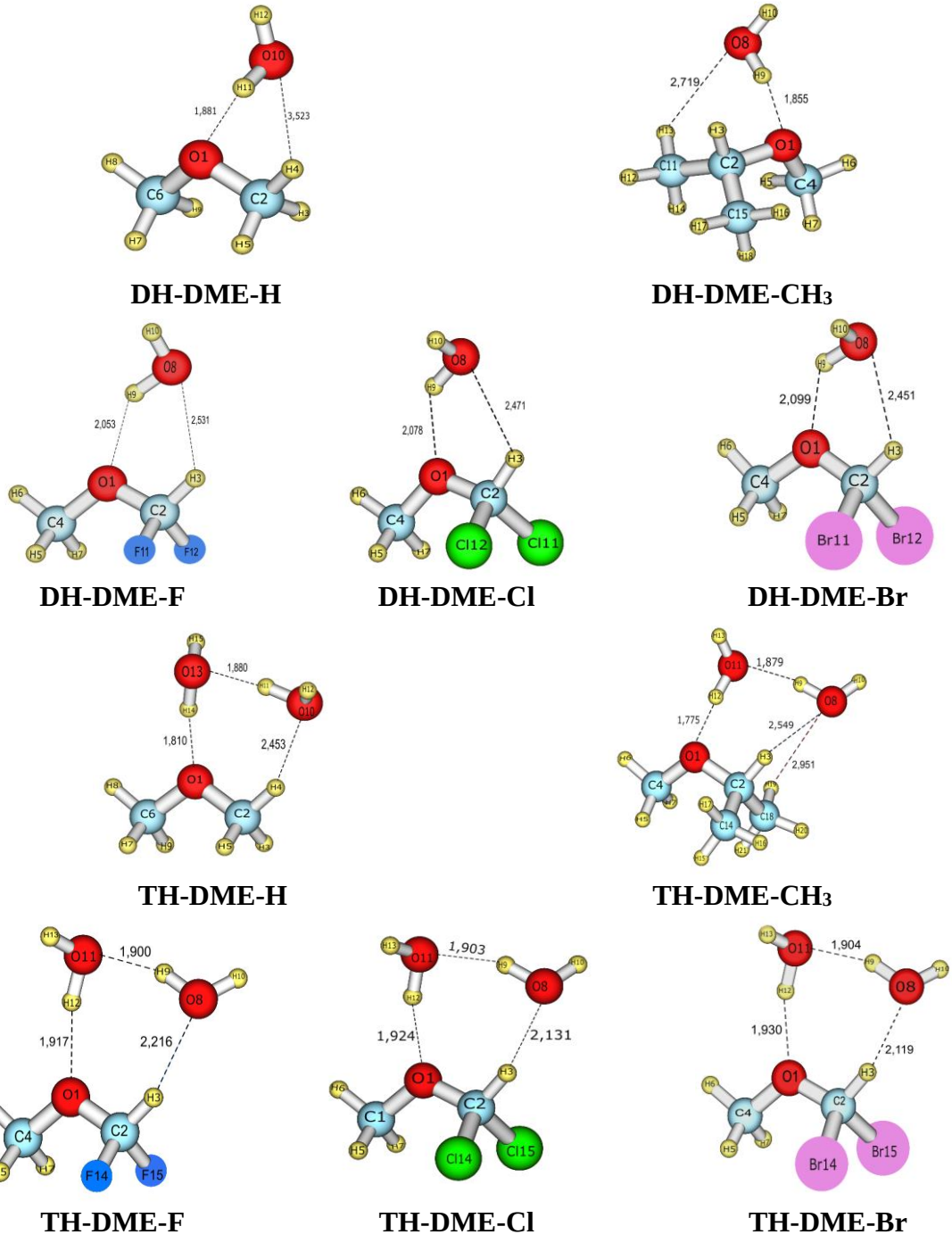

Figure 3.12. The stable structures of $CH_3OCHX_2\cdots nH_2O$ complexes

(n =1-2; X = H, F, Cl, Br, CH_3)

The complexes between CH_3OCHX_2 with $1,2H_2O$ are bound by the O−H···O and C−H···O HBs. As shown in Fig. 3.10, geometry of all **DH-DME-X** is stabilized by one O−H···O and one C−H···O HB. For complexes with $2H_2O$, it creates a heptagon in all structural shapes where three molecules connect mutual.

Table 3.20. Selected parameters at BCPs taken from AIM results for complexes of CH_3OCHX_2 with 1,2H_2O at MP2/6-311++G(2d,2p)

Complex	Interaction	$\rho(r)$ (au)	$\nabla^2\rho(r)$ (au)	$H(r)$ (au)	E_{HB} (kJ.mol^{-1})
DH-DME-H	O1···H11−O10	0.0293	0.096	0.000	-32.0
DH-DME-F	O1···H9−O8	0.0184	0.073	0.002	-19.3
	C2−H3···O8	0.0086	0.035	0.001	-8.1
DH-DME-Cl	O1···H9−O8	0.0179	0.070	0.002	-18.6
	C2−H3···O8	0.0103	0.038	0.001	-9.5
DH-DME-Br	O1···H9−O8	0.0172	0.068	0.002	-17.9
	C2−H3···O8	0.0109	0.040	0.001	-10.0
DH-DME-CH_3	O1···H9−O8	0.0311	0.100	-0.001	-34.4
	C11−H13···O8	0.0055	0.022	0.001	-4.9
TH-DME-H	O1···H14−O13	0.0323	0.107	0.000	-36.6
	C2−H4···O10	0.0092	0.031	0.001	-7.9
	O10−H11···O13	0.0286	0.095	0.000	-31.0
TH-DME-F	O1···H12−O11	0.0245	0.088	0.001	-26.2
	C2−H3···O8	0.0150	0.053	0.001	-13.6
	O8−H9···O11	0.0273	0.093	0.000	-29.6
TH-DME-Cl	O1···H12−O11	0.0242	0.087	0.001	-25.8
	C2−H3···O8	0.0181	0.062	0.001	-16.9
	O8−H9···O11	0.0271	0.093	0.000	-29.4
TH-DME-Br	O1···H12−O11	0.0238	0.086	0.001	-25.3
	C2−H3···O8	0.0188	0.064	0.001	-17.6
	O8−H9···O11	0.0271	0.093	0.000	-29.4
TH-DME-CH_3	O1···H12−O11	0.0367	0.113	-0.002	-42.2
	C2−H3···O8	0.0074	0.028	0.001	-6.6
	O8−H9···O11	0.0285	0.095	0.000	-30.9
	C18−H19···O8	0.0047	0.018	0.001	-3.8

From AIM data, the O−H···O HBs in plays as the most important interaction in strengthening complexes. In particular, for complexes with 1H_2O, O−H···O HB overcomes the C−H···O HB which is observed through $\rho(r)$ and E_{HB} values. Indeed, the $\rho(r)$ at BCPs of O−H···O is estimated of 0.0172-0.0311 au while that of C−H···O is about from 0.0055-0.0103 au. The E_{HB}(O−H···O) values are also largely negative than those of C−H···O HBs. It is found that the substitution of halogen atom into

dimethyl ether results to a decrease in strength of O−H···O HB while the CH_3 substituent makes that interaction becomes stronger. It is in agreement with the results found in complexes $CH_3OCHX_2\cdots CO_2$.

In going to the complexes with $2H_2O$, both $\rho(r)$ and E_{HB} values of O−H···O HBs remarkably increase as compared to those in binary complexes. The addition of one H_2O molecule leads to the existence of the O−H···O between two H_2O molecules along with the conventional O−H···O between CH_3CHX_2 and H_2O, and the C−H···O HBs. Based on the $\rho(r)$ and E_{HB} values, the strength of these HBs is increased in order C−H···O < O−H···O (between two H_2O) < O1···H−O (between CH_3CHX_2 and H_2O). Thus, the O1···H−O still is the main driver in stabilizing complexes besides the additional role of the remaining interactions.

For the same X, it is noteworthy that the strength of O1···H−O HBs in ternary complexes are found to becomes stronger as compared to the binary one. Thus, it is predicted that the cooperative effect between these HBs makes the O1···H−O HBs stronger, and also leads to the increase in the overall stability. When X is going from H to halogen atom, strength of O1···H−O HB is decreased from -32 $kJ.mol^{-1}$ to about -18 $kJ.mol^{-1}$ while C···H−O HB is stronger. The substitution of two methyl groups also strengthens the O···H−O HB.

Table 3.21. Interaction energy and cooperative energy of complexes $CH_3OCHX_2\cdots 1,2H_2O$ at MP2/aug-cc-pVTZ//MP2/6-311++G(2d,2p) (X = H, F, Cl, Br, CH_3)

Complex	$\mathbf{E_{int}}$	**Complex**	$\mathbf{E_{int}}$	$\mathbf{E_{coop}}$
DH-DME-H	-16.0	**TH-DME-H**	-37.2	-15.0
DH-DME-F	-10.1	**TH-DME-F**	-32.4	-11.9
DH-DME-Cl	-10.5	**TH-DME-Cl**	-34.0	-11.5
DH-DME-Br	-10.6	**TH-DME-Br**	-34.1	-10.8
DH-DME-CH_3	-19.3	**TH-DME-CH_3**	-41.8	-17.2

Table 3.21 represents the interaction energy and cooperative energy of $CH_3OCHX_2\cdots nH_2O$ at MP2/aug-cc-pVTZ//MP2/6-311++G(2d,2p). The interaction

energy of **DH-DME-X** ranges from -10.1 to -19.3 kJ.mol^{-1}. The stability is increased as **F** < **Cl** ≈ **Br** < **H** < **CH$_3$**. The results on stability is consistent with that predicted in AIM analysis, in which the subsitution of di-halogen atom leads to a decrease in strength of $CH_3OCHX_2\cdots nH_2O$ and the substitution of dimethyl groups results in an inverse trend. The addition of one H_2O molecule enhances the stability of complexes about 11-22 kJ.mol^{-1}. Indeed, the E_{int} of **TH-DME-X** ranges from -37.2 to -41.8 kJ.mol^{-1}. The change in stability is in good agreement with the strength of O1···H−O HB demonstrating the primary role of that HB again.

In comparison with complexes $CH_3OCHX_2\cdots nCO_2$, for n=1, the E_{int} values of $CH_3OCHX_2\cdots 1CO_2$ and $CH_3OCHX_2\cdots 1H_2O$ are approximate. However, the interactions of CH_3OCHX_2 with $2H_2O$ is considerably stronger than that with $2CO_2$. The E_{int} values of $CH_3OCHX_2\cdots 2H_2O$ are more negative than those of $CH_3OCHX_2\cdots nCO_2$ roundly 9-19 kJ.mol^{-1}. It is explained by the larger cooperative effect between HBs in $CH_3OCHX_2\cdots 2H_2O$ as compared to that in $CH_3OCHX_2\cdots 2CO_2$. Indeed, the E_{coop} of **TH-DME-X** ranges from -10.8 to -17.2 kJ.mol^{-1} while that of **TC-DME-X** is from -1.0 to -3.7 kJ.mol^{-1}.

The EDT and $E^{(2)}$ values taken from NBO analysis for complexes $CH_3OCHX_2\cdots nH_2O$ are given in Table A10 in *Appendix*. The EDT value of CH_3OCHX_2 monomer is positive and in range of 0.0029-0.0238 e, indicating the electron delocalization from CH_3OCHX_2 to H_2O molecules. The primary role of O1···H−O is also observed through the high $E^{(2)}$ values (from 8.6 to 65.2 kJ.mol^{-1}).

3.5.4. Interactions of CH_3OCHX_2 with $1CO_2$ and $1H_2O$ (X =H, F, Cl, Br, CH_3)

The stable structures of complexes formed by interactions between CH_3OCHX_2 with $1CO_2$ and $1H_2O$ are presented in Fig. 3.13 (denoted as **TCH-DME-X**) where X = H, F, Cl, Br, CH_3.

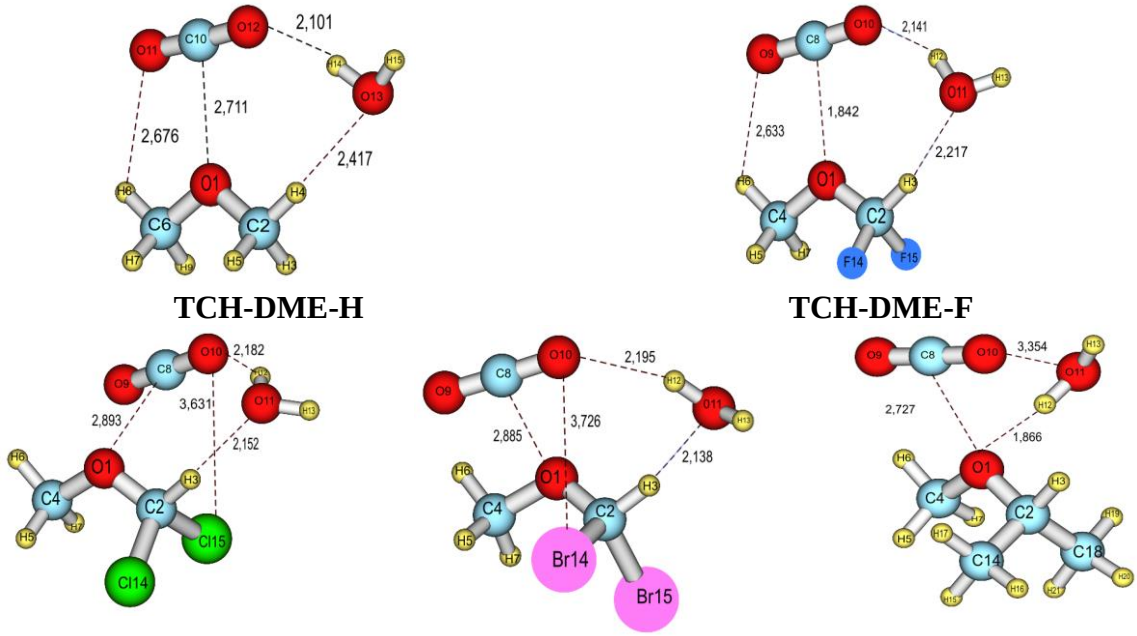

TCH-DME-H **TCH-DME-F**

TCH-DME-Cl **TCH-DME-Br** **TCH-DME-CH$_3$**

Figure 3.13. Stable structures of complexes $CH_3OCHX_2\cdots1CO_2\cdots1H_2O$ (X = H, F, Cl, Br, CH_3)

The selected parameters at BCPs from AIM results are collected in Table A11 of *Appendix*. The topological graphs of complexes $CH_3OCHX_2\cdots1CO_2\cdots1H_2O$ indicates the simultaneous existence of C···O TtB between CH_3OCHX_2 and CO_2 molecule and C−H···O HB between CH_3OCHX_2 and H_2O one. Furthermore, it also appears the connection between CO_2 and H_2O moiety through the O−H···O_{CO2} HB. The $\rho(r)$ value at BCPs of C8(10)···O1 TtBs in complexes **TCH-DME-X** is increased as order Cl < Br ≈ F < H < CH_3, as observed in complexes between CH_3OCHX_2 and nCO_2 or nH_2O (n=1-2) in previous sections. The calculated values of $\rho(r)$ at BCPs of O···C TtBs, O−H···O and C−H···O HBs, Cl/Br···O and O···O ChB lie in the range of 0.0097-0.0131 au, 0.0116-0.0306 au, 0.0062-0.0179 au, 0.0045 - 0.0048 au and 0.0050 au, respectively. Combined with the positive values of $\nabla^2\rho(r)$ and $H(r)$ (*cf.* Table A11), it is suggested that all intermolecular interactions of complexes with the substitutions are weakly noncovalent interactions.[132]

The $\rho(r)$ value of O1···C8 TtB in **TCH-DME-H** and **TCH-DME-CH$_3$** is greater than that in the remaining complexes. The strength of O−H···O HB in two previous complexes is also higher than the corresponding in complexes substituted

halogen which is described through the $\rho(r)$ and E_{HB} values (*cf.* Table A11). The effect of halogen substitution leads to not only the weaker of O1···C8, but also the stronger of C−H···O HB by 5-9 kJ.mol^{-1}. In addition, it exists the C−Cl/Br···O halogen bond in **TCH-DME-Cl/Br** complexes.

Table 3.22 summarizes all values of interaction energy and cooperative energy at MP2/aug-cc-pVTZ//MP2/6-311++G(2d,2p) level of theory. All complexes are stable with the E_{int} lying from -21.2 to -31.8 kJ.mol^{-1}. Accordingly, the stability of complexes $CH_3OCHX_2\cdots1CO_2\cdots1H_2O$ is increased in the order of substitution: **H~F<Cl<Br<CH$_3$**. It is remarkable that the stability trend of $CH_3OCHX_2\cdots1CO_2\cdots1H_2O$ is different with that of $CH_3OCHX_2\cdots2CO_2$ and $CH_3OCHX_2\cdots2H_2O$. Combined with the AIM results, the **TCH-DME-H/CH$_3$** is mainly stabilized by the O−H···O HB and O···C while C−H···O HB plays the main role in the **TCH-DME-F/Cl/Br** among multiple weak noncovalent interactions. The E_{int} of $CH_3OCHX_2\cdots1CO_2\cdots1H_2O$ is also estimated to be more negative than that of corresponding binary $CH_3OCHX_2\cdots1CO_2/1H_2O$. It demonstrates that the addition of a H_2O or CO_2 molecule into the $CH_3OCHX_2\cdots1CO_2/1H_2O$ leads to the enhancement in stability of the formed ternary complexes. Explicitly, for complexes of DME, a greater increase is found for the addition of H_2O (from -13.3 to -21.2 kJ.mol^{-1}) as comparison with the addition of CO_2 (from -16 to -21.2 kJ.mol^{-1}). Another evidence is that the stability of ternary complexes with the same X is followed the order: **$CH_3OCHX_2\cdots2H_2O$** > **$CH_3OCHX_2\cdots1CO_2\cdots1H_2O$** > **$CH_3OCHX_2\cdots2CO_2$**. This trend also is also observed for complexes with the substitution of halogen and methyl group into 2H in DME.

Table 3.22. Interaction energy and cooperative energy of complexes $CH_3OCHX_2\cdots1CO_2\cdots1H_2O$ (X = H, F, Cl, Br, CH_3)

Complexes	**E_{int}**	**E_{coop}**
TCH-DME-H	-21.2	-7.5
TCH-DME-F	-21.5	-5.4
TCH-DME-Cl	-24.9	-5.2
TCH-DME-Br	-26.1	-3.3
TCH-DME-CH$_3$	-31.8	-3.5

The cooperative energies between intermolecular interactions in complexes $CH_3OCHX_2\cdots 1CO_2\cdots 1H_2O$ vary from -3.3 to -7.5 kJ.mol^{-1}, which is more negative than those values of $CH_3OCHX_2\cdots 2CO_2$ (from -1.0 to -3.7 kJ.mol^{-1}) and is less negative than those of $CH_3OCHX_2\cdots 2H_2O$ (from -10.8 to -17.2 kJ.mol^{-1}) (*ca*. Table 3.21). It is consistent with the changes of stability in going from complexes with $2CO_2$,

The NBO analyses are performed at MP2/6-311++G(2d,2p) to determine the orbital interactions in complexes $CH_3OCHX_2\cdots 1CO_2\cdots 1H_2O$, as shown in Table 3.23. The EDT values of CH_3OCHX_2 component in **TCH-DME-H** and **TCH-DME-CH_3** are positive in range of 0.0031-0.0248 e, while those of **TCH-DME-F/Cl/Br** are negative from -0.0069 to 0.0049 e. It is in good agreement with the electron withdrawing effect of halogen atom in **TCH-DME-F/Cl/Br** and the electron releasing one of methyl groups in **TCH-DME-CH_3**. In general, the orbital interactions n(O)→π*(C=O), n(O)→σ*(O−H) and n(O)→σ*(C−H) represent the C···O TtB, O−H···O and C−H···O HBs. The n(Cl/Br)→σ*(C=O) delocalization proves for the interactions between Cl/Br with C=O group of CO_2 and plays an additional role to the complex stabilization.

The $E^{(2)}$ values of (O)→π*(C=O) and n(O)→σ*(O−H) delocalizations are higher than those of n(O)→σ*(C−H) indicating the important role of C···O TtB and O−H···O HB in **TCH-DME-H/CH_3** complexes. Especially, the $E^{(2)}$ value of O−H···O HB in **TCH-DME-CH_3** is highest, of 42 kJ.mol^{-1} demonstrating the great electron releasing effect of methyl groups as compare to the corresponding value of 7.3 kJ.mol^{-1} in complexes of dimethyl ether. The stabilization energy of n(O)→σ*(C−H) in **TCH-DME-F/Cl/Br** ranges from 14.9 to 17.1 kJ.mol^{-1} which is higher than that of n(O)→σ*(O−H) and n(O)→ π*(C=O) (about 3.9-7.9 kJ.mol^{-1} and 5.6 kJ.mol^{-1}, respectively). It confirms the important role of C−H···O in halogen-derivated complexes.

Table 3.23. EDT and $E^{(2)}$ for $CH_3OCHX_2\cdots 1CO_2\cdots 1H_2O$ (X = H, F, Cl, Br, CH_3) at MP2/6-311++G(2d,2p) level of theory

Complex	EDT/e	Delocalization	E(2)/kJ.mol^{-1}
TCH-DME-H	0.0031[(a)]	n(O1) → π*(C10=O11)	10.4
	-0.0035[(b)]	n(O12) → σ*(O13−H14)	7.3
	0.0004[(c)]	n(O13) → σ*(C2−H4)	5.2
TCH-DME-F	-0.0049[(a)]	n(O1) → π*(C8=O9)	5.7
	-0.0001[(b)]	n(O10) → σ*(O11−H12)	7.9
	0.0050[(c)]	n(O11) → σ*(C2−H3)	14.9
TCH-DME-Cl		n(O1) → π*(C8=O9)	5.6
	-0.0055[(a)]	n(Cl15) → π*(C8=O9)	1.3
	-0.0032[(b)]	n(O10) → σ*(O11−H12)	3.9
	0.0087[(c)]	n(O11) → σ*(C2−H3)	16.4
		n(O11) → σ*(C2−Cl14)	0.7
TCH-DME-Br		n(O1) → π*(C8=O9)	5.6
	-0.0069[(a)]	n(Br14) → π*(C8=O9)	1.4
	-0.0032[(b)]	n(O10) → σ*(O11−H12)	3.4
	0.0101[(c)]	n(O11) → σ*(C2−H3)	17.1
		n(O11) → σ*(C2−Br15)	0.9
TCH-DME-CH_3	0.0248[(a)]	n(O1) → π*(C8=O9)	2.9
	-0.0041[(b)]	n(O1) → π*(C8=O10)	2.6
	-0.0207[(c)]	n(O1) → σ*(O11−H12)	42.5

[(a), (b), (c)] are EDT values of CH_3OCHX_2, CO_2 and H_2O, respectively.

The changes in bond length, stretching vibrational frequency of C/O−H involved HBs are collected in Table 3.24. The C−H···O HBs in complexes **TCH-DME-H/CH_3** belong to the blue-shifting HB, which is described through a shortened bond length of C−H of 0.0009-0.0010 Å and an increase of stretching vibrational frequency of 18.9-24.9 cm^{-1}. In contrast, the O−H···O HBs in all complexes **$CH_3OCHX_2\cdots 1CO_2\cdots 1H_2O$** are red-shifted of 30.9-229.1 cm^{-1} and an increase in bond length of O−H about 0.0021-0.0110 Å, as compared to those in isolated monomers.

Table 3.24. Changes of bond length C(O)−H (in Å) and stretching frequency (Δν(C/O-H), in cm^{-1}) of C-H and O-H bonds involved in HB of complexes $CH_3OCHX_2\cdots 1CO_2\cdots 1H_2O$ (X = H, F, Cl, Br, CH_3)

Complex	Interaction	Δr (Å)	Δν (cm^{-1})	Δσ*(C(O)−H) (e)	Δ%s(C(O)) (%)
TCH-DME-H	C2−H4···O13	-0.0009	18.9	0.0007	0.92
	O13−H14···O12	0.0025	-37.4	0.0028	1.30
TCH-DME-F	C2−H3···O11	-0.0010	24.9	-0.0012	1.38
	O11−H12···O10	0.0021	-30.9	0.0021	1.21
	C4−H6···O9	0.0001	0.4	0.0005	0.14
TCH-DME-Cl	C2−H3···O11	0.0008	1.3	-0.0010	1.87
	O11−H12···O10	0.0024	-33.7	0.0016	1.00
TCH-DME-Br	C2−H3···O11	0.0013	-6.4	0.0000	2.06
	O11−H12···O10	0.0024	-33.9	0.0014	0.93
TCH-DME-CH_3	O11−H12···O1	0.0110	-229.1	0.0233	3.01

3.5.5. Remarks

The investigation into interactions of CH_3OCH_3 and the substituted-derivative CH_3OCHX_2 (X = F, Cl, Br, CH_3) at high level of theory was performed to explore the stability, properties and effect of di-halogen and dimethyl substitution.

For binary complexes $CH_3OCHX_2\cdots 1CO_2/H_2O$, the stability is increased as order of substitution as F < Cl < Br < H < CH_3. The upward trend of stability for ternary complexes is different, due to the existence of the Cl/Br···C=O TtB and Cl/Br···O interactions. In general, the halogenated-substituted derivatives cause a decrease in the complex strength while methyl-substituted one leads to a stabilization enhancement.

For the same X, the addition of H_2O contributes a large amount to the complex stabilization, as compared to the addition of CO_2. AIM results found that all intermolecular interactions are weakly noncovalent interactions. The C···O TtB still plays the main contribution into the stability of complexes with the complement of C−H···O HB in complexes with $1,2CO_2$. The complexes of $1,2H_2O$ are stabilized significantly by O−H···O HBs. This HB is also found to contribute to the positive cooperative effect leading to the greater cooperativity in $CH_3OCHX_2\cdots 2H_2O$ in

comparison with in $CH_3OCHX_2\cdots 2CO_2$.

SAPT2+ results for $CH_3OCHX_2\cdots 1CO_2$ complexes that the attractive electrostatic energy is the main contribution overcoming dispersion and induction energetic components in stabilizing the complexes.

3.6. Interactions of dimethyl sulfide with nCO_2 (n=1-2)

This section is based on the results of Ref. 146.

In this section, complexes of dimethyl sulfide (DMS) with nCO_2 and nH_2O are denoted as **DX-DMS-n,** and **TX-DMS-n**, for dimer and trimer, respectively; **X** stands for **C** (CO_2) or **H** (H_2O) and **n** = 1, 2, 3, ... are numerical orders of isomers.

3.6.1. Geometric structures and AIM analysis

The geometric shapes and topolographies of complexes formed by interactions between DMS and CO_2 ($DMS\cdots nCO_2$) (n=1-2) at MP2/6-311++G(2d,2p) are shown in Fig. 3.14.

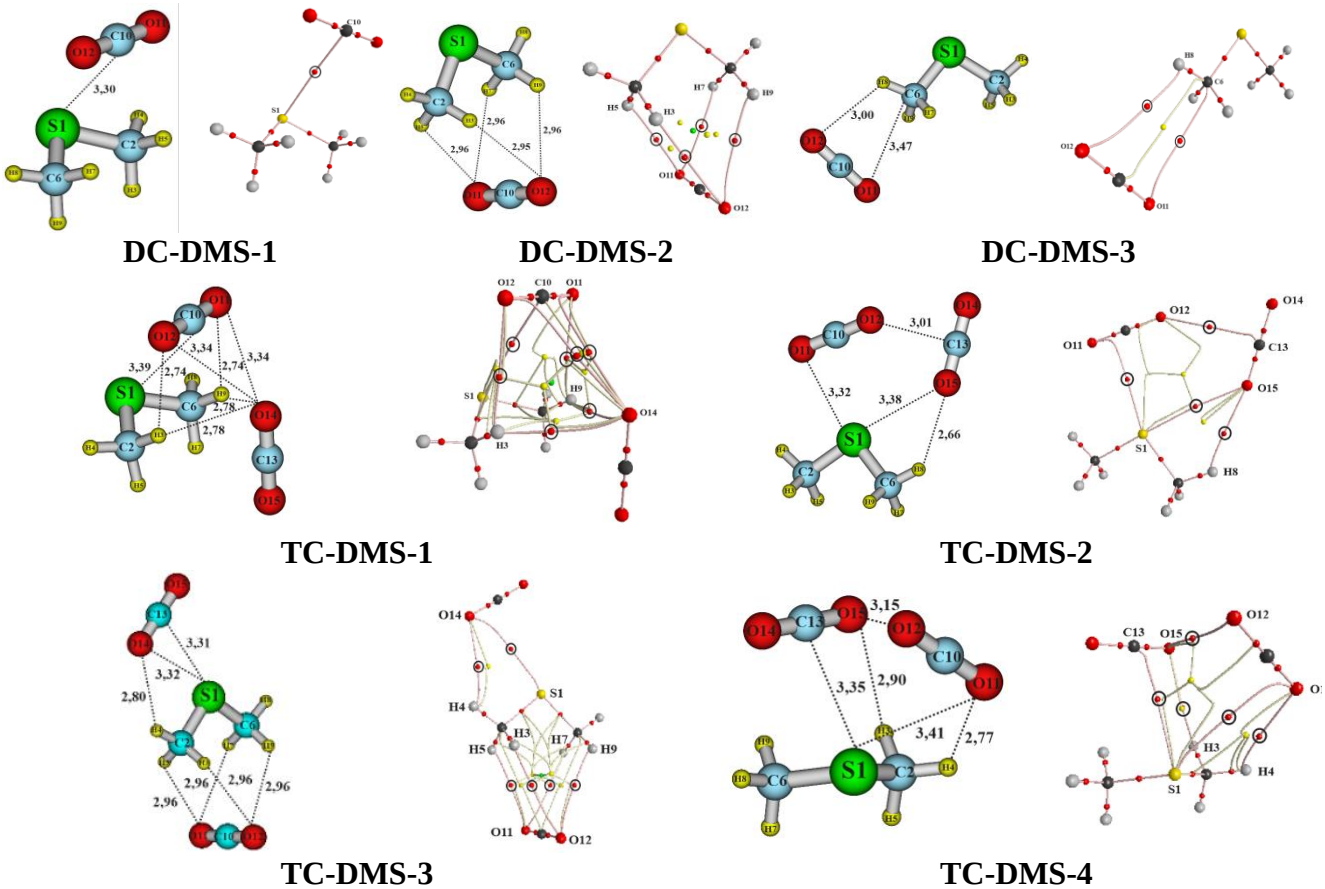

Figure 3.14. Optimized structures and topological geometries of $(CH_3)_2S$ and nCO_2 (n = 1-2) (all distances are in Å)

Fig. 3.14 shows that the distances of the O···H, S···C, C···O, S···O và O···O contacts are in the ranges of 2.66−3.04, 3.30−3.39, 3.01−3.47, 3.32−3.52 and 3.10−3.34 Å, respectively; which are smaller than the sum of van der Waals radii of the two atoms involving interactions (being 2.72, 3.22, 3.55, 3.37 and 3.04 Å for the corresponding pairs of H and O, S and C, C and O, S and O, O and O atoms). The DMS···nCO_2 (n = 1-2) complexes are formed by the intermolecular contacts which are HBs and/or tetrel interactions and/or chalcogen interactions.

Table 3.25. Selected parameters at the BCPs of intermolecular contacts of $(CH_3)_2S$···1,2CO_2 complexes

Complex	Contact	$\rho(r)$ (au)	$\nabla^2\rho(r)$ (au)	$H(r)$ (au)
DC-DMS-1	S1···C10−O12	0.008	0.030	0.0015
DC-DMS-2	C2−H5···O11	0.004	0.015	0.0007
	C6−H7···O11	0.004	0.015	0.0007
	C2−H3···O12	0.004	0.015	0.0007
	C6−H9···O12	0.004	0.015	0.0007
DC-DMS-3	C6−H8···O12	0.004	0.015	0.0008
	O11···C6	0.004	0.016	0.0010
TC-DMS-1	S1···C10−O12	0.006	0.026	0.0014
	C2−H3···O12	0.006	0.022	0.0009
	C6−H9···O11	0.006	0.022	0.0009
	C2−H3···O14	0.005	0.020	0.0009
	C6−H9···O14	0.005	0.020	0.0009
	O11···O14	0.004	0.020	0.0011
	O12···O14	0.004	0.020	0.0011
TC-DMS-2	S1···O11	0.007	0.029	0.0013
	O12···C13−O14	0.006	0.027	0.0013
	C6−H8···O15	0.005	0.021	0.0010
	S1···O15	0.004	0.018	0.0008
TC-DMS-3	C2−H5···O11	0.004	0.015	0.0007
	C2−H3···O12	0.004	0.015	0.0007
	C6−H7···O11	0.004	0.015	0.0007
	C6−H9···O12	0.004	0.015	0.0007
	C2−H4···O14	0.005	0.018	0.0007
	S1···O14	0.007	0.026	0.0011
TC-DMS-4	S1···O11	0.007	0.025	0.0011
	S1···C13−O14	0.008	0.027	0.0013
	O12···O15	0.007	0.028	0.0011
	C2−H4···O11	0.005	0.020	0.0008
	C2−H3···O15	0.004	0.016	0.0008

The obtained results from AIM analysis are collected in Table 3.25. All the values of $\rho(r)$, $\nabla^2\rho(r)$ and $H(r)$ at BCPs of all intermolecular interactions are in the ranges of 0.004-0.008 au, 0.015-0.022 au and 0.0007-0.0015 au, respectively. These values fall within the critical limits for the formation of weak and noncovalent interaction in nature.[132] Accordingly, all intermolecular contacts in the complexes are noncovalent weak interactions. For DMS···CO_2 binary complexes, the value of $\rho(r)$ at the BCP of S···C=O TtBs in **DC-DMS-1** is *ca.* 0.0004 au larger than that of other interactions in **DC-DMS-2** and **DC-DMS-3**. These results imply a larger strength of the S···C=O TtB relative to the C−H···O HB. As a consequence, it is roughly predicted that **DC-DMS-1** is the most stable complex of DMS···CO_2. There are four C−H···O HBs in **DC-DMS-2** while **DC-DMS-3** is formed by only one C−H···O HB and one C···O TtB with the comparable values of electron densities at BCPs of the contacts. As a result, the stability of DMS···CO_2 binary complexes decreases in the ordering of **DC-DMS-1** > **DC-DMS-2** > **DC-DMS-3**.

In going from DMS···CO_2 binary to DMS···2CO_2 ternary complexes, S(O)···O chalcogen bonds are found along with conventional TtBs and HBs mentioned above. For DMS···2CO_2 system, S···C=O TtB in **TC-DMS-4** dominates the remaining intermolecular contacts which is due to the highest value of electron density at its BCP (0.008 au). It is clear that there is a slight increase of $\rho(r)$ at the BCPs of intermolecular interactions in sequence from C−H···O to S(O)···O, O···C=O and then to S···C=O, implying a strengthening increase in this trend. In a word, the stability of complexes between DMS and nCO_2 (n = 1-2) is mainly contributed by S···C=O TtB with an additional complement from C−H···O HB and S(O)···O ChB. This observation is quite consistent with that taken from the complexes of dimethyl ether and CO_2 in which the TtB overwhelming the C−H···O HB has a significant impact on the stability of complex.[147]

3.6.2. Interaction and cooperativity energy and energetic components

Interaction and cooperative energies of complexes DMS···nCO_2 at MP2/aug-cc-pVTZ//MP2/6-311++G(2d,2p) are tabulated in Table 3.26. The interaction

energies of the complexes are negative and range from -2.7 to -22.0 kJ.mol^{-1} (with both ZPE and BSSE corrections) indicating that the complexes investigated are quite stable. The ternary complexes are *ca.* 10-12 kJ.mol^{-1} more stable than the binary ones. This suggests that an addition of one CO_2 molecule to DMS···CO_2 leads to an increase in stability of complex.

Table 3.26. Interaction energies and cooperative energies of complexes DMS···nCO_2

Complex	E_{int}	Complex	E_{int}	E_{coop}
DC-DMS-1	-9.9	**TC-DMS-1**	-15.2	-1.0
DC-DMS-2	-3.9	**TC-DMS-2**	-16.9	-0.6
DC-DMS-3	-2.7	**TC-DMS-3**	-12.5	-0.4
		TC-DMS-4	-22.0	-0.8

All values are in kJ.mol^{-1}.

For the binary system, the interaction energy is more negative for **DC-DMS-1** than for **DC-DMS-2** and **DC-DMS-3** by *ca.* 6.0 and 7.2 kJ.mol^{-1}, respectively. This indicates a decrease in the stability of complexes in going from **DC-DMS-1** to **DC-DMS-2** and then to **DC-DMS-3**, which is consistent with AIM analysis above. In comparison with other organic molecules, the interaction energy of **DC-DMS-1** is less negative that that of $(CH_3)_2O$···1CO_2 and $(CH_3)_2CO$···1CO_2 by *ca.* 3.8 and 1.2 kJ.mol^{-1}. It is predicted that the solubility of DME and DMSO in scCO_2 is slightly better than DMS.[40] For ternary complexes, **TC-DMS-4** has the most negative interaction energy with -22.0 kJ.mol^{-1} while **TC-DMS-3** is the least stable complex with an energetic value of -12.5 kJ.mol^{-1}. As shown in Table 3.19, the stability of ternary complexes decreases in the trend of **TC-DMS-4** > **TC-DMS-2** > **TC-DMS-1** > **TC-DMS-3**, which is in good agreement with the obtained results from AIM analysis above. The values of E_{coop} with ZPE and BSSE corrections of trimer are also given in the Table 3.26. All E_{coop} values are slightly negative and fall within the range of -0.4 to -1.0 kJ.mol^{-1}, indicating that the cooperativity of intermolecular interactions takes place in complexes and leads to an enhance in the strength of ternary complexes.

SAPT2+ analysis is used to evaluate contribution of different energetic components to total stabilization energy of the binary complexes, which include

electrostatic (E_{elest}), exchange energy (E_{exch}), induction (E_{ind}), dispersion (E_{disp}) and the second and high order level correlation energy ($\delta E_{int,r}^{HF}$).

Table 3.27. Contributions of different energetic components into stabilization energy of complexes DMS···nCO_2 using SAPT2+ approach (kJ.mol^{-1})

Complex	$\mathbf{E_{elest}}$	$\mathbf{E_{exch}}$	$\mathbf{E_{ind}}$	$\mathbf{E_{disp}}$	$\boldsymbol{\delta E_{int,r}^{HF}}$
DC-DMS-1	-15.3(30.1)	46.3	-21.3(42.1)	-13.1(25.9)	-1.0(1.9)
DC-DMS-2	-0.6(4.1)	14.1	-4.2(29.3)	-9.3(64.3)	-0.3(2.2)
DC-DMS-3	-1.0(11.3)	7.5	-2.2(24.4)	-5.5(62.3)	-0.2(1.9)

Values in brackets are the percentages (%) of corresponding energetic components contributing to total stabilization energy.

Table 3.27 shows that there are three mainly energetic components contributing to stability of DMS···CO_2 complexes. A larger role of induction term (42.1%) as compared to both electrostatic (30.1%) and dispersion (25.9%) terms is found for **DC-DMS-1**, while **DC-DMS-2** and **DC-DMS-3** are mainly determined by dispersion term of 62.3−64.3% overwhelming induction (24.4-29.3%) and electrostatic (4.1-11.3%) term. Contribution of the second and high order level correlation energy to stabilization of binary complexes is quite small. Therefore, the stability of DMS···CO_2 is contributed mainly by induction component as compared to other energetic components.

3.6.3. Vibrational and NBO analyses

The stretching vibrational frequency and NBO analyses for DMS···nCO_2 complexes (n=1-2) and relevant monomers are performed at MP2/6-311++G(2d,2p). EDT and electron transfer process and donor-acceptor stabilization energy are gathered in Table 3.28.

There are different directions of electron density transfer between CO_2 and DMS upon complexation. The EDT values of DMS in **DC-DMS-1**, **TC-DMS-(1-4)** are positive while those values in the remaining complexes are negative. These results show that electron density is transferred from DMS to CO_2 in stable complexes including **DC-DMS-1** and **TC-DMS-4.** The presence of electron transfer processes from n(O) to σ*(C−H) anti-bonding orbitals and from n(S), n(O) to

π*(C=O) anti-bonding orbitals confirm the formation of C−H···O HBs and >C=O···S(O) TtBs in the complexes investigated. Moreover, π(C=O)→σ*(S−C) and n(O)→σ*(S−C) processes are found to be represented for S···O ChBs.

Table 3.28. Selected results of vibrational and NBO analysis of complexes DMS···nCO_2 at MP2/6-311++G(2d,2p)

Complex	**EDT** (e)	**Delocalization**	$\mathbf{E_{inter}}$ (kJ.mol^{-1})	$\mathbf{\Delta r_{C-H}}$ (Å)	$\mathbf{\Delta \nu_{C-H}}$ (cm^{-1})
DC-DMS-1	0.0085[a)]	n(S1)→π*(C10=O12)	7.2	-	-
DC-DMS-2	-0.0004[a)]	n(O11)→σ*(C2−H5)	0.2	0.0005	-3.5
		n(O11)→σ*(C6−H7)	0.2	0.0004	-3.0
		n(O12)→σ*(C2−H3)	0.3	0.0004	-2.7
		n(O12)→σ*(C6−H9)	0.3	0.0004	-3.0
DC-DMS-3	-0.0006[a)]	n(O12)→σ*(C6−H8)	0.2	-0.0002	-6.6
TC-DMS-1	0.0048[a)] -0.0060[b)] 0.0012[c)]	n(S1)→π*(C10=O11)	4.9	-	-
		n(O12)→σ*(C2−H3)	0.5	-0.0005	9.9
		n(O11)→σ*(C6−H9)	0.5	-0.0005	10.1
		n(O14)→σ*(C2−H3)	0.7	-0.0005	9.9
		n(O14)→σ*(C6−H9)	0.7	-0.0005	10.1
		n(O14)→π*(C10=O11)	2.0	-	-
TC-DMS-2	0.0028[a)] -0.0023[b)] -0.0005[c)]	n(S1)→π*(C10=O11)	3.2	-	-
		π(C10−O11)→σ*(S1−C6)	1.7	-	-
		n(O12)→π*(C13=O14)	2.8	-	-
		n(O15)→σ*(C6−H8)	1.0	-0.0015	11.5
		n(O15)→π*(S1−C2)	1.5	-	-
TC-DMS-3	0.0031[a)] -0.0028[b)] -0.0003[c)]	π(C10−O11)→σ*(C2−H5)	0.3	0.0003	-1.3
		π(C10−O12)→σ*(C2−H3)	0.2	0.0003	-1.3
		π(C10−O11)→σ*(C6−H7)	0.3	0.0003	-1.0
		π(C10−O12)→σ*(C6−H9)	0.2	0.0003	-1.0
		n(O14)→σ*(C2−H4)	0.8	-0.0009	3.1
		n(O11)→π*(C6−S1)	0.8	-	-
		n(S1)→π*(C13=O15)	2.5	-	-
TC-DMS-4	0.0108[a)] -0.0034[b)] -0.0074[c)]	n(S1)→π*(C10=O11)	3.6	-	-
		n(S1)→π*(C13=O14)	5.5	-	-
		n(O12)→π*(C13=O14)	3.6	-	-
		n(O15)→π*(C10=O11)	1.6	-	-
		n(O11)→σ*(C2−H4)	0.3	-0.0012	6.7
		n(O15)→σ*(C2−H3)	0.3	0.0002	1.1

[a), b), c)] *for charge of DMS, CO_2, CO_2*

n: nonbonded (lone-pair) orbital, σ: anti σ-bond, π*: anti π-bond*

For binary complexes, the E_{inter} value of n(S)→π*(C=O) in **DC-DMS-1** is 7.2 kJ.mol^{-1}, while they are *ca.* 0.3 kJ.mol^{-1} for electron transfer from n(O) to σ*(C−H) in **DC-DMS-2** and **DC-DMS-3**. This affirms that the stability of DMS···1CO_2 complexes increases in the sequence: **DC-DMS-3** < **DC-DMS-2** < **DC-DMS-1**. The same tendency is also obtained for DMS···2CO_2 ternary complexes. The >C=O···S(O) TtBs dominate the other interactions in stabilization of complexes (*cf.* Table 3.21). Four >C=O···S(O) TtBs are found in **TC-DMS-4** with the largest E_{inter} value of 5.5 kJ.mol^{-1}, showing that **TC-DMS-4** is the most stable complex for DMS···2CO_2 ternary system. The **TC-DMS-1** and **TC-DMS-2** are stabilized mainly by two S(O)···C=O TtBs with the E_{inter} values ranging from 2.0 to 4.9 kJ.mol^{-1}. Meanwhile, **TC-DMS-3** is only formed by S···C=O and other weak interactions (E_{inter} values of 0.2-0.8 kJ.mol^{-1}). Accordingly, the stability of ternary complexes decreases in the ordering **TC-DMS-4** > **TC-DMS-2** > **TC-DMS-1** > **TC-DMS-3**, which is consistent with the results of interaction energy in Table 3.19. These results also show that intermolecular interactions have increasing order of stability in going from C−H···O to S···O to O···C=O and then to S···C=O.

When adding one CO_2 molecule to DMS···1CO_2, the stabilization energy of n(S)→π*(C=O) processes are lowers by 1.7-4.7 kJ.mol^{-1} and that of n(O)→σ*(C−H) processes rise slightly by 0-1.7 kJ.mol^{-1}. This indicates that when the cooperativity of intermolecular interactions happens, the strength of >C=O···S TtBs decreases while it is increased for C−H···O HBs. In summary, NBO results confirm again that the S···C=O TtB plays a primary role into the stability of DMS···nCO_2 complexes while the other interactions act as an additional component.

The characteristics of the C−H···O hydrogen bond are investigated *via* the changes of C-H bond length and its stretching frequency in complexes compared to relevant monomers, as described in Table 3.21. In general, the C−H bond lengths in ternary complexes are shortened by 0.0002−0.0015 Å and accompanied by an increase in stretching frequency of 3.1−11.5 cm^{-1}. However, a small elongation of C−H bond length of 0.0001−0.0007 Å and a decrease of its corresponding

stretching frequency of 1.0−6.0 cm^{-1} in **DC-DMS-2** and **DC-DMS-3** are estimated. Nevertheless, both changes of C-H bond lengths and stretching frequencies are quite small and do not rule, causing difficulty in assigning exactly to kind of C−H···O hydrogen bond in the systems. This assignment will be explored in our next work on the basis of deeper investigations.

3.6.4. Remarks

The theoretical investigation on interactions between DMS and CO_2 induce nine stable structures in which three for DMS···1CO_2 binary and six for DMS···2CO_2 ternary complexes.

The interaction energies of DMS···nCO_2 (n=1-2) complexes range from -8.3 to -22.0 $kJ.mol^{-1}$ at the MP2/aug-cc-pVTZ//MP2/6-311++G(2d,2p) level. The complex stabilization is mainly determined by S(O)···C=O TtB overcoming the O(S)···O ChB and C−H···O HB. When a CO_2 molecule is added to DMS···1CO_2 dimer, the stability of complexes is enhanced due to the slightly cooperative effect of intermolecular interactions. The SAPT2+ analysis shows a dominating contribution of induction term as compared to other energetic terms to the overall stabilization energy of DMS···nCO_2 complexes. For HBs, the changes of C-H bond lengths and stretching frequencies are quite small and complicated to distinguish type of HBs. This problem is hoped to be solved in the future work.

3.7. Growth pattern of the C_2H_5OH···nCO_2 complexes (n=1-5)

This section is based on the results of Ref. 148.

3.7.1. Structural pattern of the C_2H_5OH···nCO_2 complexes (n=1-5)

The stable configurations and geometric parameters of C_2H_5OH···nCO_2 (n=1−5) complexes at the MP2/6−311++G(2d,2p) level are presented in Fig. 3.15a-b. The dash lines in Fig. 3.15a-b represent the intermolecular interactions which are taken from AIM topological analysis. The molecular graphs of some complexes formed are provided in Fig. A11 of *Appendix*, with the aim of finding out intermolecular interactions formed. The existence of BCPs is considered as the indicator for the formation of interactions.

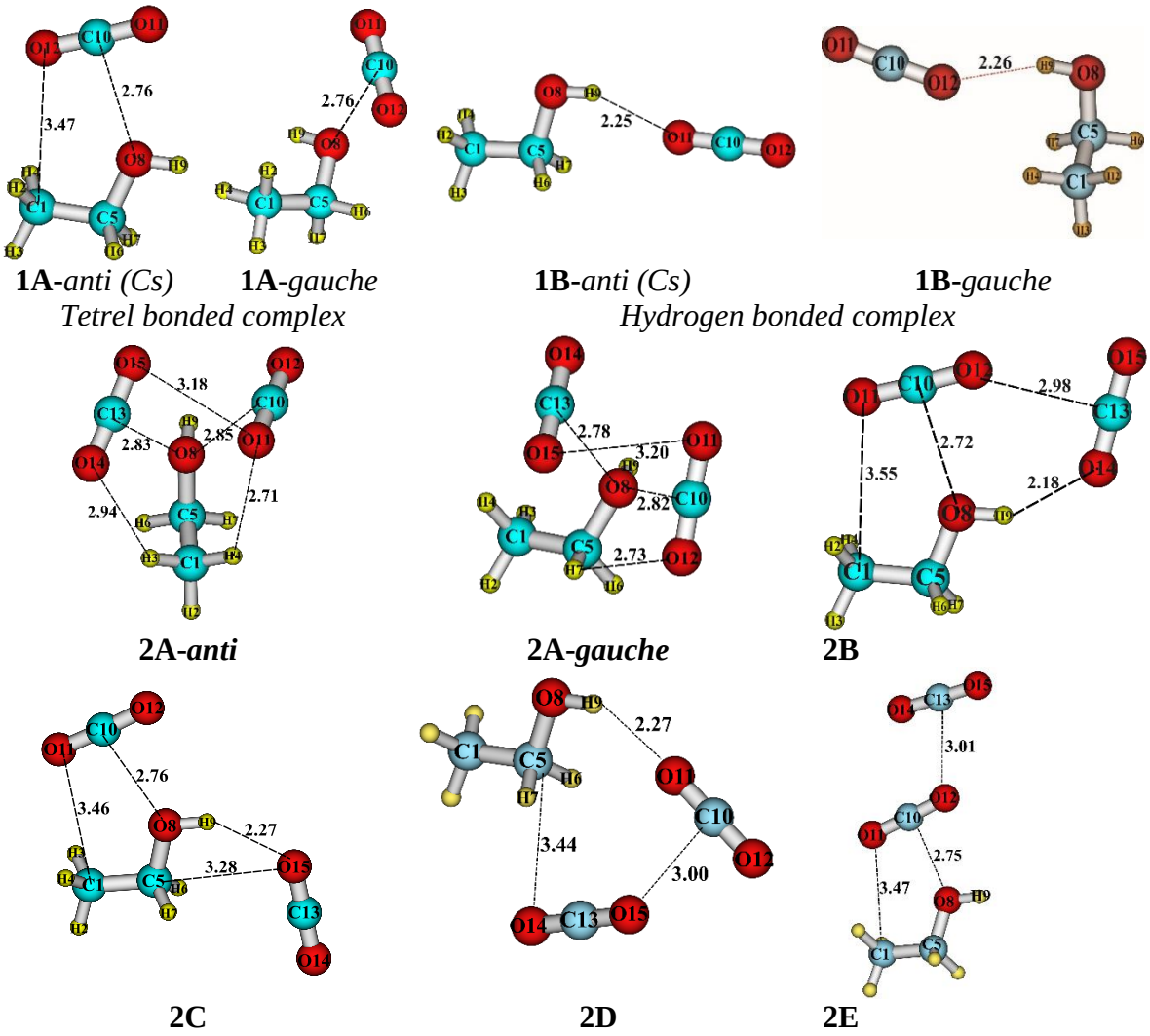

Figure 3.15a. Optimized structures of $C_2H_5OH\cdots nCO_2$ (n=1-2)

From Fig. 3.14a-b, geometries adopted by interactions between ethanol and nCO_2 molecules are consistent with Saitow *et al.*[58] that the high attractive energy of ethanol in $scCO_2$ was driven by the large negative charge on the oxygen atom of ethanol (O8). Values of $\rho(r)$, $\nabla^2(\rho(r))$ and $H(r)$ at BCPs of intermolecular interactions are summarized in Table A12 of *Appendix*. These values lie in the ranges of 0.003-0.013, 0.012-0.052, and 0.001-0.002 au, respectively, indicating that all interactions formed are weakly noncovalent.[132]

For binary complexes, two types of geometries are observed: i) tetrel bonded model (**1A-***anti*/*gauche*) and ii) hydrogen bonded one (**1B-***anti*/*gauche*). In particular, the *anti* and *gauche* structures are formed from the corresponding *anti* and *gauche* isomers of ethanol which are distinguished by the orientation of the OH

bond with respect to CCO plane. The *anti* conformer of ethanol is predicted to be more stable than the *gauche* one by 0.5 kcal.mol^{-1} at CCSD(T)/aug-cc-pVTZ.[149] The O8···C_{CO2} distances of **1A**-*anti* and **1A**-*gauche* are very close to those in previous studies.[49,57] The calculated rotational constants of these structures are given in Table 3.29. Our predicted rotational spectra of **1A**-*anti* fit well with the experimental data, as previous studies did.[48,49,58,150]

Table 3.29. Rotational constant and vibrational frequencies of OH group of isolated ethanol and C_2H_5OH···nCO_2 complexes

	A (MHz)	**B** (MHz)	**C** (MHz)		ν_{OH} (cm^{-1})	**Intensity** (10^{-40}.esu^2.cm^2)
1A-*anti*	6090.39	1721.79	1365.04	**C_2H_5OH**	3881	38.1
1A-*gauche*	5989.29	1706.24	1526.29	**1A-*anti***	3876	42.6
1B-*anti*	18475.91	0807.35	0781.04	**2A-*anti***	3866	42.9
1B-*gauche*	8652.14	1024.63	0951.94	**3A**	3857	124.1
Exptl[150]	6128.02	1677.25	1340.85	**4A**	3852	164.5
				5A	3858	127.8

When the number of CO_2 molecules increases, multiple interactions between C_2H_5OH and CO_2 molecules are observed. Indeed, six ternary structures are determined to be the minima on PES of C_2H_5OH···$2CO_2$. According to previous studies, the **2A**-*anti* complex was suggested as the minima for C_2H_5OH···$2CO_2$ system[57,58] while the *gauche* conformer and other four ternary complexes have not been reported so far. As shown in Fig. 3.14a, **2A**-*anti* and **2A**-*gauche* are the rearrangements of C_2H_5OH corresponding conformers and two CO_2 molecules *via* two O8···C TtB and C−H···O HBs. It is worth noting that two CO_2 in **2A** are oriented to associate with two electron lone pairs of the oxygen atom O8 in C_2H_5OH. This result confirms the geometrical arrangements reported previously using molecular dynamic simulation.[57] The **2B**-**2D** structures are mainly formed *via* O−H···O HB, whereas, three components in **2E** associate as layers from C_2H_5OH to the first CO_2 and next to the remaining CO_2.

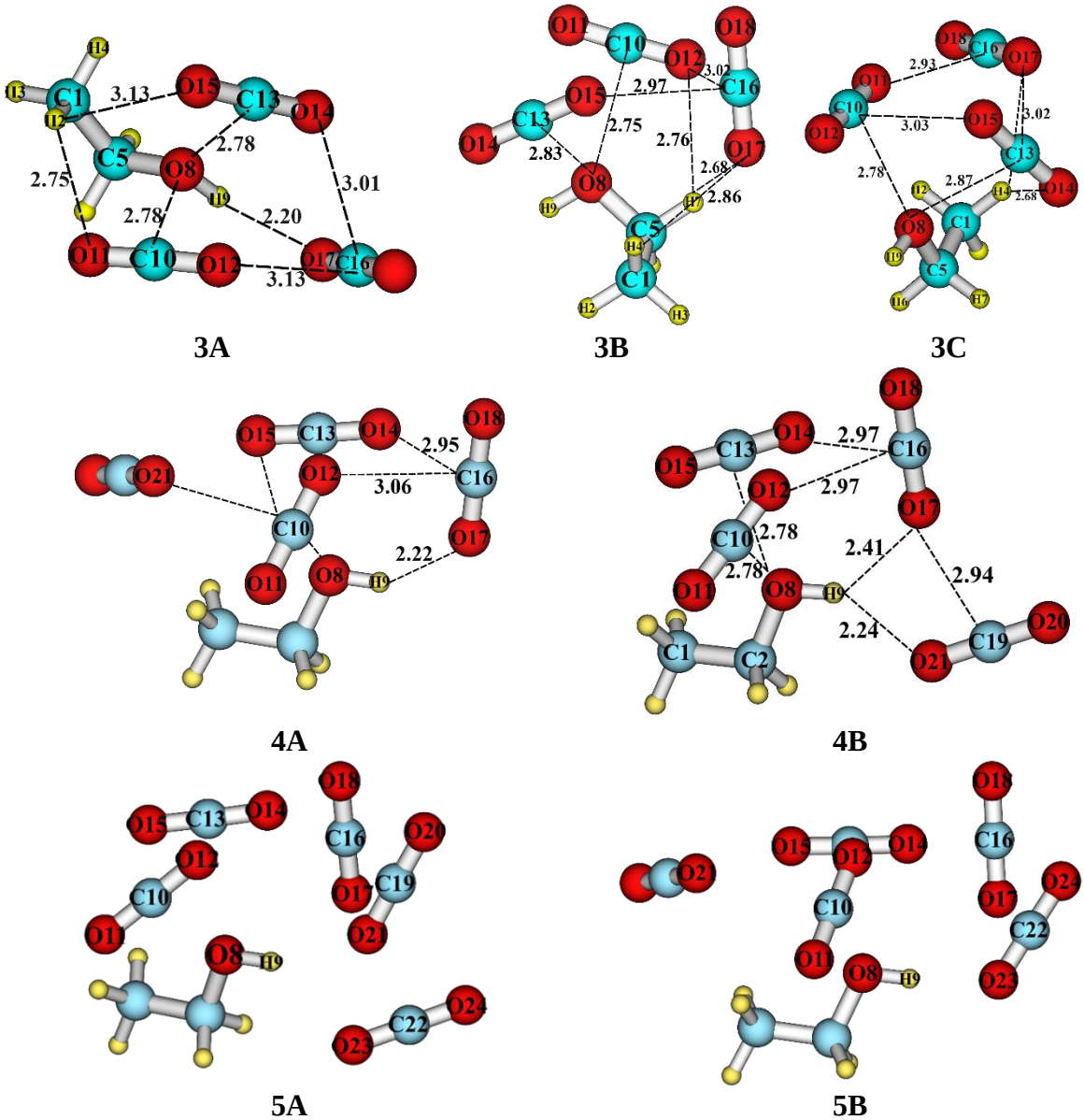

Figure 3.15b. Optimized structures of $C_2H_5OH\cdots nCO_2$ (n=3-5)

For n=3-4, the stable shapes of complexes are out-of-plane positioning of CO_2 (out-of-plane here means that the O-C-O axis of CO_2 does not lie on the CCO plane of C_2H_5OH) (*cf.* Fig. 3.15b). Interestingly, all sub-molecules interact with one another to form cage structures. The complexes with $3CO_2$ are obtained from the corresponding **2A**-*anti* or **2A**-*gauche* geometries with different positions of the third CO_2. For the conformers containing four CO_2 molecules, the fourth CO_2 molecule is likely to connect to neighbour CO_2 molecules rather than the C_2H_5OH as observed in the smaller complexes with $\leq 3CO_2$ molecules. The same way is also found for

stable structures with $5CO_2$. Complexes of ethanol with nCO_2 (n=1–5) seem to be similar to other carbonyl-containing molecules, in which CO_2 molecules surround the functional groups (=O, >C=O, and –OH) of the host molecules.[45,151] From the optimized geometries, it is suggested that CO_2 prefers to orient around the -OH functional group to interact with the lone pair or negative region of O8 of ethanol.

3.7.2. Complex stability, and changes of OH stretching frequency and intensity under variation of CO_2 molecules

The energetic characteristics of the $C_2H_5OH\cdots nCO_2$ complexes (n=1-5) at MP2/aug-cc-pVTZ//MP2/6-311++G(2d,2p) are gathered in Table 3.30. The binding energies with ZPE and BSSE corrections are generally negative, in the range between -4.6 kJ.mol^{-1} of **1B** complex and -61.9 kJ.mol^{-1} of **5A** one. Their stabilities rise in the order $1CO_2 < 2CO_2 < 3CO_2 < 4CO_2 < 5CO_2$. It is proposed that the addition of CO_2 molecules leads to the stability enhancement of investigated complexes.

Table 3.30. Binding energy ($\mathbf{E_b}$) of $C_2H_5OH\cdots nCO_2$ complexes (n=1-5) (in kJ.mol^{-1}) calculated at the MP2/aug-cc-pVTZ//MP2/6-311++G(2d,2p) level of theory

Complexes	E_b	Complexes	E_b
1A-*anti*	-11.4	**3A**	-38.2
1A-*gauche*	-10.7	**3B**	-35.6
1B-*anti*	-5.1	**3C**	-34.3
1B-*gauche*	-4.6	**4A**	-48.6
2A-*anti*	-23.9	**4B**	-47.9
2A-*gauche*	-23.6	**5A**	-61.9
2B	-22.1	**5B**	-59.7
2C	-17.0		
2D	-12.5		
2E	-16.2		

As shown in Table 3.26, the binding energies of **1A-*anti*** and **1A-*gauche*** complexes are -11.4 and -10.7 kJ.mol^{-1}, respectively. These values are more negative than those of hydrogen bonded structures by 5.6–6.8 kJ.mol^{-1}. Hence, the tetrel bonded model is the energetic-favourable structure of $C_2H_5OH\cdots 1CO_2$ in comparison with the hydrogen bonded one which is consistent with the previous

static analyses.[49,58,152,153] Both *anti* isomers are found to be more negative than the gauche ones by 0.5–0.7 kJ.mol^{-1}. Thus, the *anti*-typed geometry corresponds to characteristic structure for ethanol complexes that exhibits large attractive energy. Electron density at BCPs adopted from AIM calculations is considered as a diagnostic of bond strength, in which a larger $\rho(r)$ value means a stronger strength and *vice versa*, for the same type of interaction.[154,155] The $\rho(r)$ at BCP of O8···C TtB in **1A**-*anti* and **1A**-*gauche* are 0.010 and 0.011 au (*ca*. Table A12 of Appendix). Nevertheless, **1A**-*anti* is reinforced by a C=O···C1 secondary TtB with $\rho(r)$ at BCP of 0.004 au. Therefore, the slightly higher stability of **1A**-*anti* as compared to **1A**-*gauche* is due to an additional role of C=O···C1 TtB. With the aim of CO_2 capture, the interaction capacity of CO_2 with ethanol is weaker than that of carbonyl/sulfoxide compounds, compatible with that of methanol, methylamine, and obviously stronger than alkanes such as methane, ethane and ethylene.[40,45,58,124,147]

For complexes with $2CO_2$, **2A** conformers display the approximate binding energies. The remaining complexes are less stable than **2A** by roughly 1.5–7.7 kJ.mol^{-1}. The increasing stability of ternary complexes is estimated in the order of **2D** < **2E** < **2C** < **2B** < **2A**-*gauche* ≈ **2A**-*anti*. Combined with their geometries, the TtBs between CO_2 and ethanol are still preferred in case of $2CO_2$ molecules. For comparison purposes, the geometrical and energetic calculations on complexes of $(CO_2)_n$ (n=2-3) were employed at the same level of theory as in the present work. The minima and their binding energies were previously elucidated.[156,157,158] The calculated binding energies for the minima of these complexes are of -4.4 and -12.3 kJ.mol^{-1} for $(CO_2)_2$ and $(CO_2)_3$, respectively. Both of them are less negative than those of relevant complexes between ethanol and 1,2 molecules of CO_2 (**1A**-*anti* and **2A**-*anti*). Hence, the solvent-solvent interactions between CO_2 molecules are obviously less stable than the solute-solvent ones between CO_2 and ethanol.

To thoroughly investigate the combinations of ethanol with CO_2, dimers of ethanol and their complexes with CO_2 have been recalculated at MP2/aug-cc-

pVTZ//MP2/6-311++G(2d,2p) (details of calculations and results are provided in *Appendix* section). In fact, the ethanol dimers are systematically studied using both theoretical and experimental approaches, especially the high resolution Fourier transform microwave spectroscopy by Hearn *et al.*[159,160,161,162,163] Ethanol dimer is substantial stronger than the binary complexes of ethanol and CO_2. Indeed, the binding energy of ethanol dimer was estimated to be -20.8 kJ.mol^{-1} at MP2/6-311++G(3df,2dp)[160] while that of ethanol$\cdots CO_2$ in this work is roughly -11.4 kJ.mol^{-1}. For (ethanol)$_2\cdots CO_2$ complexes, the most stable configurations between three typical geometries of ethanol dimer and CO_2, and their binding energies are presented in Fig. A12 and Table A13. The calculated results show that the bindings of ethanol dimers with CO_2 are negative in range of 16.6-17.9 kJ.mol^{-1} at MP2/aug-cc-pVTZ//MP2/6-311++G(2d,2p) which are significantly more stable than those of ethanol with CO_2. It is interesting that in all combinations of *(*$C_2H_5OH)_2$ with CO_2, the C_2H_5OH fragments likely exists in the *anti* type, even though the *gauche-gauche* one was confirmed to be the minimum on the PES.

Going to $3CO_2$ system, their binding energies are significantly more negative than those of complexes involving $1,2CO_2$. The **3A** complex is the global minimum of $C_2H_5OH\cdots 3CO_2$ system while the **3C** one is the most weakly bound complex with binding energies of -38.2 and -34.3 kJ.mol^{-1}, respectively. All stable structures of $3CO_2$ system found in this study are more stable than that reported by Kajiya and Saitow by around 1-6 kJ.mol^{-1} in relative energy at 6-311++G(2d,2p).[58] The complexes between C_2H_5OH with $4,5CO_2$ have binding energies in range of -47.9 and -61.9 kJ.mol^{-1}. This implies that the complex stabilization is enhanced when CO_2 guest molecule is added to the previous ethanol host complex. The electron density at BCP of $C_{CO2}\cdots O8$ contact changes insignificantly when going from n=1 to n=5 (*cf.* Table A12). In order to evaluate the cooperativity in the ternary complexes of ethanol with $2CO_2$ and compare with that of $(CO_2)_3$ trimer, the cooperative energies of **2A**-*anti* and $(CO_2)_3$ were computed using many-body procedure.[164] Those values are estimated of -7.8 and -8.6 kJ.mol^{-1}, respectively, indicating the

larger positive cooperativity of $(CO_2)_3$ trimer as compared to that of **2A**-*anti*. The positive cooperativity contributes amount of roughly 30% to the binding energy of **2A**-*anti*, however, it increases to 70% in case of $(CO_2)_3$ trimer. Accordingly, the positive cooperative effect plays a vital role in the formation of $(CO_2)_3$ trimer and its contribution is much smaller in the binding of ethanol and $2CO_2$ molecules. This finding of $C_2H_5OH\cdots nCO_2$ (n=1–5) complexes is consistent with the positive cooperativity in other complexes stabilized by TtB.[165,166] On the basis of the energetic preferred structures, the minimum structures follow an addition pathway in which the structure with nCO_2 is built from the previous one with (n-1) CO_2. The geometric formation and energetic data also reveal the important role of oxygen site of ethanol in attracting CO_2 molecules, as previously found in complexes of carbonyl compounds with CO_2.[45,151]

To evaluate in more detail the stability of complexes with the increasing number of CO_2 molecules, the binding energy per CO_2 (ΔE_n) is used as a scoring for the average strength of interactions formed by C_2H_5OH host and nCO_2 guest molecules. The changes of ΔE_n with different basis sets are presented in Fig. 3.16. The magnitude of ΔE_n values is estimated to decrease from n = 1, get minima at n = 3 and then it increases with n = 4 and 5. Let us consider the **3A** structure, two CO_2 molecules locate at the electron n-pair of oxygen, and the last CO_2 associates with O-H to form HB. In other words, the contribution of O atom of ethanol gradually increases from n=1 and gains the maximum with n=3. The fourth and fifth CO_2 molecules tend to connect to other CO_2 molecules instead of ethanol to establish ethanol:4,5CO_2 system. It proves the potential ability of ethanol to bind with 3 molecules of CO_2.

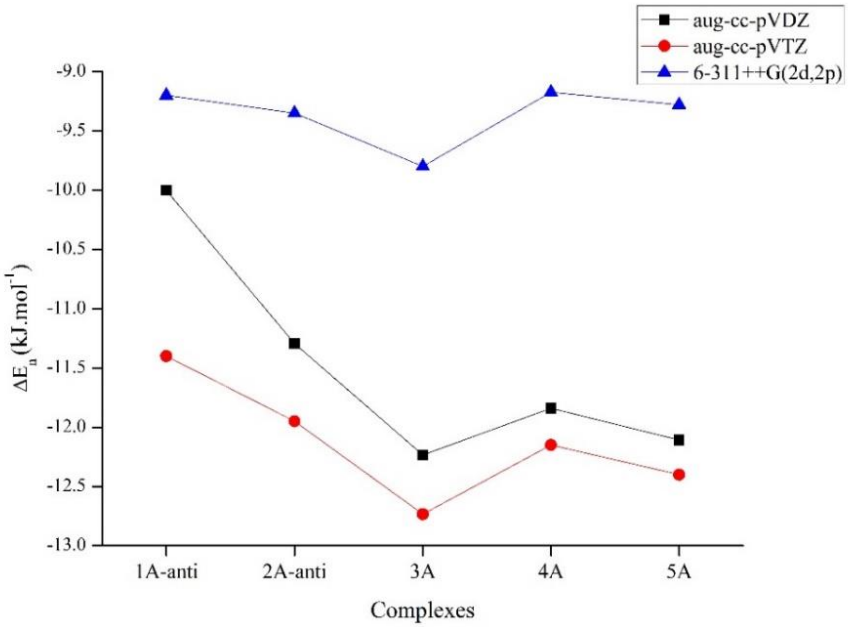

Figure 3.16. The binding energies per carbon dioxide

The changes of OH stretching mode along with the addition of CO_2 are also considered in Table 3.25. A red shift varying from 5 to 19 cm^{-1} is observed in the stretching mode of OH group in complexes compared to that of isolated C_2H_5OH. The ν_{OH} stretching mode of ethanol interacting with $1CO_2$ molecule was previously reported to be lower than that of isolated ethanol and consistent with the experiment results.[49] For n=2 and n=3, the ν_{OH} stretching modes of $C_2H_5OH\cdots nCO_2$ are found to be remarkably decreased by 9-10 cm^{-1} as compared to the corresponding values with $(n-1)CO_2$. The vibrational intensity also shows an increase, up to 126.4 ($x10^{-40}.esu^2.cm^2$). The intensity of OH mode is significantly enhanced from 42.9 at n=2 to 124.1 ($x10^{-40}.esu^2.cm^2$), at n=3. This result is another evidence for the relative strong interactions of ethanol with 3 molecules of CO_2. Thus, in solvent perspective, the concentration ratio of 1:3 between ethanol and $scCO_2$ is predicted to be a potential ratio for the good solubility.

3.7.3. Intermolecular interaction analysis

NCI two-dimension (2D) and three-dimension (3D) plots of $C_2H_5OH\cdots nCO_2$ complexes (n=1–5) are shown in Fig. 3.17. The low-density and low-reduced gradient at the negative region of λ_2 eigenvalue of all 2Dplots demonstrate the weak

and noncovalent attractive interactions between ethanol and CO_2 molecules. To further understand the difference of properties between tetrel and HBs, 2Dplots of **1A**-*anti* and **1B**-*anti* are also considered in Fig. 3.17.

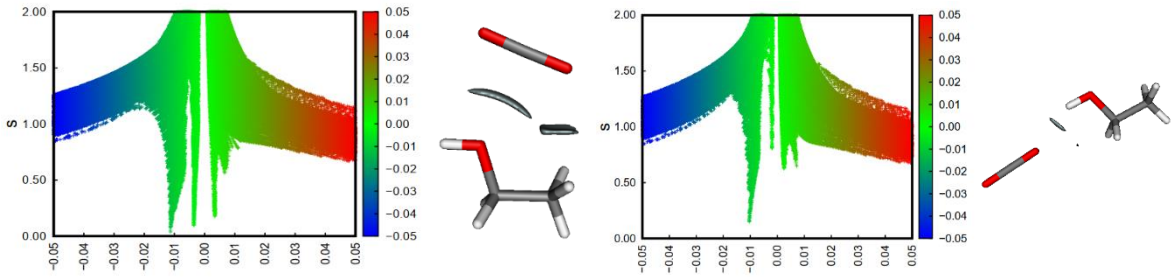

(a) **1A-*anti*** (b) **1B-*anti***

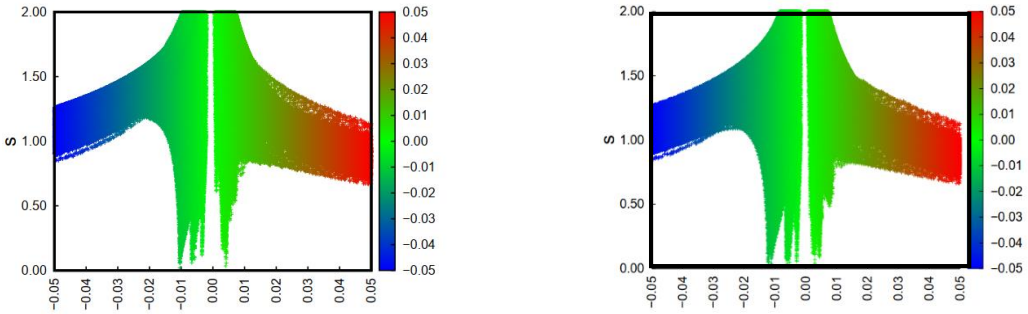

(c) **2A-*anti*** (d) **3A**

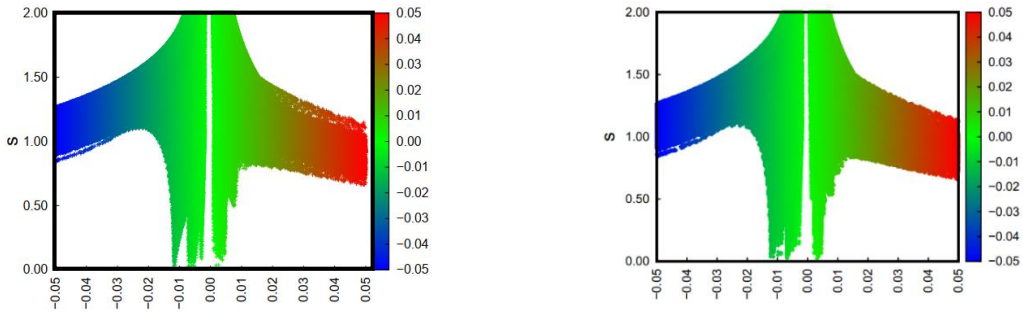

(e) **4A** (f) **5A**

Figure 3.17. NCIplot of tetrel model and hydrogen model with gradient isosurface of s=0.65.

2D plot of RDG *versus* the electron density multiplied by the sign of the λ_2 second Hessian eigenvalue. Data was obtained by evaluating MP2/6-311++G(2d,2p) level of theory

In two cases, the attractive interactions between C_2H_5OH and CO_2 are observed, which obviously dominate the repulsive interactions, and are consistent with the results of Kajiya and Saitow.[58] The 2Dplot of **1A-***anti* has a peak in negative site of $(\lambda_2).\rho(r)$ with the electron density of about 0.01 au, confirming again the noncovalent attractive nature of O8···C TtB which also obtained from AIM analysis. The larger volume of gradient isosurface of **1A-***anti* describes a stronger strength of O8···C TtB as compared to the O−H···O hydrogen one of **1B-***anti*. Furthermore, as expected, the $C1\cdots O_{CO2}$ is also detected *via* the isosurface between O of CO_2 and C of ethanol. From n=1 to n=3, the spikes expand in the negative site of $\text{sign}(\lambda_2).\rho(r)$, indicating the increasing of the attractive interactions contributing to the stabilization of the corresponding complexes (*cf*. (a-d) of Fig. 3.17). However, at n=4–5, it is observed the unchanged of the attractive spike as compared to complexes of $3CO_2$ (*cf*. (e-f) of Fig. 3.17). It confirms the higher stability of complexes with $3CO_2$ in the sequence of 1-5 CO_2.

In order to identify the characteristic of intermolecular interactions and evaluate the strength of interactions, the NBO calculations were conducted at the ωB97X-D/aug-cc-pVTZ level of theory. The charge of C_2H_5OH unit, orbital interactions and their donor-acceptor stabilization energies are collected in Table 3.31. The other intermolecular components found in the NBO analysis with the $E^{(2)}$ values lower than 0.5 kJ.mol^{-1} are not discussed here.

In general, second-order energies of $n(O8)\rightarrow\pi^*(C{=}O)$ are significantly higher than those of other delocalization processes, revealing the decisive role of $O8\cdots C_{CO2}$ TtB in orbital perspective. For complexes of $1CO_2$, $E^{(2)}(n(O8)\rightarrow\pi^*(C{=}O))$ of **1A-***anti* and **1A-***gauche* are estimated of 6.0 and 7.3 kJ.mol^{-1}, respectively. An additive contact from a nucleophilic section π(C=O) to an electrophilic one $\sigma^*(C{-}H)$ of **1A-***anti* complex is found with an $E^{(2)}$ of 1.0 kJ.mol^{-1}. Furthermore, the second-order interactions of $n(O8)\rightarrow\pi^*(C{=}O)$ are significantly higher than those of $n(O11)\rightarrow\sigma^*(O8{-}H9)$ by 2.3-3.3 kJ.mol^{-1}. This emphasizes the dominant role of C···O8 TtB relative to O8−H9···O11 HB in stabilizing the complexes investigated.

Table 3.31. NBO analysis of $C_2H_5OH\cdots nCO_2$ complexes (n=1-4) at ωB97X-D/aug-cc-pVTZ

Complexes	**Charge**[*] (*m*e)	**Orbital interactions**	**E(2)** (kJ.mol^{-1})
1A-*anti*	2.44	n(O8)→π*(C10−O12)	6.0
		π(C10−O12)→σ*(C1−H3)	1.1
1A-*gauche*	3.45	n(O8)→π*(C10−O11)	7.3
1B-*anti*	-0.38	n(O11)→σ*(O8−H9)	3.7
1B-*gauche*	-3.03	n(O11)→σ*(O8−H9)	8.1
2A-*anti*	4.49	n(O8)→π*(C10−O12)	5.7
		n(O8)→π*(C13−O14)	5.4
		n(O11)→π*(C13−O14)	1.6
		n(O15)→π*(C10−O12)	3.0
		n(O14)→σ*(C1−H3)	0.5
2A-*gauche*	5.61	n(O8)→π*(C10−O12)	5.6
		n(O8)→π*(C13−O14)	7.4
		n(O11)→π*(C13−O14)	2.0
		n(O15)→π*(C10−O12)	2.1
3A	5.11	n(O8)→π*(C10−O11)	8.6
		n(O8)→π*(C13−O15)	5.9
		n(O17)→σ*(O8−H9)	6.7
		n(O12)→π*(C13−O15)	3.1
		n(O12)→π*(C16−O18)	2.6
		n(O14)→π*(C16−O18)	2.8
4A	4.98	n(O8)→π*(C10−O11)	9.7
		n(O8)→π*(C13−O15)	8.0
		n(O17)→σ*(O8−H9)	4.5
		n(O12)→π*(C13−O15)	2.3
		n(O12)→π*(C16−O18)	3.2
		n(O14)→π*(C16−O18)	4.0
		n(O15)→π*(C19−O20)	2.1
		n(O21)→π*(C10−O11)	3.4
5A	2.72	n(O8)→π*(C10−O11)	8.0
		n(O8)→π*(C13−O15)	6.8
		n(O12)→π*(C13−O15)	3.3
		n(O12)→π*(C16−O18)	3.1
		n(O14)→π*(C16−O18)	3.4
		n(O14)→π*(C19−O20)	3.1
		n(O17)→σ*(O8−H9)	2.5
		n(O17)→π*(C19−O20)	3.9
		n(O17)→π*(C22−O24)	2.0

[*] *Charge of C_2H_5OH unit*

n: nonbonded (lone-pair) orbital, σ: anti σ-bond, π*: anti π-bond*

For the most stable complexes, the positive charge values of C_2H_5OH unit are observed, indicating that a fraction of electronic charge is transferred from C_2H_5OH host to CO_2 guest molecule (*cf.* Table 3.31), in line with the attractive factor of O site of ethanol. As a consequence, C_2H_5OH behaves as an electron donor (Lewis base) while CO_2 molecules prefer to be electron acceptor (Lewis acid) upon complexation. The small charge transfer is observed and, the electrostatic force is expected to drive intermolecular interactions.

3.7.4. Role of physical energetic components

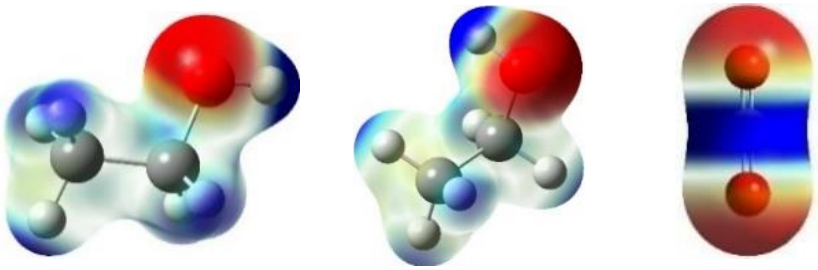

C_2H_5OH (*anti*) (isovalue=0.035) | C_2H_5OH (*gauche*) (isovalue=0.035) | CO_2 (isovalue=0.015)

Figure 3.18. MEP surface of monomers including C_2H_5OH (*anti* and *gauche*) and CO_2 at MP2/aug-cc-pVTZ

Molecular electrostatic potential is also an important tool to determine intermolecular interactions. The MEP of monomers are displayed in Fig. 3.18, where red regions correspond to the maximal negative potentials and blue regions indicates positive ones. Values of charges at the surface of monomers are represented by different colours, with the potential increase in the ordering: red < orange < yellow < green < blue. All negative potentials are associated with the oxygen atoms, while the positive potentials are mainly located at C of CO_2 and H atoms of C_2H_5OH. It is accounted for the formation of the O···C=O, O−H···O and C−H···O contacts in C_2H_5OH···nCO_2 complexes (n=1–5). It is worth noting that C atom of CO_2 and O atom of C_2H_5OH possess the maximum of positive and negative potentials, respectively; compared to other location in corresponding monomers. These results prove that the bonding feature of C_2H_5OH···nCO_2 systems (n=1–5) is

$O_{ethanol}\cdots C_{CO2}$ TtB and all intermolecular interactions are mainly held by the electrostatic attraction.

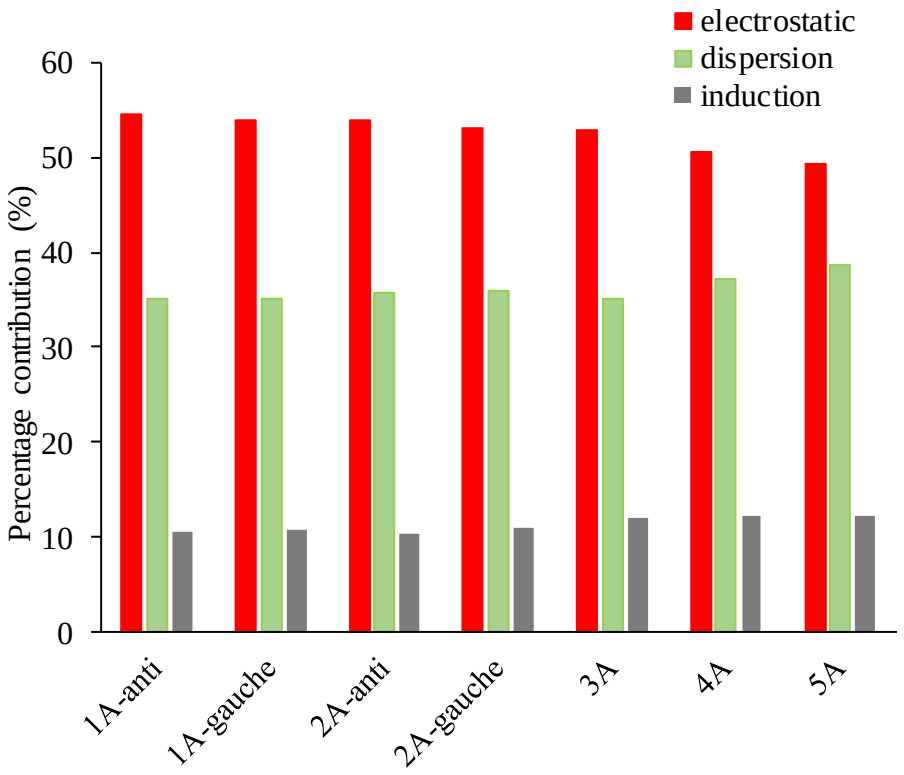

Figure 3.19. Contributions (%) of different energetic components into stabilization energy of $C_2H_5OH\cdots nCO_2$ complexes at MP2/aug-cc-pVDZ

To further explore the contribution of the different energetic components to the total stabilization energy of the complexes, the SAPT2+ calculations are performed to separate the interaction energy into exchange, electrostatic, induction and dispersion terms as given in Fig. 3.19. A significantly large role of attractive electrostatic is observed in comparison with induction and dispersion terms. It is speculated that electrostatic component acts as a prime contributor of 49–57 % to the binding of $C_2H_5OH\cdots nCO_2$ complexes. The dispersion force also provides a large percentage of 35-38% to the overall stabilization, while the contribution of induction energy is only of 10–12 %.

3.7.5. Remarks

Based on the high-level computations on $C_2H_5OH\cdots nCO_2$ (n=1–5) systems, seventeen stable structures are found, in which CO_2 molecules preferentially solvate around -OH of ethanol as the solvation site. The obtained results are in agreement with previous studies of the equilibrium configurations of small complexes (n=1-2), however, the stable geometries of larger complexes with n=3-5 are discovered for the first time and exhibit an increasing trend of stability. A growth pattern in geometry is found that the stable complexes are formed based on the structures of (n-1) CO_2 ones when adding CO_2 molecule, with an exception of n=5.

The binding energies with ZPE and BSSE corrections range from -4.6 to -61.9 $kJ.mol^{-1}$ at MP2/aug-cc-pVTZ//MP2/6-311++G(2d,2p) for the complexes investigated. It is noted that the binding of C_2H_5OH with 3 CO_2 molecules has a remarkable stability, which is expected for the good solubility of ethanol in $scCO_2$ solvent at ratio 1:3.

The weakly noncovalent nature of intermolecular interactions between C_2H_5OH and CO_2 molecules is elucidated by means of different approaches including AIM, NBO and NCI. It is found that the positive cooperativity between the noncovalent interactions in $C_2H_5OH\cdots 2CO_2$ is slightly weaker than that of $(CO_2)_3$ pure systems. With the addition of CO_2 molecules, the C···O TtB overwhelming the C/O−H···O HBs is maintained as the bonding characteristics and mainly contributes to the strength of $C_2H_5OH\cdots nCO_2$ complexes. SAPT and MEP results present the major role of electrostatic energy overcoming the dispersion and induction terms in stabilizing the complexes. These findings are expected to be useful for understanding the ethanol solvation in $scCO_2$.

CONCLUSIONS

The systematic investigation on complexes of functional organic molecules with CO_2 and/or H_2O using appropriate high level of theory is studied. These following results are hoped to contribute to the thorough understanding of the solvation process of organic functional molecules (including dimethyl sulfoxide, acetone, thioacetone, methanol, ethanol, ethanethiol, dimethyl ether and its halogen/methyl substitution) by carbon dioxide with and without the presence of water, the stability and bonding features of mentioned systems in aspect of theoretical viewpoint.

- The geometrical structures of complexes between dimethyl sulfoxide, acetone, thioacetone, dimethyl ether and its halogen/methyl-substituted derivatives, methanol, ethanethiol, dimethyl sulfide with $1,2CO_2$ and/or $1,2H_2O$ molecules are figured out that the guess CO_2/H_2O molecules preferentially solvate around the functional group of organic compounds, as the solvation site. The complexes of organic compounds with CO_2 molecules prefer the formations of C···O TtBs, while those with the presence of H_2O are stabilized by O–H···O/S HBs.
- Dimethyl sulfoxide, acetone, dimethyl ether is recognized to be more effective than ethanol, methanol, ethanethiol, thioacetone, dimethyl sulfide in aiming of carbon dioxide capture. The halogenated-substituted derivatives cause a decrease in the complex strength while methyl-substituted one leads to a stabilization enhancement. Remarkably, it is found that the interactions of CO_2 and/or H_2O with functional groups containing oxygen are more stable than those containing sulfur atom, and the larger positive cooperativity of ternary complexes is estimated in the complexes with O-containing organic molecules relative to S-containing ones.
- The addition of CO_2 or H_2O molecules into binary complexes leads to an increase in the stability of the resulting complexes, and it is significantly larger for the H_2O than CO_2 addition.

- The positive cooperative effect is found in all investigated systems indicating the mutual influence of intermolecular interactions in complexes of organic compounds with CO_2 and/or H_2O. It is interesting that the O–H···O HBs contribute largely into the cooperativity among other weak interactions including C···O/S TtBs, C-H···O HBs and O···O ChBs. A larger positive cooperativity is also found in case of H_2O relative to CO_2 addition.
- The complexes of $1,2CO_2$ are primarily stabilized by C···O tetrel bonds. For complexes relevant H_2O, the O–H···O/S dominating other weak interactions plays a decisive role in stabilizing the complexes. The stabilities of investigated complexes are contributed mainly by electrostatic energy, and a smaller contribution of dispersion and induction term.
- For complexes $C_2H_5OH···nCO_2$ (n=1-5), a growth pattern in geometry is found that the stable complexes are formed based on the structures of (n-1) CO_2 ones when adding CO_2 molecule, with the exception of n=5. With the addition of CO_2 molecules, the C···O TtB overwhelming the C/O−H···O HBs is maintained as the bonding characteristics and mainly contributes to the strength of $C_2H_5OH···nCO_2$ complexes.
- All O−H···O HBs in the systems investigated belong to red-shifting HBs while the characteristic of C−H···O HBs is complicated. In most cases, the C−H···O HBs is blue-shifting, however, their magnitude depends on the strength of C−H···O HBs.

FUTURE DIRECTIONS

Finally, it is not possible to finish this dissertation without thinking in the following stage, which is related to future directions of the present research. From problems and ideas which are appeared in the research process, theoretical works are suggested as follow:

1. Theoretical quantum calculations to evaluate the interactions of organic compounds with other functional groups such as: amines, amino acids; and the effect of halogen substitution to these complexes;

2. Molecular dynamic calculations to determine the thermodynamic properties and interactions of complexes with more than two CO_2 molecules. It will give information to the solvation process and the effective ratio of dissolution of organic compounds in scCO_2;

3. Consider the PCM model and temperature, pressure into the quantum calculations to evaluate the effect of reaction conditions into complexes involving CO_2;

4. Use of DFT methods with range-separated dispersion-corrected functional to explore the effect of dispersion to the stability of complexes involving CO_2. Besides, examination of different contributions to the interaction energy (electrostatic, induction, dispersion, charge transfer) by means of different methods;

5. Use of machine learning to analyze the relationship between the electron density and the type of noncovalent interactions based on a number of data from theoretical quantum calculations.

LIST OF PUBLICATIONS CONTRIBUTING TO THE DISSERTATION

1) The growth pattern, stability and properties of complexes of C_2H_5OH and nCO_2 (n = 1-5) molecules: a theoretical study

   Cam-Tu Dang Phan, Nguyen Thi Ai Nhung, Nguyen Tien Trung, *ACS Omega*, **2020**, 5, 14408-14416.

2) General trends in structure, stability and role of interactions in the complexes of acetone and thioacetone with carbon dioxide and water

   Phan Dang Cam-Tu, Vu Thi Ngan, Nguyen Tien Trung, *Chemical Physics*, **2020**, 530, 110580(1-8).

3) Insights into the cooperativity between multiple interactions of dimethyl sulfoxide with carbon dioxide and water

   Khanh Pham Ngoc, **Phan Dang Cam-Tu**, Dai Quoc Ho, Quan Van Vo, Vu Thi Ngan, Minh Tho Nguyen, Nguyen Tien Trung, *Journal of Computational Chemistry*, **2019**, 40, 464-474.

4) Interaction of ethanethiol with carbon dioxide and water: structure, stability and cooperativity

   Phan Dang Cam Tu, Le Minh Trong, Nguyen Le Tuan, Vu Thi Ngan, Nguyen Thi Ai Nhung, Nguyen Tien Trung, *Vietnam Journal of Chemistry*, **2018**, 56(6E2), 318-324.

5) A theoretical study on structure, stability and behavior of complexes containing CH_3OH, CO_2 and H_2O

   Phan Dang Cam Tu, Nguyen Thi Duong, Nguyen Ngoc Tri, Nguyen Tien Trung, *Vietnam Journal of Chemistry*, **2018**, 56(6E2), 245-250.

6) Effects of substituents on intermolecular interaction and stability of complexes of CO_2 and CH_3OCHX_2 (X = H, F, Cl, Br, CH_3)

   Pham Thi Hoa, **Phan Dang Cam Tu**, Nguyen Tien Trung, *Journal of Science - Quy Nhon University*, **2019**, *13*(5), 75-83.

7) A theoretical study on interaction and stability of complexes between dimethyl sulfide and carbon dioxide

Truong Tan Trung, **Phan Dang Cam-Tu**, Ho Quoc Dai, Nguyen Phi Hung, Nguyen Tien Trung, *Journal of Science – Quy Nhon University* **2019**, 13(1), 95-105.

List of conferences

- Vietnamese workshop: Computational Chemistry and Applications, 19^{th}-20^{th} July **2019**, Quy Nhon, Vietnam. (**Oral presentation**)
- The 2nd Taiwan-Thailand-Vietnam Workshop on Theoretical and Computational Chemistry, 17th-20th January **2019**, Pathum Thani (Bangkok), Thailand. (**Poster presentation**)
- Vietnamese workshop of science and technology: Inorganic chemistry, 2^{nd} November **2018**, Hanoi, Vietnam.

REFERENCES

1. Eckert C.A., Knutson B.L., Debenedetii P.G. (1996) “Supercritical fluids as solvents for chemical and materials processing”, *Nature* 383, 313–318.

2. Lacis A.A., Schmidt G.A., Rind D., Ruedy R.A. (2010) “Atmospheric CO_2: Principal control knob governing Earth’s temperature”, *Science* 330(6002), 356-359.

3. Reverchon, E., Marco I.D. (2006) “Supercritical fluid extraction and fractionation of natural matter”, *J. Supercrit. Fluids* 386, 146-166.

4. Herrero M., Cifuentes A., Ibanez E. (2006) “Sub- and supercritical fluid extraction of functional ingredients from different natural sources: Plants, food-by-products, algae and microalgae - A review”, *Food Chem.* 98, 136-148.

5. Milan N.S., Branislava G.N., Momčilo Đ.S. (2011) “Critical review of supercritical fluid extraction of selected spice plant materials”, *Maced. J. Chem. Chem. Eng.* 30(2), 197-220.

6. Marongiu B., Piras A., Pani F., Porcedda S., Ballero M. (2003) “Extraction, separation and isolation of essential oils from natural matrices by supercritical CO_2”, *Flavour Fragr. J.* 18, 505-509.

7. Fried J.R., Hu N. (2003) “The molecular basis of CO_2 interaction with polymers containing fluorinated groups: computational chemistry of model compounds and molecular simulation of poly[bis(2,2,2-trifluoroethoxy)phosphazene]”, *Polymer* 44, 4363-4372.

8. Raveendran P., Wallen S.L. (2003) “Exploring CO_2-philicity: Effects of stepwise fluorination”, *J. Phys. Chem. B* 1007, 1473-1477.

9. Raveendran P., Wallen S.L. (2002) “Cooperative C−H···O hydrogen bonding in CO_2−lewis base complexes: Implications for solvation in supercritical CO_2”, *J. Am. Chem. Soc.* 124(42) 12590-12599.

10. Li G., Zhou D., Xu Q.Q., Qiao G.Y., Yin J.Z. (2018) “Solubility of ionic liquid

[Bmim]Ac in supercritical CO_2 containing different cosolvents", *J. Chem. Eng. Data* 63(5), 1596–1602.

11. Lee H.M., Youn I.S., Saleh M., Lee J.W., Kim K.S. (2015) "Interactions of CO_2 with various functional molecules", *Phys. Chem. Chem. Phys.* 17, 10925-10933.

12. Dalvi V.H., Srinivasan V., Rossky P.J. (2010) "Understanding the effectiveness of fluorocarbon ligands in dispersing nanoparticles in supercritical carbon dioxide", *J. Phys. Chem. C* 114(37), 15553-15561.

13. Nunes A.V.M., Almeida A.P.C., Marques S.R., de Sousa A.R.S., Casimiro T., Duarte C.M.M. (2010) "Processing Triacetyl-B-cyclodextrin in the liquid phase using supercritical CO_2", *J. Supercrit. Fluids* 54, 357-361.

14. Azofra L.M., Altarsha M., Ruiz-Lopez M.F., Ingrosso F. (2013) "A theoretical investigation of the CO_2-philicity of amides and carbamides", *Theoret. Chem. Acc.* 132, 1-9.

15. San-Fabián E., Ingrosso F., Lambert A., Bernal-Uruchurtu M.I., Ruiz-López M.F. (2014) "Theoretical insights on electron donor–acceptor interactions involving carbon dioxide", *Chem. Phys. Lett.* 601, 98–102.

16. Reverchon E. (1999) "Supercritical antisolvent precipitation of micro- and nano-particles", *J. Supercrit. Fulids* 15, 1−21.

17. Vieceli J., Benjamin I. (2003) "Selective Adsorption of DMSO from an Aqueous Solution at the Surface of Self-Assembled Monolayers", *Langmuir* 19, 5383−5388.

18. Reverchon E., Adami R. (2006) "Nanomaterials and supercritical fluids", *J. Supercrit. Fluids* 37, 1−22.

19. Perez de Diego' Y., Pellikaan H.C., Wubbolts F.E., Borchard G., Witkamp G.J., Jansensa P.J. (2006) "Opening new operating windows for polymer and protein micronisation using the PCA process", *J. Supercrit. Fluids* 36, 216–224.

20. Andreatta A.E., Florusse L.J., Bottini S.B., Peters C.J. (2007) "Phase equilibria

of dimethyl sulfoxide (DMSO) + carbon dioxide, and DMSO + carbon dioxide + water mixtures", *J. Supercrit. Fluids* 42, 60–68.

21. Perez de Diego' Y., Wubbolts F.E., Witkamp G.J., de Loos T.W., Jansens P.J. (2005) "Measurements of the phase behaviour of the system dextran/DMSO/CO_2 at high pressures", *J. Supercrit. Fluids* 35, 1−9.

22. Phuong V.T., Trang N.T.T., Vo V., Trung N.T. (2014) "A comparative study on interaction capacity of CO_2 with the >S=O and >S=S groups in some doubly methylated and halogenated derivatives of CH_3SOCH_3 and CH_3SSCH_3", *Chem. Phys. Lett.* 598, 75-80.

23. Kirchner B., Reiher M. (2002) "The secret of dimethyl sulfoxide−water mixtures. A quantum chemical study of 1DMSO−nWater clusters", *J. Am. Chem. Soc.* 124, 6206−6215.

24. Lie Y., Li H.R., Han S.J. (2003) "An all-atom simulation study on intermolecular interaction of DMSO–water system", *Chem. Phys. Lett.* 380, 542−548.

25. Wu W., Zhang J., Han B., Chen J., Liu Z., Jiang T., He J., Li W. (2003) "Solubility of room-temperature ionic liquid in supercritical CO_2 with and without organic compounds", *Chem. Commun.* 9, 1412-1413.

26. Wu W., Li W., Han B., Jiang T., Shen D., Zhang Z., Sun D., Wang B. (2004) "Effect of organic cosolvents on the solubility of ionic liquids in supercritical CO_2", *J. Chem. Eng. Data* 49, 1597-1601.

27. Zhang Z., Wu W., Liu Z., Han B., Gao H., Jiang T. (2004) "A study of tri-phasic behavior of ionic liquid-methanol-CO_2 systems at elevated pressures", *Phys. Chem. Chem. Phys.* 6, 2352-2357.

28. Dobbs J.M., Wong J.M., Johnston K.P. (1986) "Nonpolar cosolvents for solubility enhancement in supercritical fluid carbon dioxide", *J. Chem. Eng. Data* 31, 303-308.

29. Walsh J.M., Ikonomou G.D., Donohue M.D. (1987) “Supercritical phase behavior: The entrainer effect”, *Fluid Phase Equilib.* 33, 295-314.
30. Hosseini S.Z., Bozorgmehr M.R., Masrurnia M., Beyramabadi S.A. (2018) “Study of the effects of methanol, ethanol and propanol alcohols as Cosolvents on the interaction of methimazole, propranolol and phenazopyridine with carbon dioxide in supercritical conditions by molecular dynamics”, *J. Supercrit. Fluids* 140, 91-100.
31. Lee M.J., Ho C.C., Lin H.M., Wang P.Y., Lu J.S. (2014) “Solubility of Disperse Red 82 and modified Disperse Yellow 119 in supercritical carbon dioxide or nitrous oxide with ethanol as a cosolvent”, *J. Supercrit. Fluids* 95, 258-264.
32. Becker S., Werth S., Horsch M., Langenbach K., Hasse H. (2016) “Interfacial tension and adsorption in the binary system ethanol and carbon dioxide: Experiments, molecular simulation and density gradient theory” *Fluid Phase Equilib*. 427, 476-487.
33. Yoon J.H., Lee H.S., Lee H. (1993) “High-pressure vapor-liquid equilibria for carbon dioxide + methanol, carbon dioxide + ethanol, and carbon dioxide + methanol + ethanol”, *J. Chem. Eng. Data* 38, 53-55.
34. Yeo S.D., Park S.J., Kim J.W., Kim J.C. (2000) “Critical properties of carbon dioxide + methanol, + ethanol, +1-propanol, and + 1-butanol”, *J. Chem. Eng. Data* 45, 932-935.
35. Stievano M., Elvassore N. (2005) “High-pressure density and vapor-liquid equilibrium for the binary systems carbon dioxide-ethanol, carbon dioxide-acetone and carbon dioxide-dichloromethane”, *J. Supercrit. Fluids* 33, 7-14.
36. Macnaughton S.J., Foster N.R. (1994) “Solubility of DDT and 2,4-D in supercritical carbon dioxide and supercritical carbon dioxide saturated with water”, *Ind. Eng. Chem. Res.* 33 (11), 2757–2763.
37. Iheozor-Ejiofor P., Dey E.S. (2009) “Extraction of rosavin from *Rhodiola Rosea*

root using supercritical carbon dioxide with water" *J. Supercrit. Fluids* 50(1), 29–32.

38. Blatchford M.A., Raveendran P., Wallen S.L. (2003) "Spectroscopy studies of model carbonyl compounds in CO_2: Evidence for cooperative C-H···O interactions", *J. Phys. Chem. A* 107, 10311–10323.

39. Nelson M.R., Borkman R.F. (1998) "Ab initio calculations on CO_2 binding to carbonyl groups", *J. Phys. Chem. A* 102, 7860–7863.

40. Trung N.T., Nguyen M.T. (2013) "Interactions of carbon dioxide with model organic molecules: a comparative theoretical study", *Chem. Phys. Lett.* 581, 10–15.

41. Wang J., Wang M., Hao J., Fujita S., Arai M., Wu Z., Zhao F. (2010) "Theoretical study on interaction between CO_2 and carbonyl compounds: Influence of CO_2 on infrared spectroscopy and activity of C=O", J. *Supercrit. Fluid*, 54, 9–15.

42. Trung N.T., Hung N.P., Hue T.T., Nguyen M.T. (2011) "Existence of both blue-shifting hydrogen bond and lewis acid–base interaction in the complexes of carbonyls and thiocarbonyls with carbon dioxide", *Phys. Chem. Chem. Phys*. 13, 14033–14042.

43. Dai H.Q., Tri N.N., Trang N.T.T., Trung N.T. (2014) "Remarkable effects of substitution on stability of complexes and origin of the C-H···O(N) hydrogen bonds formed between acetone's derivative and CO_2, XCN (X = F, Cl, Br)", *RSC Adv*. 4, 13901–13908

44. Altarsha M., Ingrosso F., Ruiz-Lopez M.F. (2012) "A new glimpse into the CO_2-philicity of carbonyl compounds", *Chem. Phys. Chem*. 13, 3397–3403.

45. Azofra L.M., Scheiner S. (2015) "Tetrel, chalcogen, and CH··O hydrogen bonds in complexes pairing carbonyl-containing molecules with 1, 2, and 3 molecules of CO_2", *J. Chem. Phys.* 142, 1–9.

46. Li M., Lei J., Feng G., Grabow J., Gou Q. (2020) "The rotational spectrum of acetophenone-CO_2: Preferred non-covalent interactions", *Spectrochim. Acta A Mol.*

Biomol. Spectrosc. 238, 118424,

47. Ginderen P.V., Herrebout W.A., van der Veken B.J. (2003), "Van der Waals complex of dimethyl ether with carbon dioxide", *J. Phys. Chem. A* 107, 5391–5396.

48. Danten Y., Tassaing T., Besnard M. (2002) "Vibrational spectra of CO_2-electron donor--acceptor complexes from ab initio", *J. Phys. Chem. A* 106, 11831–11840.

49. Lalanne P., Tassaing T., Danten T.Y., Cansell F., Tucker S.C., Besnard M. (2004) "CO_2-ethanol interaction studied by vibrational spectroscopy in supercritical CO_2", *J. Phys. Chem. A* 108, 2617-2624.

50. Gao S., Obenchain D.A., Lei J., Feng G., Herbers S., Gou Q., Grabow J., (2019) "Tetrel bond and conformational equilibria in the formamide – CO_2 complex: A rotational study", *Phys. Chem. Chem. Phys.* 21, 7016–7020.

51. Lu T., Zhang J., Gou Q., Feng G. (2020) "Structure and C···N tetrel-bonding of the isopropylamine–CO_2 complex studied by microwave spectroscopy and theoretical calculations", *Phys. Chem. Chem. Phys.* 22, 8467–8475.

52. Cheng W., Zheng Y., Herbers S., Zheng H., Gou Q. (2021) "Conformational equilibria of 2-methoxypyridine···CO_2: Cooperative and competitive tetrel and weak hydrogen bonds", *ChemPhysChem* 22, 154.

53. Newby J.J., Peebles R.A., Peebles S.A. (2004) "Structure of the dimethyl ether−CO_2 van der Waals complex from microwave spectroscopy", *J. Phys. Chem. A* 108, 11234–11240.

54. Legon A.C., Suckley A.P. (1989) "Infrared diode-laser spectroscopy and Fourier-transform microwave spectroscopy of the (CO_2, CO) dimer in a pulsed jet", *J. Chem. Phys.* 91, 4440–4447.

55. Leopold K.R., Fraser G.T., Klemperer W. (1984) "Rotational spectrum and structure of the complex $HCNCO_2$", *J. Chem. Phys.* 80, 1039–1046.

56. Columberg G., Bauder A., Heineking N., Stahl W., Makarewicz J. (1998)

"Internal rotation effects and hyperfine structure in the rotational spectrum of a water–carbon dioxide complex", *Mol. Phys.* 93, 215–228.

57. Saharay M., Balasubramanian S. (2006) "Electron donor-acceptor interactions in ethanol-CO_2 mixtures: an Ab initio molecular dynamics study of supercritical carbon dioxide", *J. Phys. Chem. B* 110, 3782-3790.

58. Kajiya D., Saitow K. (2016) "Significant difference in attractive energies of C_2H_6 and C_2H_5OH in $scCO_2$", *J. Supercrit. Fluids* 120(2) 328-334.

59. Abboud J.L.M., Mo O., de Paz J.L.G., Yanez M., Esseffar M., Bouab W., El-Mouhtadi M., Mokhlisse R., Ballesteros E., Notario R. (1993) "Thiocarbonyl versus carbonyl compounds: A comparison of intrinsic reactivities", *J. Am. Chem. Soc.* 115, 12468-12476.

60. Murai T. (2018) "The construction and application of C=S bonds", *Top. Cur. Chem.* 376:31, 1-21.

61. Dunitz J. D., Gavezzotti A. (2009) "How molecules stick together in organic crystals: weak intermolecular interactions", *Chem. Soc. Rev.* 38, 2622-2633.

62. Volkert L.G., Conrad M. (1998) "The role of weak interactions in biological systems: The dual dynamics model", *J. Theor. Biol.* 193(2), 287-306.

63. Scheiner S. (2018) "Ability of IR and NMR spectral data to distinguish between a tetrel bond and a hydrogen bond", *J. Phys. Chem. A* 122, 7852-7862.

64. Bene J.E.D., Alkorta I., Elguero J. (2019) "Potential energy surfaces of HN(CH)SX:CO_2 for X = F, Cl, NC, CN, CCH, and H: N···C tetrel bonds and O···S chalcogen bonds", *J. Phys. Chem. A* 123, 7270-7277.

65. Southern S.A., Bryce D.L. (2015) "NMR investigations of noncovalent carbon tetrel bonds. Computational assessment and initial experimental observation", *J. Phys. Chem. A* 119, 11891-11899.

66. Brammer L. (2017) "Halogen bonding, chalcogen bonding, pnictogen bonding, tetrel bonding: origins, current status and discussion", *Faraday Discuss.* 203, 485-

507.
67. Anthony L.C. (2017) “Tetrel, pnictogen and chalcogen bonds identified in the gas phase before they had names: a systematic look at non-covalent interactions”, *Phys. Chem. Chem. Phys.* 19, 14884-14896.
68. Chalasinski G., Szczesniak M.M. (2000) “State of the art and challenges of the ab initio theory of intermolecular interactions”, *Chem. Rev.* 100(11), 4227–4252.
69. Reed A.E., Curtiss L.A., Weinhold F. (1988) “Intermolecular interactions from a natural bond, donor-acceptor viewpoint”, *Chem. Rev*. 88(6), 899–926.
70. Etter M.C. (1990) “Encoding and decoding hydrogen-bond patterns of organic compounds”, *Acc, Chem. Res.* 23(4), 120–126.
71. Gu Y., Kar T., Scheiner S. (1999) “Fundamental properties of the CH···O interaction: Is it a true hydrogen bond?”, *J. Am. Chem. Soc.* 121, 40, 9411–9422.
72. Hermansson K. (2002) “Blue-shifting hydrogen bonds”, *J. Phys. Chem. A* 106, 4695-4702.
73. Wieczorek R., Dannenberg J.J. (2003) “H-Bonding cooperativity and energetics of α-helix formation of five 17-amino acid peptides”, *J. Am. Chem. Soc.* 125, 8124−8129.
74. Chen Y.F., Viswanathan R., Dannenberg J.J. (2007) “Through hydrogen-bond vibrational coupling in hydrogen-bonding chains of 4-pyridones with implications for peptide amide absorptions: density functional theory compared with transition dipole coupling”, *J. Phys. Chem. B* 111, 8329−8334.
75. Neela Y.I., Mahadevi A.S., Sastry G.N. (2010) “Hydrogen bonding in water clusters and their ionized counterparts”, *J. Phys. Chem. B* 114, 17162−17171.
76. Parthasarathi R., Subramanian V., Sathyamurthy N. (2007) “Hydrogen bonding in protonated water clusters: an atoms-in-molecules perspective”, *J. Phys. Chem. A* 111, 13287−13290.
77. Li Q., An X., Gong B., Cheng J. (2007) “Cooperativity between O-H···O and

C-H···O hydrogen bonds involving dimethyl sulfoxide-H_2O-H_2O complex", *J. Phys. Chem. A* 111, 10166−10169.

78. Saha S., Sastry G.N. (2015) "Cooperative or anticooperative: How noncovalent interactions influence each other", *J. Phys. Chem. B* 119, 11121-11135

79. Hartree D.R. (1928) "The wave mechanics of an atom with a non-Coulomb central field", *Math. Proc. Camb. Philos. Soc.* 24(1):111, 89-110.

80. Møller Chr., Plesset M.S. (1934) "Note on an approximation treatment for many-electron systems", *Phys. Rev.* 46, 618-622.

81. Hohenberg P., Kohn W. (1964) "Inhomogeneous Electron Gas", *Phys. Rev.* 136(3B), 864-871.

82. Kohn W., Sham L.J. (1965) "Self-consistent equations including exchange and correlation effects", *Phys. Rev.* 140(4A), 1133-1138.

83. Koch W., Holthausen M.C. (2001) "A chemist's guide to density functional theory", Wiley-VCH: New York.

84. Chai J.D.; Gordon M.H. (2008) "Systematic Optimization of Long-Range Corrected Hybrid Density Functionals", *J. Chem. Phys.* 128, 084106-15.

85. Burke K. (2012) "Perspective on Density Functional Theory", *J. Chem. Phys.* 136 (15), 150901-9.

86. Dunning T.H. Jr. (1989) "Gaussian basis sets for use in correlated molecular calculations I. The atoms boron through neon and hydrogen", *J. Chem. Phys*. 90, 1007-1023.

87. Huang Z., Qin K., Deng G., Wu G., Bai Y., Xu J.F., Wang Z., Yu Z., Scherman O.A., Zhang X. (2016) "Supramolecular chemistry of cucurbiturils: tuning cooperativity with multiple noncovalent interactions from positive to negative", *Langmuir* 32(47), 12352-12360.

88. Kar T., Scheiner S. (2004) "Comparison of cooperativity in CH···O and OH···O hydrogen bonds", *J. Phys. Chem. A* 108, 9161−9168.

89. Zhao Q., Feng D., Hao J. (2011) “The cooperativity between hydrogen and halogen bond in the XY···HNC···XY (X, Y = F, Cl, Br) complexes”, *J. Mol. Model.* 17, 2817–2823.

90. Alkorta I., Blanco F., Deya P.M., Elguero J., Estarellas C., Frontera A., Quinonero D. (2010) “Cooperativity in multiple unusual weak bonds”, *Theor. Chem. Acc.* 126, 1-14.

91. Boys S.F., Bernardi F. (1970) “The calculation of small molecular interactions by the differences of separate total energies. Some procedures with reduced errors”, *Molecular Physics* 19, 553-566.

92. Per-Olov Löwdin. (1955) “Quantum theory of many-particle systems. I. Physical interpretations by means of density matrices, natural spin-orbitals, and convergence problems in the method of configurational interaction”, *Phys. Rev*. 97, 1474-1489.

93. Glendening E.D., Badenhoop J.K., Reed A.E., Carpenter J.E., Bohmann J.A., Morales C.M., Weinhold F. “NBO 5.G”; Theoretical Chemistry Institute, University of Wisconsin: Madison, 1996-2001.

94. Glendening E.D., Landis C.R., Weinhold F. (2012) “Natural bond orbital methods”, *Wires. Comput. Mol. Sci.* 2, 1-42.

95. Bader R.F.W. (1985) “Atoms in molecules”, *Acc. Chem. Res.* 18(1), 9-15.

96. Bader R.F.W. (1991) “A quantum theory of molecular structure and its applications”, *Chem. Rev.* 91, 893-928.

97. Bader R.F.W. (1990) “Atoms in molecules: A quantum theory”, Oxford: Clarendon Press.

98. Johnson E.R., Keinan S., Mori-Sánchez P., Contreras-García J., Cohen A.J., Yang W. (2010) “Revealing noncovalent interactions”, *J. Am. Chem. Soc*. 132, 6498-6506.

99. Contreras-Garcia J., Johnson E.R., Keinan S., Chaudret R., Piquemal J.P.,

Beratan D.N. Yang W. (2011) “NCIPLOT: A program for plotting noncovalent interaction regions”, *J. Chem. Theory Comput.* 7, 625-632.

100. Szalewicz K. (2012) “Symmetry-adapted perturbation theory of intermolecular forces”, *WIREs Comput. Mol. Sci.* 2, 254-272.

101. Bauzá A., Mooibroek T.J., Frontera A. (2013) “Tetrel-bonding interaction: Rediscovered supramolecular force?”, *Angew. Chem., Int. Ed.* 52, 12317–12321.

102. Peng Y.P., Sharpe S.W., Shin S.K., Wittig C., Beaudet R.A. (1992) Infrared spectroscopy of CO_2–D(H)Br: Molecular structure and its reliability, *J. Chem. Phys.* 97, 5392–5402.

103. Baiocchi F.A., Dixon T.A., Joyner C.H., Klemperer W. (1981) “CO_2–HF: A linear molecule”, *J. Chem. Phys*. 74, 6544–6550.

104. Altman R.S., Marshall M.D., Klemperer W. (1982) “The microwave spectrum and molecular structure of CO_2–HCl”, *J. Chem. Phys*. 77, 4344–4349.

105. García-Llinás X., Bauzá A., Seth S.K., Frontera A. (2017) “Importance of R–CF3···O tetrel bonding interactions in biological systems”, *J. Phys. Chem. A* 121, 5371–5376.

106. Elangannan A., Gautam R.D., Roger A.K., Joanna S., Scheiner S., Alkorta I., David C.C., Robert H.C., Joseph J.D., Hobza P., Henrik G.K., Anthony C.L., Benedetta M., David J.N. (2011) “Definition of the hydrogen bond (IUPAC Recommendations 2011)”, *Pure Appl. Chem.* 83(8), 1637-1641.

107. Jeffrey G.A. (1997) “An introduction to hydrogen bonding”, Oxford University Press.

108. Hobza P., Havlas Z. (2000) “Blue-shifting hydrogen bonds”, *Chem. Rev.* 100, 4253−4264.

109. Scheiner S., Kar T. (2002) “Red- versus blue-shifting hydrogen bonds: Are there fundamental distinctions?” *J. Phys. Chem. A* 106, 1784−1789.

110. Alabugin I.V., Manoharan M., Peabody S., Weinhold F. (2003) “Electronic

basis of improper hydrogen bonding: A subtle balance of hyperconjugation and rehybridization", *J. Am. Chem. Soc.* 125, 5973−5987.

111. Joseph J., Jemmis E.D. (2007) "Red-, blue-, or no-shift in hydrogen bonds: A unified explanation", *J. Am. Chem. Soc.* 129, 4620−4632.

112. Chang X., Zhang Y., Weng X., Su P., Wu W., Mo Y., (2016) "Red-Shifting versus blue-shifting hydrogen bonds: Perspective from ab initio valence bond theory, *J. Phys. Chem. A* 120, 2749−2756.

113. Pascal A., Franklin A.H., Eric W., Shing H.P. (2004) "Halogen bonds in biological molecules", *Proc. Natl. Acad. Sci.* 101(48) 16789-16794.

114. Espallargas M.G., Zordan F., Arroyo Marín L., Adams H., Shankland K., van de Streek J., Brammer L. (2009) "Rational modification of the hierarchy of intermolecular interactions in molecular crystal structures by using tunable halogen bonds", *Chem. Eur. J.* 15, 7554-7568.

115. Bertani R., Sgarbossa P., Venzo A., Lelj F., Amatic M., Resnati G., Pilati T., Metrangolo P., Terraneo G. (2010) "Halogen bonding in metal-organic-supramolecular networks", *Coord. Chem. Rev.* 254, 677-695.

116. Desiraju G.R., Shing H.P., Kloo L., Legon A.C., Marquardt R., Metrangolo P., Politzer P., Resnati G., Rissanen K. (2013) "Definition of the halogen bond (IUPAC Recommendations 2013)", *Pure Appl. Chem.* 85(8), 1711-1713.

117. Minyaev R.M., Minkin V.I., (1998) "Theoretical study of O→X (S, Se, Te) coordination in organic compounds", *Can. J. Chem.* 76, 776–778.

118. Junming L., Yunxiang L., Subin Y., Weiliang Z. (2011) "Theoretical and crystallographic data investigations of noncovalent S···O interactions", *Struct. Chem.* 22, 757-763.

119. Burling F.T., Goldstein B.M. (1992) "Computational studies of nonbonded sulfur oxygen and selenium-oxygen interactions in the thiazole and selenazole nucleosides", *J. Am. Chem. Soc.* 114, 2313-2320.

120. Aakeroy C.B., Bryce D.L., Desiraju G.R., Frontera A., Anthony L.C., Nicotra F., Rissanen K., Scheiner S., Terraneo G., Metrangolo P., Resnati G. (2019) "Definition of the chalcogen bond (IUPAC Recommendations 2019)", *Pure Appl.Chem.* 91(11), 1889-1892.

121. Keith T.A., AIMAll (Version 19.10.12), TK Gristmill Software, Overland Park KS, USA 2019.

122. Espinosa E., Molins E., Lecomte C. (1998) "Hydrogen bond strengths revealed by topological analyses of experimentally observed electron densities", *Chem. Phys. Lett.* 285, 170.

123. Murray J.S., Politzer P. (2011) "The Electrostatic potential: An overview", *WIREs Comput. Mol. Sci.* 1 153-163.

124. Khanh P.N., Cam-Tu P.D., Ho D.Q., Vo Q.V., Ngan V.T., Nguyen M.T., Trung N.T. (2019) "Insights into the cooperativity between multiple interactions of dimethyl sulfoxide with carbon dioxide and water", *J. Comput. Chem.* 40, 464-474.

125. Li Q.Z., An X.L., Gong B.A., Cheng J.B. (2008) "Spectroscopic and theoretical evidence for the cooperativity between red-shift hydrogen bond and blue-shift hydrogen bond in DMSO aqueous solutions", *Spectrochim. Acta A Mol. Biomol. Spectrosc.* 69(1), 211-215.

126. Koch U., Popelier P.L.A. (1995) "Characterization of C-H-O hydrogen bonds on the basis of the charge density", *J. Phys. Chem.* 99, 9747.

127. Zabardasti A., Kakanejadifard A. (2008) "Theoretical study of hydrogen bonded clusters of water and cyanic acid: Hydrogen bonding in terms of the molecular structure", *Polyhedron* 27, 2973–2977.

128. Grabowski S.J., Leszczynski J. (2009) "The enhancement of X–H···π hydrogen bond by cooperativity effects – Ab initio and QTAIM calculations", *Chem. Phys.* 355, 169–176.

129. Zio´łkowski M., Grabowski S.J., Leszczynski J. (2006) "Cooperativity in

hydrogen-bonded interactions: Ab initio and “Atoms in Molecules” Analyses”, *J. Phys. Chem. A* 110, 6514-6521.

130. Mrazkova E., Hobza P. (2003) “Hydration of sulfo and methyl groups in dimethyl sulfoxide is accompanied by the formation of red-shifted hydrogen bonds and improper blue-shifted hydrogen bonds: An ab initio quantum chemical study”, *J. Phys. Chem. A* 107, 1032−1039.

131. Cam-Tu D.P., Ngan V.T., Trung N.T. (2020) “General trends in structure, stability and role of interactions in the complexes of acetone and thioacetone with carbon dioxide and water”, *Chem. Phys.* 530, 110580(1-7).

132. Popelier P. (2000) “Atoms in Molecules”, Pearson Education Ltd., Essex, U.K.

133. Wang J., Wang M., Hao J., Fujita S., Arai M., Wu Z., Zhao F. (2010) “Theoretical study on interaction between CO_2 and carbonyl compounds: Influence of CO_2 on infrared spectroscopy and activity of C=O”, *J. Supercrit. Fluids* 54, 9-15.

134. Allen F.H., Baalham C.A., Lommerse J.P.M., Raithby P.R. (1998) “Carbonyl-carbonyl interactions can be competitive with hydrogen bonds”, *Acta Cryst.* B54, 320–329.

135. Tsuzuki S., Uchimaru T., Mikami M., Tanabe K. (1998) “Intermolecular interaction potential of the carbon dioxide dimer”, *J. Chem. Phys.* 109, 2169–2175.

136. Rebelatto E.A., Polloni A.E., Andrade K.S., Bender J.P., Corazza M.L., Lanza M., Oliveira J.V. (2018) “High-pressure phase equilibrium data for systems containing carbon dioxide, Pentadecalactone, chloroform and water”, *J. Chem. Thermodyn.* 122, 125-132.

137. Reimers J.R., Watts R.O. (1984) “The structure and vibrational spectra of small clusters of water molecules”, *Chem. Phys.* 85, 83-112.

138. Liao D.W., Mebel A.M., Chen Y.T., Lin S.H. (1997) “Theoretical study of the structure, energetics, and the π-π* electronic transition of the acetone + nH_2O (n=1-3) complexes”, *J. Phys. Chem. A* 101, 9925-9935.

139. Cam-Tu D.P., Nguyen T.D., Tri N.N., Trung N.T. (2018) “A theoretical study on structure, stability and behavior of complexes containing CH_3OH, CO_2 and H_2O”, *Vietnam J. Chem.* 56(6E2), 245-250.

140. Fileti E.E., Chaudhuri P., Canuto S. (2004) “Relative strength of hydrogen bond interaction in alcohol–water complexes”, *Chem. Phys. Lett.* 400(4-6), 494-499.

141. Erp V., Meijer T.S., Jan E. (2001) “Hydration of methanol in water. A DFT-based molecular dynamics study”, *Chem. Phys. Lett.* 333(3-4), 290–296.

142. Cam-Tu D.P., Trong L.M., Tuan N.L., Ngan V.T., Nhung N.T.A., Trung N.T. (2018) “Interaction of ethanethiol with carbon dioxide and water: structure, stability and cooperativity”, *Vietnam J. Chem.* 2018, 56(6E2), 318-324.

143. Kieninger M., Ventura O.N. (2011) “Calculations of the Infrared and Raman spectra of simple thiols and thiol – water complexes”, *J. Quantum Chem.* 111, 1843-1857.

144. Hoa P.T., Cam-Tu D.P., Trung N.T. (2019) “Effects of substituents on intermolecular interaction and stability of complexes of CO_2 and CH_3OCHX_2 (X = H, F, Cl, Br, CH_3)”, *Quy Nhon University - J. Sci.*, 13(5), 75-83.

145. Trung N.T., Trang N.T.T., Ngan V.T., Quang D.T., Tho N.M. (2016), “Complexes of carbon dioxide with dihalogenated ethylenes: structure, stability and interaction”, *RSC Adv.* 6, 31401-31409.

146. Trung T.T., Cam-Tu P.D., Dai H.Q., Hung N.P., Trung N.T. (2019) Theoretical study on interaction and stability of complexes between dimethyl sulfide and carbon dioxide, *Quy Nhon University –J. Sci.* 13(1), 95-105.

147. Kim K. H., Kim Y. (2008) “Theoretical studies for Lewis acid-base interactions and C-H···O weak hydrogen bonding in various CO_2 complexes”, *J. Phys. Chem. A* 112, 1596-1603.

148. Cam-Tu D.P., Nhung N.T.A., Trung N.T. (2020) “The growth pattern, stability

and properties of complexes of C_2H_5OH and nCO_2 (n=1-5) molecules: a theoretical study", *ACS Omega* 5, 14408-14416.

149. Scheiner S., Seybold P.G. (2009) "Quantum chemical analysis of the energetics of the anti and gauche conformers of ethanol", *Struct. Chem.* 20, 43-48.

150. McGuire B.A., Martin-Drummel M.A., McCarthy M.C. (2017) "Electron donor-acceptor nature of ethanol - CO_2 dimer", *J. Phys. Chem. A* 121(33), 6283-6287.

151. Kajiya D., Imanishi M., Saitow K. (2016) "Solvation of esters and ketones in supercritical CO_2", *Phys. Chem. B* 120, 785-792.

152. Xu W., Yang J., Hu Y. (2009) "Microscopic structure and interaction analysis for supercritical carbon dioxide−ethanol mixtures: A Monte Carlo simulation study", *J. Phys. Chem. B 1*13(14), 4781-4789.

153. Skarmoutsos I., Guardia E., Samios J. (2010) "Hydrogen bond, electron donor-acceptor dimer, and residence dynamics in supercritical CO_2-ethanol mixtures and the effect of hydrogen bonding on single reorientational and translational dynamics: A molecular dynamics simulation study", *J. Chem. Phys.* 133, 014504(1-13).

154. Bader R.F.W. (2002) "Atoms in molecules", in Encyclopedia of computational chemistry, John Wiley & Sons, Ltd.

155. Bentley J. (1998) "Behavior of electron density functions in molecular interaction", *J. Phys. Chem. A* 102, 6043-6051.

156. Illies A.J., McKee M.L., Schelgel H.B. (1987) "Ab initio study of the carbon dioxide dimer and the carbon dioxide ion complexes [$(CO_2)_2^+$ and $(CO_2)_3^+$]", *J. Phys. Chem.* 91, 3489–3494.

157. Nesbitt D. J. (1988), "High-resolution infrared spectroscopy of weakly bound molecular complexes", *Chem. Rev.* 88, 843–870.

158. Tsuzuki S., Klopper W., Luthi H.P. (1999) "High-level *ab initio* computations of structures and relative energies of two isomers of the CO_2 trimer", *J. Chem.*

Phys. 111, 3846–3854.
159. Dyczmons V. (2004) “Dimers of ethanol”, *J. Phys. Chem. A* 108, 2080-2086.
160. Hearn J.P.I., Cobley R.V., Howard, B.J. (2005) “High-resolution spectroscopy of induced chiral dimers: A study of the dimers of ethanol by Fourier transform microwave spectroscopy”, *J. Chem. Phys*. 123, 134324(1-6).
161. Emmeluth C., Dyczmons V., Kinzel T., Botschwina P., Suhm M.A., Yáñez M. (2005) “Combined jet relaxation and quantum chemical study of the pairing preferences of ethanol”, *Phys. Chem. Chem. Phys* 7, 991-997.
162. Vargas-Caamal A., Ortiz-Chi F., Moreno D., Restrepo A., Merino G., Cabellos J.L. (2015) “The rich and complex potential energy surface of the ethanol dimer”, *Theor. Chem. Acc.* 134(16), 1-9.
163. Finneran I.A., Carroll P.B., Mead G.J., Blake G.A. (2016) “Hydrogen bond competition in the ethanol–methanol dimer”, *Phys. Chem. Chem. Phys*. 18, 22565–22572.
164. Xantheas S.S. (1994) “Ab initio studies of cyclic water clusters $(H_2O)_n$, n=1–6. II. Analysis of many-body interactions”, *J. Chem. Phys.* 100, 7523–7534.
165. Marín-Luna M., Alkorta I., Elguero J. (2016), “Cooperativity in tetrel bonds”, *J. Phys. Chem. A* 120, 648-656.
166. Anila S., Suresh C. H. (2019) “Formation of large clusters of CO_2 around anions: DFT study reveals cooperative CO_2 adsorption”, *Phys. Chem. Chem. Phys*. 21, 23143-23153.